Rocuronium-specific antibodies drive perioperative anaphylaxis but can also function as reversal agents in preclinical models

Alice Dejoux, Qianqian Zhu, Christelle Ganneau, Odile Richard-Le Goff, Ophélie Godon, Julien Lemaitre, Francis Relouzat, François Huetz, Aurélien Sokal, Alexis Vandenberghe, et al.

Title: Rocuronium-specific antibodies drive perioperative anaphylaxis but can also function as reversal agents in preclinical models

Overline: IMMUNOLOGY

One Sentence Summary: Reversal agents for rocuronium were identified from rocuronium-specific antibody repertoires.

Editor's Summary:

Roc Out. Neuromuscular blocking agents (NMBAs) such as rocuronium are used during anesthesia to assist with surgeries and intubations. Although these agents are effective, they are not without risk. Patients can develop postoperative residual neuromuscular blockade that can be treated with an NMBA reversal agent, and life-threatening anaphylaxis can occur in rare cases. Here, Dejoux *et al.* isolated and characterized memory B cells from three individuals who developed reactions to NMBA treatment and had serum antibodies to rocuronium. The authors found that IgE antibodies generated from these memory B cells were sufficient to induce anaphylaxis in mice treated with rocuronium, although they were too low affinity to be used as reversal agents. This led the authors to immunize mice with rocuronium to generate antibodies of higher affinity, which were able to reverse neuromuscular blockade in rocuronium-treated nonhuman primates. Together, these data both explain why these three patients had a reaction and offer a therapeutic approach to reversing neuromuscular blockade. –Courtney Malo

Authors: Alice Dejoux[1,2,†], Qianqian Zhu[1,3,†], Christelle Ganneau[4], Odile Richard-Le Goff[1], Ophélie Godon[1], Julien Lemaitre[5], Francis Relouzat[5], François Huetz[1], Aurélien Sokal[6,7], Alexis Vandenberghe[6], Cyprien Pecalvel[8], Lise Hunault[1,2], Thomas Derenne[1,2], Caitlin Gillis[1], Bruno Iannascoli[1], Yidan Wang[1], Thierry Rose[9], Christel Mertens[10], Pascale Nicaise-Roland[11], NASA study group‡, Patrick England[12], Matthieu Mahévas[6], Luc de Chaisemartin[3,11], Roger Le Grand[5], Hélène Letscher[5], Frederick Saul[13], Cédric Pissis[13], Ahmed Haouz[13], Laurent L. Reber[8], Pascal Chappert[6], Friederike Jönsson[1,14], Didier G. Ebo[10], Gaël A. Millot[1,15,§], Sylvie Bay[4,§], Sylvie Chollet-Martin[3,11,§], Aurélie Gouel-Chéron[1,16,17,§,*] and Pierre Bruhns[1,18,§,*].

Affiliations:

[1]Institut Pasteur, Université Paris Cité, INSERM UMR1222, Antibodies in Therapy and Pathology, 75015 Paris, France.

[2]Sorbonne Université, Collège Doctoral, 75005 Paris, France.

[3]Université Paris-Saclay, INSERM, Inflammation Microbiome Immunosurveillance, 91400 Orsay, France.

[4]Institut Pasteur, Université Paris Cité, CNRS UMR3523, Chimie des Biomolécules, 75015 Paris, France.

[5]Université Paris-Saclay, INSERM, CEA, Center for Immunology of Viral, Autoimmune, Hematological and Bacterial Diseases (IMVA-HB/IDMIT), 92260 Fontenay-aux-Roses & 94250 Le Kremlin-Bicêtre, France.

[6]Institut Necker Enfants Malades, INSERM U1151/CNRS UMR 8253, Action thématique incitative sur programme-Avenir Team, Auto-Immune and Immune B cells, Université Paris Cité, Université Paris Est-Créteil, 94000 Créteil, France; INSERM U955, équipe 2. Institut Mondor de Recherche Biomédicale (IMRB), Université Paris-Est Créteil (UPEC), 94000 Créteil, France.

[7]Service de Médecine interne, Hôpital Beaujon, Assistance Publique-Hôpitaux de Paris (AP-HP), Université de Paris Cité, 92110 Clichy, France

[8]Toulouse Institute for Infectious and Inflammatory Diseases (Infinity), INSERM UMR1291, CNRS UMR5051, University Toulouse III; 31000 Toulouse, France.

[9]Institut Pasteur, Université Paris Cité, INSERM UMR1224, Biologie Cellulaire des Lymphocytes, Ligue Nationale Contre le Cancer, Équipe Labellisée Ligue 2018, 75015 Paris, France.

[10]Faculty of Medicine and Health Science, Department of Immunology-Allergology-Rheumatology, Antwerp University Hospital and the Infla-Med Center of Excellence, University of Antwerp, Antwerp, Belgium; Department of Immunology and Allergology, AZ Jan Palfijn Ghent, 9000 Ghent, Belgium.

[11]Service d'immunologie Biologique, DMU BIOGEM,, Hôpital Bichat, APHP, 75018, Paris, France.

[12]Institut Pasteur, Université Paris Cité, CNRS UMR3528, Molecular Biophysics Core Facility, 75015 Paris, France.

[13]Institut Pasteur, Université Paris Cité, CNRS UMR3528, Plate-forme Cristallographie-C2RT, 75015 Paris, France.

[14]CNRS, F-75015 Paris.

[15]Institut Pasteur, Université Paris Cité, Bioinformatics and Biostatistics Hub, 75015 Paris, France.

[16]Anaesthesiology and Critical Care Medicine Department, DMU Parabol, Bichat-Claude Bernard Hospital, AP-HP, 75018 Paris, France.

[17]Université Paris Cité, 75010 Paris, France.

[18]INSERM 1152, DHU FIRE, Labex Inflamex, Université Paris Diderot Paris 7, 75018 Paris, France.

†: Equal contribution.

§: Co-senior authorship.

‡The full list of members of the study group and their affiliations is listed at the end of the Acknowledgments.

*To whom correspondence should be addressed: **Pierre Bruhns**, Unit of Antibodies in Therapy and Pathology, Department of Immunology, Institut Pasteur, 25 rue du Docteur Roux, 75015 Paris, France. Phone: +33-145688629. E-mail: bruhns@pasteur.fr; **Aurélie Gouel-Chéron**, Anaesthesiology and Critical Care Medicine Department, DMU Parabol, Bichat-Claude Bernard Hospital, AP-HP, 75018 Paris, France. Phone : +33-140258355. E-mail: aurelie.gouel@aphp.fr

Abstract:

Neuromuscular blocking agents (NMBA) relax skeletal muscles to facilitate surgeries and ease intubation, but can lead to adverse reactions, including complications due to postoperative residual neuromuscular blockade (rNMB) and, in rare cases, anaphylaxis. Both adverse reactions vary between types of NMBAs with rocuronium, a widely used non-depolarizing NMBA, inducing among the longest rNMB durations and highest anaphylaxis incidence. rNMB induced by rocuronium can be reversed by the synthetic γ-cyclodextrin, sugammadex. However in rare cases, sugammadex can provoke anaphylaxis. Thus, additional therapeutic options are needed. Rocuronium-induced anaphylaxis is proposed to rely on preexisting rocuronium-binding antibodies. To understand the pathogenesis of rocuronium-induced anaphylaxis and to identify potential therapeutics, we investigated the memory B cell antibody repertoire of patients with suspected hypersensitivity to rocuronium. We identified polyclonal antibody repertoires with a high diversity among V(D)J genes without evidence of clonal groups. When recombinantly expressed, these antibodies demonstrated specificity and low affinity for rocuronium without

cross-reactivity for other NMBAs. Moreover, when these antibodies were expressed as human IgE, they triggered human mast cell activation and passive systemic anaphylaxis in transgenic mice, although their affinities were insufficient to serve as reversal agents. Rocuronium-specific, high-affinity antibodies were thus isolated from rocuronium-immunized mice. The highest affinity antibody was able to reverse rocuronium-induced neuromuscular blockade in nonhuman primates with kinetics similar to sugammadex. Together, these data support the hypothesis that antibodies cause anaphylactic reactions to rocuronium and pave the way for improved diagnostics and neuromuscular blockade reversal agents.

Main text:

INTRODUCTION

Neuromuscular blocking agents (NMBAs) are used in the clinic to paralyze skeletal muscles during surgery conducted under general anesthesia (*1, 2*). They help to assist airway management in programmed or emergency anesthesia by facilitating endotracheal intubation. NMBAs operate at the neuromuscular junction by competing with acetylcholine to bind nicotinic receptors. All NMBAs possess two tertiary or quaternary substituted ammonium groups at physiological pH that enable NMBAs to compete with the quaternary ammonium group of acetylcholine for binding to nicotinic receptors. NMBAs have two major side effects, acute hypersensitivity reactions and potentially life-threatening anaphylaxis (*3, 4*). Moreover, in the absence of appropriate monitoring that, despite international recommendations (*1, 2*), is not applied to more than 20% of the patients., residual neuromuscular blockade (rNMB), where NMBA remains present after the end of infusion, can lead to tracheal damage and infections (*5*).

rNMB can lead to postoperative pulmonary events, pharyngeal dysfunction, urgent tracheal reintubation, and prolonged stay in post-anesthesia care units and hospitals that lead to a high economic burden (*6*). The first option for pharmacological neuromuscular blockade reversal, neostigmine (Prostigmine; used for atracurium reversal), is restricted to situations where half of the spontaneous reversal is effective, making it inefficient for deep neuromuscular blockade (*7*). The second option is the synthetic γ-cyclodextrin sugammadex (Bridion) (*8*), which encapsulates the aminosteroid NMBAs rocuronium and vecuronium in vivo within minutes following injection, and is efficient at reversing deep neuromuscular blockade. Instant blockade reversal might also be necessary, as in difficult intubation scenarios, explaining that it has been considered economically advantageous to administer sugammadex despite a cost of $100-200 per patient, leading to a $400-3,000 economy per patient (*6*). Yet, multiple cases of anaphylaxis induced by sugammadex or by the sugammadex-rocuronium inclusion complex have been reported (*9-12*) leading to restrictions of its use in several countries (*11*). Rocuronium is the most used NMBA worldwide for full-stomach rapid sequence induction, and has become almost exclusive in countries like Japan, due to the existence of sugammadex for deep neuromuscular reversal (*13*).

The most dramatic adverse event following NMBA exposure is anaphylaxis, a severe allergic reaction that can lead to death, even after rapid recognition and correct management. In

some countries, half of perioperative anaphylaxis events are caused by NMBAs, with a global mortality rate of 4.1% (*14*). The current dogma proposes that IgE antibodies with reactivity towards NMBAs lead to mast cell and basophil activation in NMBA-allergic patients (*15*), and we reported earlier that, indeed, circulating anti-NMBA IgE concentrations, but also anti-NMBA IgG concentrations, correlate with the severity of anaphylaxis (*16*). In our view, two pathways are potentially involved in NMBA-induced anaphylaxis separately or concomitantly depending on the patient: the IgE pathway, leading to mast cell and basophil activation with histamine release as a major mediator, and the IgG pathway, leading to neutrophil and monocyte activation with platelet-activating factor (PAF) release as a major mediator (*15, 17*). Both histamine and PAF induce vasodilation, bronchoconstriction, cardiac and pulmonary failure, with probable cumulative or potentiating effects when both mediators are released (*18*). Routinely, only anti-NMBA IgEs are quantified in clinical practice, using a morphine group (termed Quaternary Ammonium Molecule; QAM) as a surrogate for NMBA in ImmunoCAP detection, as its molecular structure mimics ammonium groups present in some aminosteroid NMBAs (*19, 20*). The morphine ImmunoCAP demonstrates acceptable specificity and sensitivity for aminosteroids (e.g., rocuronium) and suxamethonium, but not for benzylisoquinolines (e.g., atracurium) (*21*).

The tertiary and quaternary substituted ammonium groups present in NMBAs have been proposed to be part of the epitope recognized by anti-NMBA antibodies in patients, as patient sera reacting with one or several NMBAs (*22*) cross-react with unrelated molecules possessing a quaternary ammonium (*23, 24*). Since anti-NMBA monoclonal antibodies (mAbs) have not been identified from patients or animals, molecular or structural evidence lacks to ascertain these hypotheses. Importantly, anaphylaxis occurs at the first exposure to aminosteroid NMBAs in half of the patients (*25*), excluding NMBA ammonium groups as primary sensitizing epitopes in the patient's history. NMBAs are small compounds (molecular weight ≈ 300-1,000 Da) with unknown properties in terms of immunogenicity; several families of compounds are however considered to sensitize towards NMBAs, including cosmetics, cleaning and bleaching products, as well as cough syrups containing morphine-based compounds (*22, 26*). Among the latter, studies proposed pholcodine, an opioid cough suppressant with two tertiary ammonium groups at physiological pH, to be a culprit molecule responsible for NMBA hypersensitivity (*27, 28*). Large variations in serum reactivity profile to NMBAs are found between individuals, from a single NMBA to NMBAs belonging to the same chemical family, and even to all NMBAs in 4% of the cases (*22*), suggesting

that B cell responses develop with one or multiple monospecificities each toward a particular compound, or that cross-reactive B cell responses develop and react towards different NMBAs.

To investigate the antibody specificity and affinity for NMBAs in patients who experienced NMBA-induced anaphylaxis, we analyzed single memory B cells with rocuronium reactivity. Memory B cell antibody repertoires were polyclonal with high V(D)J diversity, exclusive for rocuronium among NMBAs and anaphylactogenic when expressed as human IgE in vitro and in vivo in mice. Because patient-derived anti-rocuronium mAbs were of low-to-medium affinity and incapable to capture clinical doses of rocuronium in vivo, we generated high affinity rocuronium-specific mAbs from immunized mice, which could reverse rocuronium-induced neuromuscular blockade in nonhuman primates with similar kinetics as sugammadex. When co-crystallized, these latter mAbs captured rocuronium in a hydrophobic cleft in which the quaternary ammonium group is completely buried and involved in the binding. High affinity anti-NMBA mAbs thus represent a potential therapeutic avenue for the reversal of neuromuscular blockade.

RESULTS

Rocuronium-specific memory B cells were isolated from patients with NMBA allergy

Patients with presumed anaphylaxis to NMBAs during general anesthesia were included in two clinical studies (France, registered under NCT05420935, and Belgium) to obtain large volumes of blood for peripheral blood mononuclear cell (PBMC) isolation. Among these, three patients experienced fast occurring symptoms (< 5 min) of anaphylaxis and were admitted to the intensive care unit (ICU) afterwards (Table 1). Patient #1 developed a mild Ring & Messmer grade 2 anaphylaxis to atracurium in 2012 and was sampled for PBMCs in 2014 and 2023. Patient #2 and Patient #3 developed a severe grade 3 and 4 anaphylaxis, respectively, to rocuronium (Fig. 1A) in 2020, and were sampled a few weeks later. QAM IgE ImmunoCAP assays were positive only for Patient #2, although Patient #1 and Patient #3 had been previously exposed to NMBAs (Table 1). The anti-rocuronium IgE ImmunoCAP was positive only for Patient #3 (Fig. 1B). Skin prick tests and basophil activation tests with rocuronium were negative for Patient #1 but positive for Patients #2 and #3 (Table 1). Anti-rocuronium IgG concentrations were, however, elevated compared to controls in all three patients, and in both serum samples of Patient #1 at 9 years difference (Patient #1_2014 and Patient #1_2023) using enzyme-linked immunosorbent assay (ELISA; Fig. 1C), LuLISA and ImmunoCAP (fig. S1). We have previously reported that both IgE and IgG pathways exist with potentially additive or synergistic effects in human NMBA-induced anaphylaxis, and that Patient #1 had elevated serum anti-rocuronium IgG concentrations even while presenting with a grade 2 atracurium-induced anaphylaxis (*16*). In agreement with these findings, Patient #3 that developed a grade 4 anaphylaxis upon rocuronium infusion presents with elevated concentrations of both anti-rocuronium IgE and IgG (Fig.1B and C).

IgE memory B cells remain elusive and their existence is still disputed (*29*), as their survival may be extremely limited (*30-33*). As it has been proposed that IgE plasmablasts (and plasma cells) are continuously derived from IgG memory B cells (*34*), we decided to explore the IgG memory B cell compartment as a surrogate for the IgE B cell compartment with the goal of defining the rocuronium-specific antibody repertoire in these patients. We single-sorted $CD27^+$ memory B cells from frozen PBMCs from these three patients based on expression of memory B cell markers (IgD^- $CD19^+$ $CD27^+$). We further used fluorescently-labeled monomeric human serum albumin-rocuronium conjugate (HSA-roc) to label B cell receptors (BCRs) with affinity for

rocuronium. We also excluded cells expressing markers of other immune cells ($CD3^-$, $CD14^-$, $CD35^-$) and B cells with affinity for HSA alone (Fig.1D). The percentage of HSA-roc^+ HSA^- among $CD27^+$ IgD^- memory B cells varied between patients with a mean of 4.6% (range from 2.75 to 6.5%) for both sorts of Patient #1_2014, 1% for Patient #1_2023, 2% for Patient #2 and 3.6% for Patient #3 (fig. S2A and B). The percentage of $CD27^+$ cells among antigen-specific $CD3^-$ $CD14^-$ $CD19^+$ $CD38^-$ IgD^- cells varied from 58 to 89% (fig. S2C).

Characteristics of anti-rocuronium memory B cell repertoires from patients with NMBA allergy

In order to test the specificity towards rocuronium of the antibodies corresponding to the BCRs expressed by these memory B cells before V(D)J sequencing of their heavy chain variable region (V_H) and light chain variable region (V_L), we cultured these single cells in an in vitro culture assay allowing their differentiation in antibody-secreting cells (*35, 36*). After 25 days of culture, supernatants with detectable amounts of IgG were further tested for rocuronium specificity by ELISA using HSA-rocuronium as an antigen in the absence or presence of free rocuronium (competitive inhibition ELISA). We obtained 57 supernatants with rocuronium specificity from the $CD27^+$ memory B cell cultures of Patient #1_2014, 128 for Patient #1_2023, 45 for Patient #2 and 23 for Patient #3 (table S1). These represented only a minor fraction of the monoclonal cultures, from 1.3% to 16.7%, indicating poor selectivity of the allophycocyanin (APC)-labeled HSA-roc to label antigen-specific BCRs for B cell sorting. This selectivity did not increase with sorts using antigen labeled with two different fluorophores (HSA-rocuronium-APC versus HSA-rocuronium-AlexaFluor488), or when selecting $CD45RB^+$ memory B cells (*37*) instead of $CD27^+$ memory B cells (fig. S3). As expected from serum reactivity to rocuronium in humans (*16*), rocuronium-binding $CD27^+$ memory B cells and $CD45RB^+$ memory B cells could also be identified and sorted from PBMCs of a healthy donor, but with lower numbers of strong rocuronium binders among the monoclonal cultures from these sorted PBMCs compared with monoclonal cultures from PBMCs sorted from Patient #1_2023 (fig. S4).

RNA of the 240 monoclonal cell cultures (data file S1) was extracted to perform V(D)J sequencing of their V_H-V_L domains. Using the repertoire-profiler bioinformatic pipeline (*38*), we established the anti-rocuronium antibody repertoire profile of the three patients. We obtained a total of 211 V_H and 191 V_L sequences (Fig. 1E) with an average of approximately 14 nucleotide

mutations in the V_H and approximately 7 in the V_L compared to germline for Patient #1 and Patient #2 (fig. S5). The V_H and V_L sequences of Patient #3 were less mutated with a majority of non- or poorly-mutated sequences.

Analyses of V-J gene usage identified highly diverse and polyclonal repertoires, both within and between patients, for both the V_H and V_L sequences. Indeed, the proportion of B cells with V_H sequences coded by identical V-J genes was lower than 11% for all patients. The V_L sequences were similarly diverse, with identical V-J genes lower than 9% except for Patient #3 for whom 23% of the sequences (five out of 22) were coded by KV3-20*01_J1*01 (Fig. 1E). The alignment of the 211 V_H amino acid sequences revealed 22 groups of at least three members with identical V-J genes but dissimilarities in their sequences and complementarity determining regions (CDRs; fig. S6A). Because of this high diversity, attempts to identify clonal groups inside a patient defined by at least 3 distinct complementary determining region 3 (CDR3) of identical length and identical V-J gene usage failed (fig. S6B). We found, however, two to four identical V_H sequences in seven instances in Patient #1_2023, once in Patient #2 and once in Patient #3 (Table 2). As we obtained PBMC samples 9 years apart from Patient #1, we compared their antibody repertoires over time in the absence of any exposure to NMBAs between the samplings. The repertoires of Patient #1_2014 and Patient #1_2023 were distinct, with only rare similarities of V-J gene usage. V4−39*01_J4*02 was the most predominant for the V_H representing 4 out of 49 (approximately 10%) and 8 out of 98 (approximately 8%) of the rearrangements, respectively (Fig. 1E). Six clonal groups for the V_L were identified with sequences present in samples from both 2014 and 2023 (KL2-11_KJ1, KV3-20_KJ2, KV1-39_KJ4 and KV2-28_KJ4); however, the amino acid sequence alignment of the corresponding 39 V_H sequences represented in 9 different V(D)J recombinations revealed dissimilarities in their sequences and CDRs, with no V_H clonal groups identified (fig. S7A).

Among the 211 V_H and 191 V_L sequences identified (Fig. 1E), 152 were paired V_H-V_L sequences, including 25 V_H-V_L pairs from Patient #1_2014, 76 from Patient #1_2023, 32 from Patient #2 and 19 from Patient #3 (tables S1 and 2). Amino acid alignments led to the identification of five B cells clones identified at least twice with identical V_H-V_L amino acid sequences. The sequences of the shared mAbs had a large diversity in mutation load compared with the germline sequence (up to 41 amino acid mutations in the V_H and 20 in the V_L) and some possessed long CDR3 motifs (Table 2). Only one paired V_H-V_L with identical V-J usage (V3-7*01-J4*02 and

KV4-1*01_KJ1*01) was identified from the two repertoires of Patient #1 (2014 and 2023). The amino acid alignment of those two mAbs revealed greater than 80% homology in the V_H and in the V_L with mutations in the frameworks and CDRs (fig. S7B). Altogether, these data show that the four anti-rocuronium repertoires we characterized are diverse, with neither predominant gene usage nor evidence of clonal groups.

Anti-rocuronium antibodies from patients are specific, of low affinity, and anaphylactogenic

To further characterize the V_H-V_L pairs identified from single-cell sorting of rocuronium-binding memory B cells, we recombinantly expressed those corresponding to monoclonal cell cultures with the highest anti-rocuronium signal as aglycosylated effectorless (Fc engineered heavy chain mutation $N_{297}A$) human IgG1 mAbs. Anti-rocuronium ELISA using HSA-rocuronium as an antigen enabled a first ranking of the antibodies with mostly poor binding, except mAb h1F10 (Fig. 2A, fig. S8A, and Table 3). Competitive inhibition ELISA demonstrated their specificity for rocuronium as only free rocuronium, but not free molecules with the same aminosteroid scaffold, such as the closely related homologue vecuronium, the 5α-dihydrotestosterone (5α-DHT) that lacks quaternary ammonium groups, or pholcodine (Fig. 2B and fig. S8B). The mAbs were also not reactive towards irrelevant antigens such as ovalbumin, amoxicillin, and peanut extract (fig. S8C). From the memory B cells sorted initially based on their binding to HSA-rocuronium-APC, only 1.3 to 16% expressed antibodies that bound free rocuronium, suggesting a frequency of antigen-specific B cells ranging from 0.04 to 0.2% in PBMC samples from the three patients (tables S1 and 2). The avidity of the mAbs towards HSA-rocuronium (molar ratio rocuronium:HSA of 15:1) was measured using Bio-layer interferometry (BLI) with the conjugate covalently bound to the sensors. All antibodies had similar profiles with a fast association and a biphasic dissociation. The dissociation constants (K_D) of these mAbs ranged from 21 to 922 nM, with half the antibodies in the 21 to 50 nM range (Table 3 and fig. S9A), and mAb h1F10 displaying the best avidity (Fig. 2C). The very small size of rocuronium (530 Da) is incompatible with the relatively poor sensitivity of BLI, but at the lower limit of detection for Surface Plasmon Resonance (SPR). Using SPR with the mAbs captured onto the chip, we confirmed that among the mAbs with the highest avidity for HSA-rocuronium, five mAbs bound free rocuronium in solution, in a transitory mode with a very fast association and dissociation (Table 3 and fig. S9B), with mAb 1F10 displaying the best affinity for rocuronium with a K_D of 140 μM (Fig. 2D).

Next, we produced h1F10 as a human IgE to investigate if this V_H-V_L rearrangement represents an allergy-related B cell clone in Patient #1_2014 by promoting human mast cell activation or inducing anaphylaxis in mice in the presence of rocuronium. Human mast cells and basophils express the high-affinity IgE receptor (FcεRI) that allows them to be sensitized (pre-armed) with IgE in vivo for immediate cell activation following IgE engagement with allergens, leading to rapid anaphylactogenic mediator release. Human mast cells derived from PBMCs of healthy donors sensitized with h1F10 IgE dose-dependently degranulated in the presence of HSA-rocuronium but, as expected (*39*), unsensitized mast cells did not (Fig. 2E). To test the anaphylactogenic potential of IgE h1F10, we used mice expressing human FcεRI, sensitized them with h1F10 and challenged them with HSA-rocuronium in a classical model of passive systemic anaphylaxis. IgE h1F10-senstized mice, but not unsensitized mice, displayed a pronounced drop in central body temperature (Fig. 2F), a hallmark of anaphylaxis in mice (*40*). Thus, although identified from an IgG-expressing memory B cell, the h1F10 V_H-V_L rearrangement generates a rocuronium-specific antibody of medium-low affinity that, when produced as an IgE, demonstrates potential for human mast cell activation and induction of anaphylaxis in mice humanized for FcεRI.

As h1F10 was of sufficient affinity to measure its interaction with free rocuronium by SPR, and capable of inducing mast cell activation and passive systemic anaphylaxis when expressed as an IgE, we wondered if it could also capture circulating rocuronium and promote reversal of neuromuscular blockade. This possibility would represent an alternative to sugammadex for cases of sugammadex- or sugammadex-rocuronium hypersensitivity (*9-12*). We first defined the lethal dose of rocuronium in wild-type C57BL/6 mice at 160 μg/kg (Fig. 2G). We then established a prophylactic model to prevent neuromuscular blockade in mice, which consisted of pretreatment with a rocuronium capture molecule, followed by intravenous injection of a lethal dose of rocuronium and vitality assessment. In this model, only sugammadex protected mice from rocuronium-induced neuromuscular blockade. h1F10 and the other sixteen anti-rocuronium mAbs (Table 3) that we produced as fully human IgG1 ($N_{297}A$) antibodies were unable to confer protection (Fig. 2G). We hypothesized that the affinity of these antibodies was too weak to exert capture functions in vivo that would be necessary to cause reversal of neuromuscular blockade.

Generation of high-affinity anti-rocuronium mAbs

To investigate the potential use of mAbs as capture reagents for rocuronium, we decided to immunize mice against rocuronium and identify high-affinity mAbs. As we failed to induce anti-rocuronium antibody responses in mice using free rocuronium in adjuvant, we immunized mice with rocuronium coupled to keyhole limpet hemocyanin (KLH), as a large size carrier protein that favors bystander activation. Hybridomas were generated from the mice displaying the highest anti-rocuronium titers (Fig. 3A), and their variable domains were sequenced, leading to the identification of only two different V_H-V_L pairs. Both used KV2-112*KJ2 V_Ls, but different V_Hs (mAb m1B6, HV1-63*J4; mAb m2B1, HV1-81*J2). Using ELISA and competitive inhibition ELISA, we confirmed that mAb m1B6 (IgG1,κ) and mAb m2B1 (IgG1,κ) bound specifically rocuronium but not any other NMBA, including analogues vecuronium and pancuronium, suxamethonium, 5α-DHT, diisopentyl succinate, and pholcodine (Fig. 3B and C). Both mAbs had a very high avidity for HSA-rocuronium measured by BLI (fig. S10A), 800- and 57-times higher, respectively, than mAb 1F10. Whereas mAb m2B1 had only a 140-times better affinity for free rocuronium measured by SPR than mAb 1F10 (K_D=1 μM versus 140 μM), mAb m1B6 displayed a 25,000-times better affinity (K_D=5.5 nM versus 140 μM) (fig. S10B and Table 3).

To understand how anti-rocuronium mAbs m1B6 and m2B1 bind rocuronium, we produced monovalent formats of mAb m2B1 and m1B6 as Fab fragment and single-chain variable fragment (scFv), respectively, and generated their co-crystals with rocuronium. We solved the X-ray structures of Fab-m2B1 and scFV-m1B6 in complex with rocuronium at a 1.65 Å and 1.70 Å resolution, respectively, with electron density for rocuronium observed in the binding sites in the two solved structures (Fig. 4A, fig. S11, and table S2). Both antibodies make extensive hydrophobic interactions (van der Waals bonds) with rocuronium involving the V_H and V_L in each antibody. The Fab-m2B1-rocuronium contacts involved residues Glu50, Tyr52, Ser54, Tyr56, Gly96, Val97, Ans98, and His100 of the antibody heavy chain and Tyr27, Tyr32, Leu91, Val92, Glu93, Tyr94, and Tyr96 of the light chain (Fig. 4B). The scFv-m1B6-rocuronium contacts involved residues Trp33, Try52, Ser54, Tyr56, Trp99, Ser100, Tyr100A and Tyr100B of the heavy chain and Tyr27, Tyr32, Leu91, Val92, Glu93, Tyr94, Tyr96 of the light chain (Fig. 4B). The ring A of rocuronium has been reported to exist in twist-boat and chair conformations (*41*). In the structure of the scFv-m1B6-rocuronium complex, rocuronium ring A adopts the chair conformation; however, in the Fab-m2B1-rocuronium complex, the rocuronium ring A was not sufficiently well-defined within the electron density maps to be determined. The rocuronium

hydroxyl group was fully exposed to solvent, in agreement with the use of this group as an attachment point to the rocuronium-carrier proteins used herein for immunization and screening, whereas the acetoxyl group was buried inside the binding pocket of both antibodies. Finally, both co-crystal structures revealed that the allylpyrrolidine substituent containing the quaternary ammonium is completely buried and makes numerous van der Waals contacts with the antibody light chain (Fig. 4), emphasizing the important role of this group in the rocuronium binding mode, in agreement with hypotheses extrapolated from serum cross-reactivity in patients (*22, 42*). The specificity for rocuronium and not vecuronium or pancuronium could be explained by the fact that no space remained in the hydrophobic pocket formed by the V_H and the V_L of either antibody to accommodate the methylpiperidine substituent of vecuronium and pancuronium, and by numerous hydrophobic contacts made by the allyl group of rocuronium.

High-affinity anti-rocuronium antibodies protect from and reverse neuromuscular blockade in mice and nonhuman primates

Rocuronium capture may serve two purposes: (i) rocuronium binding and sequestration to prevent interaction with IgE on mast cell and basophil to reduce or stop anaphylaxis, as suggested by some case reports (*43-45*), and (ii) reversion of neuromuscular blockade to shorten patient's recovery time and associated complications (*6*). To test the efficacy of the high affinity anti-rocuronium mAbs isolated from mice on rocuronium capture, we first used the prophylactic model of rocuronium-induced neuromuscular blockade (Fig. 2G) with a fixed dose of rocuronium of 4 µg per mouse, inducing lethality in less than 2 min. Both mAb 1B6 and mAb 2B1 protected mice for neuromuscular blockade in a dose-dependent manner. mAb 1B6 was more efficient at lower antibody doses (Fig. 5A), as expected when considering the affinities of mAb 1B6 and mAb 2B1 for free rocuronium.

Neuromuscular blockade is monitored in anesthetized and intubated patients in clinical practice using the Train-Of-Four (TOF) method that compares the twitch response (T1, T2, T3, T4) to four consecutive electric impulses applied by a TOF apparatus on the ulnar nerve through electrodes. Deep neuromuscular blockade corresponds to the absence of response at any of the stimulus, and recovery from neuromuscular blockade to a TOF ratio (T4/T1) greater than 90%. Loss and recovery of spontaneous ventilation is also recorded to calculate the time to retrieve spontaneous ventilation. Because of the small size of mice, TOF devices were not adaptable even

using pediatric equipment, and we moved to cynomolgus macaques to evaluate the efficacy of mAb 1B6 to reverse deep neuromuscular blockade induced by rocuronium in a model that closely reflects the clinical setting. We first established the lowest dose of rocuronium to induce a profound myorelaxation (200 μg/kg) in macaques and the lowest sugammadex dose for fast recovery (<1 minute; 2 mg/kg) as a control. Animals were anesthetized, placed under mechanically assisted ventilation, and the myorelaxation status was assessed by TOF monitoring (measured using two TOF instruments, each connected to one upper-limb) and time to retrieval of spontaneous ventilation (Fig. 5B) (*46*). At 200 μg/kg rocuronium injected as a bolus, the spontaneous reversal of neuromuscular blockade happened at an average of 28.5 min when monitoring TOF ratio and spontaneous ventilation at 15.5 min (Fig. 5C to F). Injection of mAb 1B6 to macaques under deep neuromuscular blockade induced by rocuronium dose-dependently decreased the time to complete neuromuscular blockade reversal. 2.5 mg/kg of mAb 1B6 were sufficient to reduce from 28.5 min to 16 min the recovery of TOF ratio>90% and to reduce from 15.5 min to 5 min recovery of spontaneous ventilation (Fig. 5D). To obtain the same speed of TOF ratio and spontaneous ventilation recovery than obtained with 1 mg/kg sugammadex, a minimum of 10 mg/kg of mAb 1B6 were required (Fig. 5E and fig. S12). Physiological parameters and blood counts remained unaltered during the experiments (fig. S13), indicating that mAb 1B6 does not induce obvious adverse events, even at high doses. These results validate the therapeutic effect of rocuronium-specific mAb 1B6 on rocuronium-induced neuromuscular blockade. They serve as a proof of concept that antibodies may be potential drugs for the reversal of neuromuscular blockade of NMBAs, and, as it has been suggested for sugammadex (*43-45*), may be able to mitigate or even reverse anaphylaxis.

DISCUSSION

This study reports anti-NMBA antibody repertoires from NMBA-allergic patients. Memory B cell repertoires of patients with suspected hypersensitivity to NMBA and evidence of anti-rocuronium antibodies in their serum demonstrated high polyclonality, with no evidence of clonal groups, suggestive of diverse sources of immunization against compounds chemically or structurally related to rocuronium. However, no crossreactivity for other NMBAs or structurally-related molecules could be detected, and the affinities for rocuronium were rather poor, with K_D around hundred micromolar for free rocuronium. These affinities were sufficient to trigger in vitro mast cell activation and in vivo anaphylaxis in mice, indicating that some of these antibodies may have contributed to rocuronium-induced anaphylaxis in patients. Two high-affinity anti-rocuronium mAbs generated from rocuronium-immunized mice also demonstrated selectivity for rocuronium, explained by the structure of their paratope, and demonstrated the ability to capture rocuronium in vivo. The highest affinity mAb provided a proof of concept for antibodies as reversal agents for rocuronium-induced deep neuromuscular blockade that may provide an option for patients with allergy to sugammadex.

Rocuronium represents an advantageous model of NMBA, as it is widely used for standard endotracheal intubation and for rapid sequence induction, although it has one of the longest residual neuromuscular blockade durations and has among the highest anaphylaxis incidences (*4, 47-49*). This aminosteroid non-depolarizing NMBA was designed as a mono-quaternary ammonium compound (allylated pyrrolidinium group attached to the D ring), unlike its bis-quaternary closely related analog pancuronium (*50*). It is therefore a weaker antagonist at the neuromuscular junction than pancuronium, making rocuronium easier to outcompete for reversal of neuromuscular blockade. With vecuronium, rocuronium is the only NMBA on the market possessing a reversal reagent for deep neuromuscular blockade (*8*), and has been adopted as sole NMBA in countries like Japan due to this drug-antidote pair, despite the cost of the antidote. How rocuronium induces anaphylaxis remains unclear, as IgE receptors on mast cells and basophils require aggregation to enable cell activation and degranulation; the most probable hypothesis proposes that rocuronium haptenizes onto a large molecule upon infusion (*51*). A previous study using IgE-stripped human basophils sensitized with patient serum containing anti-rocuronium IgE indeed reported that only haptenized rocuronium, but not free rocuronium, induced basophil

activation in vitro (*52*). To evaluate IgE-mediated anaphylaxis, allergy work-up mostly includes degranulated biomarkers from mast cells and basophils, specific IgE measurements (during the anaphylaxis and later work-up), and skin tests and basophil activation tests (BAT) to all molecules suspected as the culprit agent (six to eight weeks after the anaphylaxis) (*53*). Rocuronium-specific IgEs are still quantified with the morphine antigen surrogate in clinical practice (QAM ImmunoCAP). An anti-rocuronium IgE ImmunoCAP is commercially available, but is not yet validated for clinical practice. Exploration of anti-rocuronium IgE antibodies in patients' sera relies on the hypothesis that its quaternary ammonium is part of the epitope bound by anti-QAM antibodies with, however, poor structural and chemical resemblance between rocuronium and the morphine antigen. Anti-QAM ImmunoCAP are also used for screening for hypersensitivity against widely different chemical structures as suxamethonium and atracurium, although with poor sensitivity and specificity (*21, 24, 54-58*). To avoid this caveat in our study, we used rocuronium derivatives by extending the OH group with a functionalized linker for grafting on carrier proteins such as KLH or HSA, which were used for memory B cell sorting, ELISA, avidity measurements, vaccination, and functional assays. This strategy allowed for identification of anti-rocuronium antibodies with no crossreactivity for other NMBAs. Validated by other groups, some of these rocuronium-based assays could become diagnostic tools in NMBA-suspected allergies.

B cells with rocuronium reactivity were sorted from two patients with a history of rocuronium-induced anaphylaxis and from one with atracurium-induced anaphylaxis. For several reasons, we chose to sort IgG-expressing memory B cells and not IgE-expressing B cells to identify anti-rocuronium antibody repertoires. First, all three patients had evidence of anti-rocuronium IgG in their sera but only one had anti-rocuronium IgE; second, IgE-expressing memory B cells elude identification in blood samples (*30, 32*); and third, IgE antibody-expressing cells have been reported to result from an intermediary switch to IgG rather than directly from IgM-expressing B cells (*59*). Very recently, type 2–polarized memory B cells defined either as $CD23^{+}$ $IgG1^{+}$ (*60*) or as IgG1 or IgG4-expressing $CD23^{hi}$, interleukin (IL)-$4R\alpha^{hi}$, and $CD32^{low}$ (*61*) have been identified from allergic patients to hold the allergen-specific IgE memory. Rocuronium haptenized on HSA allowed for the sorting and culture of single memory B cells from all three patients into IgG-secreting cells coupled to screening for both rocuronium reactivity and specificity by competitive ELISA in their culture supernatant. The latter consideration is fundamental, as greater than 80% of the cultures were excluded because of low reactivity and specificity; this curated the repertoire

data by eliminating false positives. The false positive fraction was similar when sorting CD45RB$^+$ memory B cells (*37*), and when sorting memory B cells binding HSA-rocuronium labeled with two different fluorochromes. Thus, the highly polyclonal anti-rocuronium antibody repertoires we describe herein, with a high diversity among V(D)J gene usage, corresponds only to bona fide anti-rocuronium antibodies. It remains unclear however if the memory B cell sorting method, using monomeric carrier proteins coupled to approximately 15 rocuronium molecules each, might have biased B cell selection towards higher avidity B cell clones.

No evidence of common gene usage, nor of clonal groups, could be found within and between these patients, even between the repertoires of the same patient sampled 9 years apart with no exposure to any NMBA during this period. The underlying reason for the high polyclonality of anti-rocuronium antibody repertoires might be the absence of exposure to rocuronium before the initial anaphylactic episode in the perioperative setting in all these patients, with exposure to other compounds present in cough syrup, cosmetics, hair dyes, household cleaning products or drugs at the probable initiation of the immune reaction towards rocuronium (*12*). One of the most incriminated culprits is pholcodine, an opioid cough suppressant containing two tertiary ammonium groups, which is now considered a risk factor for anaphylaxis to NMBA (*28*) and was withdrawn from the European market in December 2022. These difficult to quantify exposures may have led to a diverse repertoire of memory B cells with cross-reactivity to rocuronium; if Patient #1, who demonstrated different V(D)J recombination 9 years apart, is representative of rocuronium-allergic individuals, one could hypothesize that their repertoires would not to be stable over time. However, none of the mAbs corresponding to these V(D)J rearrangements demonstrated cross-reactivity for any other NMBA, including vecuronium and pancuronium, which differ only slightly from rocuronium. This result agrees with our previous data showing that polyclonal IgG from Patient #1 purified on a rocuronium-bound column showed exquisite specificity for rocuronium, with no binding to atracurium, pancuronium or vecuronium, although partial cross-reactivity with suxamethonium was detected (*16*). This preference may be the result of (i) a particular exposure of these patients to rocuronium-resembling molecules, (ii) the stringency of the cell sort using rocuronium-haptenized HSA, or (iii) the modification (functionalized linker) made to rocuronium to allow protein engraftment. As a comparison in the rocuronium-immunized mouse, from all hybridomas analyzed, only two different V_H-V_L combinations could be identified (mAb m1B6, IGVH1-63*J4 x KV2-112*KJ2; mAb m2B1,

IGVH1-81*J2 x KV2-112*KJ2), suggestive of a very restricted oligoclonal repertoire. These results agree with the affinity for rocuronium determined for these human or mouse antibodies: poor affinity when antibodies were isolated from polyclonal repertoires of cross-reactive BCRs to rocuronium (as none of the patients had been pre-exposed to rocuronium) and high affinity from oligoclonal repertoires of "antigen-trained" B cells.

The mAb 1F10 isolated from Patient #1_2014 showed the best affinity towards rocuronium from all the antibodies identified from humans we studied herein, although this patient had been included after presenting with a grade 2 hypersensitivity reaction to atracurium (*16*), with no previous exposure to rocuronium. This mAb expressed as a human IgE gave positive results in a mast cell activation test, which has recently been proposed as an alternative for basophil activation tests (*62*), and was able to induce severe hypothermia in a mouse model of rocuronium-induced anaphylaxis. Even though this mAb was isolated from an IgG-expressing B cell, it may represent an IgE that is expressed and secreted by a class-switched activated B cell, as recently reported (*60, 61*), or expressed by a plasmablast or plasma cell involved in hypersensitivity to rocuronium. Allergy-related IgE plasma cells have indeed recently been identified in the bone marrow of chronically exposed mice and allergic individuals (*63, 64*). From our study, it remains unclear, however, if such IgE plasma cells exist in patients exposed to a variety of compounds and not chronically to a given antigen, and will merit further investigation if bone marrow samples from NMBA-allergic individuals become available.

The specificity for rocuronium of all the above-mentioned antibodies, with no crossreactivity for other NMBAs, can be explained for the antibodies raised from immunized mice by their co-crystal structures with rocuronium. These indicated a similar binding between the two pairs of V_H-V_L corresponding to mAbs 1B6 and 2B1, which possess different V-J rearrangements of the heavy chain but an identical V-J rearrangement of the light chain with only two amino acid differences. Both antibodies bound rocuronium through a hydrophobic pocket formed by residues from the V_H and V_L chains, that do directly interact with the ammonium group that had been hypothesized to be the main epitope involved in NMBA hypersensitivity (*22*). The quaternary ammonium group and the uncharged 5α-dihydrotestosterone counterpart were required for binding. The closely related NMBAs vecuronium and pancuronium were also unable to bind, as their side chains differ and cannot fit into the tight hydrophobic binding cleft of these two antibodies. Indeed, the ring D substituent in vecuronium/pancuronium is a 6-atom piperidinium

cycle instead of a 5-atom pyrrolidinium cycle in rocuronium (resulting in a lack of space). In addition, the hydrogen bond between rocuronium and the serine residue at position 54 in the antibody heavy chain (at least in the chair conformation) cannot be established with vecuronium or with pancuronium, as the rocuronium morpholino heterocycle involved is replaced by a piperidin and piperidinium (devoid of an oxygen atom) in these compounds, respectively. One could speculate that these specificities are the result of high selective pressure in rocuronium-immunized mice and that these may not be present in antibodies generated in humans by exposure to various ammonium-containing compounds (*3*).

Ten years ago, almost 40% to 60% of patients in post anesthesia care suffered from residual neuromuscular blockade (*5, 30, 65-68*). The increased use of neuromuscular monitoring in some countries allowed for this incidence to drop drastically, for example to 3 to 5% in recent years in France and Portugal (*69, 70*). However, it remains an issue and even today it can have major adverse outcomes by prolonging postoperative recovery, affecting respiratory function, and causing muscle weakness with sometimes fatal outcomes (*5, 71*). Similarly to the rocuronium-reversal agent sugammadex, both anti-rocuronium mAbs identified from immunized mice with high-affinity for rocuronium demonstrated ability to capture rocuronium in vivo dose-dependently in a prophylactic model of rocuronium-induced paralysis in mice. This rodent model, however, does not recapitulate the state of deep neuromuscular blockade that is difficult to reverse in patients. Currently, only rocuronium- and vecuronium-induced deep neuromuscular blockade can be reversed almost immediately by sugammadex, with no solution available for deep blockade induced by atracurium, the most used NMBA worldwide, nor pancuronium or others. This possibility is of major importance for clinicians, especially for patients with unexpected impossible mechanical ventilation or tracheal intubation. Importantly, anti-rocuronium mAb m1B6 demonstrated efficiency at reversing deep neuromuscular blockade in cynomolgus macaques in this study, with similar kinetics at 5.3×10^{-8} M (10 mg/kg) as sugammadex at 4.5×10^{-7} M (1 mg/kg).

This study has limitations. We included only three patients in this proof-of-concept study, with heterologous phenotypes in terms of NMBA hypersensitivity as the main inclusion criteria was high serum concentrations of anti-rocuronium IgG. In addition, we established antibody repertoires from IgG^+ memory B cells as surrogates for IgE^+ memory B cells, which may not be representative of the IgE antibody repertoire. Further studies focusing on a larger cohort and on anti-NMBA IgE producing cells, in particular long-lived bone marrow IgE plasma cells (*63, 64*),

should shed light on this question. In addition, we used the MT4 antibody clone rather than the MEM55 antibody clone to stain CD45RB on memory B cells which may lead to identification of different subpopulations (*72*). Finally, the costs of production of sugammadex and a monoclonal antibody are incomparably in favor of sugammadex (*73*), but we believe this proof-of-concept study provides an alternative for reversal of deep neuromuscular blockade in patients with hypersensitivity to sugammadex (*12, 48*) or sugammadex-rocuronium inclusion complexes (*11*).

In conclusion, this work reports on the underlying causes of anaphylactic reactions to NMBAs. By characterizing the memory B cell anti-rocuronium antibody repertoires from three patients and producing high-affinity anti-rocuronium antibodies in mice, we have developed potential diagnostic tools for rocuronium hypersensitivity. Moreover, the murine and nonhuman primate studies provide proof-of-concept for antibodies as drugs for the reversal of neuromuscular blockade.

MATERIALS AND METHODS

Study Design

Three patients that suffered previously from anaphylactic reactions to NMBAs in the were selected based on the concentration of anti-rocuronium IgG in their serum. The design of the study and detailed clinical characteristics of Patient #1 have been described elsewhere (*16, 74*). The study "Anesthesia-associated allergy: from new pathogenic insights to reliable diagnoses" was approved by the Belgian ethical committee under #B300202042710 and is sponsored by the University of Antwerp, registered under #8300201316408 in Belgium, and enabled the collection of blood from Patient #2 and Patient #3.

BALB/c mice, C57BL/6J mice and Human FcεRI^{tg} mouse FcεRI$^{-/-}$ mice on the C57BL/6 background (*78*) aged 7-12 weeks were randomly assigned to the study for rocuronium immunizations, reversal agents experiments and anaphylaxis experiments, respectively. Sample sizes were determined to be appropriate for determining the effects of each procedure. No power calculation was performed. The experimenters were not blinded to the study.

Eighteen adult cynomolgus macaques (*Macaca fascicularis*), aged 4 to 7 years, were randomly assigned to each of the six groups in the study. Sample sizes were determined to be appropriate for determining rocuronium and reversal agents effects. No power calculation was performed. The experimenters were not blinded to the study.

Clinical study

Three clinical studies were approved for the recruitment of NMBA-allergic patients. The French multicentric NASA ("Neutrophil Activation in Systemic Anaphylaxis") study involved 11 Anesthesia and Intensive Care departments in the Ile-de-France region in France. The study was approved for all centers by an Institutional Review Board (ethical committee "*Comité de Protection des Personnes Ile-de-France 1*", reference 2012-avril-12880), and registered before the first inclusion at ClinicalTrials.gov (Identifier: NCT0163722). The design of the study and detailed clinical characteristics of the patients have been described elsewhere (*16, 74*), and its ancillary study NASAmAbs enabled the collection of 190 mL of blood from Patient #1_2014. The second French multicentric study was MEDIREP ("Repertoire and Properties of Anti-drug Antibodies

Involved in Immediate Hypersensitivity in the Operating Room") was approved by an Institutional Review Board (ethical committee "*Comité de Protection des Personnes Ile-de-France IV*", reference 2022-A00709-34) on May 2022 and registered before the first inclusion at ClinicalTrials.gov (Identifier: NCT05420935), allowing for the inclusion of Patient #1_2023. The study "Anesthesia-associated allergy: from new pathogenic insights to reliable diagnoses" was approved by the Belgian ethical committee under #B300202042710 and is sponsored by the University of Antwerp, registered under #8300201316408 in Belgium, and enabled the collection of blood from Patient #2 and Patient #3. Written informed consent was obtained from the patients or their legal representative before study inclusion. Patient characteristics are described in Table 1.

Classical anaphylaxis parameters

As part of standard care procedures, the following circulating parameters were assessed as previously described (*55*): histamine (EIA, Immunotech, Beckman Coulter) and tryptase (FEIA, ImmunoCAP 250 Phadia, Thermo Fisher) in plasma and anti-quaternary ammonium-specific IgE (FEIA, ImmunoCAP 250 Phadia, Thermo Fisher) in serum. A value less than 0.35 kU/L of specific IgE was considered negative, as recommended (*55*). Tryptase concentrations two hours following acute hypersensitivity reaction (AHR) were considered elevated when greater than (1.2 x [baseline tryptase] + 2 µg/L) as recommended (*75*). A histamine concentration above 20 nmol/L 30 minutes following AHR was considered elevated. Data are summarized in Table 1. In addition, specific IgE concentrations for rocuronium were assessed using the non-clinically-validated rocuronium ImmunoCAP (Phadia AB; ImmunCAP#c202) (*76*), obtained as experimental prototypes made for research use, and with the LuLISA technique using an anti-IgE nanobody-luciferase tandem (1:50) as previously described (*77*).

Mice

C57BL/6J mice (JAX #000664) were purchased from Charles River, and used for experiments after maintaining the mice for at least one week in SPF conditions after arrival in Institut Pasteur's animal facility. Human FcεRI^{tg} mouse FcεRI$^{-/-}$ mice on the C57BL/6 background were described previously (*78*). Mice were bred at Institut Pasteur and used for experiments at 7-12 weeks of age.

All animal care and experimentation were conducted in compliance with the guidelines and specific approval of the Animal Ethics committee CETEA number 89 (Institut Pasteur) registered under #170043, #2013-0103 and #27465 and by the French Ministry of Research under agreement #00513.02.

Production and characterization of rocuronium bioconjugates

Hapten-protein couplings were performed using active ester derivatives of rocuronium and KLH or monomeric HSA as the carrier protein. A carboxylate function was first introduced by adding succinic anhydride to rocuronium bromide in the presence of 4-(dimethylamino)-pyridine in pyridine. After stirring overnight at room temperature under argon, the solvent was removed under vacuum. The crude compound was purified by reverse-phase flash chromatography, resulting in a rocuronium derivative with a carboxylic acid (Roc-COOH) at the 3-position of the steroid scaffold. The compound was characterized by mass spectrometry and by nuclear magnetic resonance analysis. All quantities of products were calculated relative to the carrier protein. The functionalized rocuronium (200 equivalent) was dissolved in 0.05 M MES + 0.5 M NaCl buffer (pH 5.6) and combined with 1-ethyl-3-(3-dimethylaminopropyl) carbodiimide (400 equivalent) in the presence of N-hydroxysulfosuccinimide (200 equivalent). After stirring at room temperature for 5 min, the pH was adjusted to 7.2 with 2 M NaOH. This solution was progressively added to the carrier protein dissolved in 100mM phosphate-buffered saline (PBS) at pH 7.2. After 3 hours of gentle agitation at room temperature, samples were buffer exchanged into 20mM HEPES and 300mM NaCl with minitrap desalting columns. The exact measurement of the concentration of the bioconjugates was achieved by quantitative amino acid analysis. The average density of conjugated rocuronium derivatives was evaluated by matrix-assisted laser desorption/ionization time-of-flight mass spectrometry. The HSA-rocuronium conjugates used for all experiments were monomeric with an average engraftment of 15 rocuronium molecules per HSA molecule, determined with the mean of the gaussian distribution of the m/z (mass-to-charge ratio) as previously described by matrix-assisted laser desorption/ionization time-of-flight mass spectrometry (*16*).

Human B cell single cell culture

Culture supernatants from single cell cultured memory B cells were generated according to the protocol previously described by Sokal *et al.* (*36*). After thawing, PBMCs were counted and stained with antibodies directed against surface markers: CD27-brilliant violet (BV) 421^+ (Clone M-T2711, BD Biosciences) or CD45RB-$BV421^+$ (Clone MT4 BD Biosciences), CD3/CD14-allophycocyanin (APC)-cyanine (Cy)-7^- CD19-phycoerythrin (PE)-Texas Red^+ (anti-CD3, Clone SK7, Fischer Scientific; anti-CD14, Clone MφP9 BD Biosciences; anti-CD19, clone HIB19 BD Biosciences), CD38-Peridinin-chlorophyll-protein (PerCP)-$Cy5.5^+$ (Clone HIT2 BD Biosciences), IgD-PE^- (Clone W18340F BioLegend), HSA-AlexaFluor488^- or HSA-Roc-AlexaFluor488^+, HSA-Roc-APC^+). HSA and HSA-rocuronium were conjugated to fluorescent probes using Alexa Fluor 488 and 647 microscale labeling kits (Invitrogen) following manufacturer's instructions. Conjugates with a mean of 15 rocuronium molecules grafted on a HSA carrier were used for the sort. Cells were then sorted using the ultra-purity mode (single cell) on Aria III in 96-well plates containing MS40Lo cells expressing CD40L (a kind gift from Garnett Kelsoe) (*79*). Cells were cultured for 25 days at 37°C with 5% CO2 in RPMI-1640 (Invitrogen) supplemented with 10% HyClone fetal bovine serum (FBS, Thermo Scientific), 10 mM HEPES, 1 mM sodium pyruvate, 100 units/mL penicillin, 100 mg/mL streptomycin, and MEM non-essential amino acids (all Invitrogen) with the addition of recombinant human B-cell activating factor (BAFF, 10 ng/ml), IL-2 (50 ng/ml), IL-4 (10 ng/ml), and IL-21 (10 ng/ml; all Peprotech). The supernatant was removed and replaced every 3 to 4 days of the culture and harvested on day 18, 21 and 25 of cell culture. Clones corresponding to supernatants with the highest ratio of optical density (OD) values from anti-rocuronium ELISA divided by OD value of the anti-IgG ELISA were considered to possess reactivity towards rocuronium (at least to HSA-rocuronium) and were selected to be recombinantly expressed as mAbs.

V_H-V_L sequencing from monoclonal cell cultures

Clones of interest were sequenced first by RNA extraction using NucleoSpin96 RNA extraction kit (Macherey-Nagel) according to the manufacturer's instruction. A reverse transcription step was then performed using the SuperScript IV enzyme (Thermo Fisher) in a 14 ml final volume (42°C 10 min, 25°C 10 min, 50°C 60 min, 94°C 5 min) with 4 ml of RNA and random hexamers (Thermo Fisher scientific). A polymerase chain reaction (PCR) was further performed based on the protocol established by Tiller *et al.* (*80*). Briefly, 3.5 ml of cDNA was used as template and amplified in a

total volume of 40 ml with a mix of primers and using the HotStar_Taq DNA polymerase (Qiagen) and 50 cycles of PCR (94°C 30 s, 58°C for V_H and kappa/60°C for lambda 30 s, 72°C 60 s). Sanger sequencing was performed by Eurofins.

Gene synthesis, cloning, and mAb production

V_H and V_L synthesis in pUC19-Igγ1.N297A or pUC-kappachain/pUC-lambdachain-expressing vectors were performed by Synbio Technologies. Antibodies were produced by transient co-transfection of V_H-C_H and V_L-C_L expression plasmids into exponentially growing Freestyle HEK 293-F that were cultured in serum-free Freestyle 293 Expression Medium (Life Technologies) in suspension at 37°C in a humidified 8% CO_2 incubator on a shaker platform rotating at 110 rpm. Twenty-four hours before transfection, cells were harvested by centrifugation at 300 x g for 5 min and resuspended in expression medium at a density of 1 x 10^6 cells/ml, and cultured overnight in the same conditions as mentioned above. To produce mAbs, 40 µg of each V_H and V_L expressing plasmids were diluted in 80 µl of FectoPRO reagent (Polyplus) at a final DNA concentration of 0.8 µg/ml, incubated for 10 minutes at room temperature before addition to the cells. Twenty-four hours post-transfection, cells were diluted 1:1 with expression medium. Cells were cultured for 6 days after transfection, and then supernatants were harvested, centrifuged at 1800 g for 40 min, and filtered (0.2 µm). Antibodies were purified by affinity chromatography using an AKTA pure FPLC instrument (GE Healthcare) on a HiTrap Protein A Column (GE Healthcare) and desalted on a HiTrap Desalting Column (GE Healthcare).

Production of mouse anti-rocuronium hybridomas

Female C57Bl/6J were immunized subcutaneously with 10 µg KLH-Rocuronium combined with adjuvant alum 1:1 (v:v) and 20 ng pertussis toxin in physiological saline 0.9% NaCl three times at 3-week intervals. Mice were boosted with 10 µg KLH-Rocuronium without adjuvant three weeks after the last immunization. Four days later the cervical lymph nodes were removed and fused with myeloma cells P3X63Ag8.653 for hybridoma generation using the ClonaCell-HY Hybridoma kit (StemCell Technologies). After screening, the positive clones were expanded in T250cm^2 flasks, cells were introduced in 2L rollers and incubated in rotating rollers at 37°C for 10 days. The supernatant was filtered and purified with Protein A-affinity chromatography columns.

Anti-rocuronium ELISA

96-well plates (Costar) were coated with HSA-rocuronium (mean of 15 rocuronium molecules grafted on a HSA carrier molecule) or HSA at 1 µg/mL in PBS 1X (Gibco) overnight at 4°C overnight, washed 3 times with PBS Tween 20 0.5% (PBST), blocked with PBS-3% bovine serum albumin (BSA) for mAb detection or PBS + FBS low IgG to screen human serum, and washed three times with PBST. Murine sera (diluted 1:250,000-1:5,000-1:100) or pure cell culture supernatant or monoclonal antibodies were incubated for 2 hours at room temperature and bound antibodies were detected with horseradish peroxidase (HRP)-conjugated goat anti mouse or human IgG (Bethyl Laboratories) at 1:10,000. The secondary was revealed using OPD substrate (Sigma-Aldrich) and the reaction stopped with 2M H_2SO_4 and absorbance was subsequently recorded at 490 nm and corrected at 620 nm using a spectrophotometer (Biophotometer, Eppendorff). The final OD reported in all graphs and tables corresponds to the subtraction of the OD value of the HSA-rocuronium ELISA minus the OD value of the HSA ELISA. OD values were considered positive if they were at least three times higher than the OD value of the negative control.

Cross-reactivity with classical allergens (e.g., peanut extract, amoxicillin and ovalbumin) was assayed using 1 µg/mL of allergens for coating, using afterwards the same protocol as for the HSA-rocuronium ELISA.

Competition ELISA

To ascertain antibody reactivity to rocuronium, and not towards the linker employed to attach rocuronium to HSA, or a neo-epitope formed between rocuronium, the linker and HSA, a competitive inhibition ELISA was developed. This inhibition ELISA also enabled to detect cross-binding of antibodies to a panel of different NMBAs. 96-well plates (Costar) were coated with 1µg/ml HSA-rocuronium at 4°C overnight, washed 3 times with PBST, blocked with PBST containing 3% BSA at room temperature for 2 hours.

For inhibition ELISAs of single B cell cultures, supernatants were incubated with 3,000 µM of free rocuronium at room temperature for 20 min. HSA-rocuronium was coated at 1 µg/mL (0.227 µM of rocuronium). 3,000 µM of free rocuronium thus corresponds to an excess of approximately 13,000-fold. For purified antibodies, 300 ng/mL (for murine mAbs) or 1,500 ng/mL (for human mAbs) were pre-incubated with 5-fold serial dilution of free rocuronium (Kalcex), vecuronium

(Sigma-Aldrich), pancuronium (Euromedex), suxamethonium (Fischer Scientific), or NMBA control devoid of the quaternary ammonium including 5α-DHT (Merck), diisopentyl succinate (AK Scientific), and pholcodine (Sigma-Aldrich) at concentrations ranging from 15,000 µM to 0.96µM.

The antibody-NMBA mixture was added to the ELISA plates and incubated at room temperature for 2 hours, washed 3 times and revealed with HRP-conjugated goat anti-mouse/human IgG (Bethyl Laboratories) at 1:10,000 dilution. Plates were revealed using an OPD substrate (Sigma-Aldrich). The reaction was stopped with 2M H2SO4 and absorbance was subsequently recorded at 490 nm and corrected at 620 nm using a spectrophotometer (Biophotometer, Eppendorff). Antibodies in the supernatant of B cell culture were considered rocuronium specific if more than 50% of the signal was inhibited in presence of free rocuronium. For purified mAbs, the half-maximal inhibitory concentration (IC_{50}) was measured using a non-linear fit of [Inhibitor] versus response with a variable slope (four parameters) using GraphPad Prism.

Affinity measurements using Bio-Layer Interferometry (BLI)

Affinity of mAbs for rocuronium was tested using Bio-layer interferometry with the OctetRED 384 system. Amine Reactive Second-Generation (AR2G) biosensors were covalently immobilized with HSA-rocuronium (mean of 15 rocuronium molecules per HSA carrier molecule), then inserted in wells containing different concentrations of antibodies for 1,800 seconds (association phase). The antigen-antibody complex was dissociated by introducing the biosensor in the reference buffer (PBS+BSA). Curves were retrieved as raw data from the Octet Data Analysis software and processed in the Scrubber2 software prior to analyses with the Biaevaluation software. IgG-free buffer was used as reference and for background subtraction. Fitting curves and KD values were obtained using the 1:1 Langmuir model.

Affinity measurements using Surface Plasmon Resonance (SPR)

CM5 chips (Cytiva) were primed using PBS, washed 3 times with NaOH (50 mM) and SDS (0.1%) 180seconds each time (5µL/min). At least 5,000 RU of antibody was covalently bound to CM5 chip by activating using 1:1 NHS:EDC (6,000 seconds), injecting the antibody (900 seconds) in acetate buffer pH5.5 and quenching with EtNH2 (600 seconds). Free rocuronium was injected (30

μL/min) in PBS-BSA (1 mg/mL) at different concentrations. Signal was subtracted to the reference canal bound with a non-specific antibody. K_D was determined using a kinetic analysis (RI fixed to 0, model 1:1 binding) with Biaeval software.

Antibody repertoire analysis and representative mAb selection

Docker (*81*) / Apptainer *(82)*, Nextflow (*83*) and Git (*84*) were used to better control reproducibility aspects (*85*). The Nextflow pipeline developed to analyze batches of nucleotide sequence fasta files, representing the raw single cell Sanger sequencing of the V_H-V_L IgG domains, is available at https://zenodo.org/records/13221082, and is detailed below. Most of the process is based on tools from the *immcantation portal* (*86*), specifically from the change-O toolset (*38*). V_H and V_L sequences, although single cell paired, could only be analyzed independently (V_H sequences, then V_L sequences). First, the *AssignGenes.py igblast* tool was run to detect and annotate the V, D, J, CDR and FWR domains in each sequence, using the *imgt* database (*87*). Then, *MakeDb.py igblast* converted the result into a readable tsv file. The *ParseDb.py select* tool kept productive sequences, that is those for which: (1) the coding region had an open reading frame, (2) no defects were present in the start codon, splicing sites, or regulatory elements, (3) no internal stop codons were found, and (4) junction regions were in frame. The clustering of sequences into clonal groups was performed as follows: (1) grouping of the sequences according to same V and J genes (allelic variation not considered) and same length of the CDR3, (2) for each group, computation of the distance score D = (Hamming distance) / (CDR3 length) between each 2 x 2 sequences, (3) determination of the D threshold, that determine whether 2 sequences derive from the same germline cell sequence or not, using the *distToNearest()* function of the *shazam* R package, (4) clone assignment for each sequence, with the same ID for sequences belonging to a same clonal group, using the *DefineClones.py* tool. Of note, a few sequences may have been lost at that stage, as they did not fit the criteria required by this tool. Then, the putative germline sequence of each clonal group was inferred using the *CreateGermlines.py* tool. Finally, a single *all_passed_seq.tsv* file was obtained for each batch of V_H or V_L initial fasta files, containing, for each sequence, the V, D, J gene and allelic names returned by the *AssignGenes.py igblast* tool, the clone ID, the putative germline sequence before somatic hypermutations, and the putative V, D, J gene and allelic names of the germline sequence returned by the *CreateGermlines.py* tool.

Donut plots in Fig. 1E and fig. S6A were drawn after gathering the sequences of the all_passed_seq.tsv file according to the V and J gene and allelic names of their putative germline sequence. Amino acid sequence alignments and percentage identity calculations were performed with Jalview software using MUltiple Sequence Comparison by Log- Expectation (Muscle) and colored by percentage identity. Number of mutations were obtained with IMGT database by comparing sequences with germlines and plotted as histograms using GraphPad Prism.

Human mast cell activation test

$CD34^+$ precursor cells were isolated from peripheral blood mononuclear cells of healthy donors (provided by the French Blood Bank EFS). $CD34^+$ cells were maintained for 1 week under serum-free conditions using StemSpan medium (9655 Stemcell Technologies) supplemented with recombinant human IL-6 (50 ng/ml; 200-06 Peprotech), human IL-3 (10 ng/ml; 200-03 Peprotech), 3% supernatant of CHO transfectants secreting murine stem cell factor (SCF; a gift from P. Dubreuil, corresponding to approximately 50 ng/ml SCF) and ciprofloxacin (10 ng/mL; 17850-5G-F Sigma Aldrich). Thereafter, the cells were maintained in IMDM Glutamax I (31980048), 2-mercaptoethanol (31-350-010), insulin-transferrin selenium (2506865) (all from Gibco), sodium pyruvate (S8636 Sigma Aldrich), 0.5% BSA (A2153 Sigma Aldrich), Penicillin/Streptomycin (100 Units/mL / 100µg/mL; Life Technologies), IL-6 (50 ng/ml 200-06 Peprotech) and 3% supernatant of CHO transfectants secreting mouse SCF. Mast cells were considered ready for experiments after 10 to 12 weeks of culture, when >95% of the cells stained positive for both CD117 (KIT, APC-labeled clone YB5.B8; BD Biosciences) and human FcεRI (using PE/Cy7-labeled clone AER37; BioLegend) by flow cytometry. Cells were ready for experiments after approximately 10 weeks in culture (at which time >95% of all cells were $CD117^+$ $FcεRI^+$).

Human mast cells were sensitized overnight with the anti-rocuronium antibody h1F10 produced in a human IgE format at 1 µg/mL. Cells were then washed and stimulated with increasing doses of HSA-rocuronium in Tyrode's buffer. Mast cell degranulation was measured by flow cytometry using fluorescent avidin (5 µg/mL; A2170 Invitrogen) which binds to heparin contained in mast cell granules. Data were acquired using a MACSQuant MQ10 flow cytometer (Miltenyi) and analyzed with FlowJo v10.8.1 software (TreeStar).

Passive Systemic anaphylaxis in mice

hFcεRI^{tg} mFcεRI$^{-/-}$ mice (*78*) were injected intravenously with 20 µg of anti-rocuronium human IgE h1F10 at 0h and 24h and challenged at 48h with 267 µg of HSA-roc. Control mice were injected with irrelevant human IgE and physiological serum. Central temperature was monitored using a digital thermometer with rectal probe (YSI), and time of death was recorded.

Prophylaxis of neuromuscular blockade in mice

C57BL/6 mice were pre-injected intravenously with roc-specific antibodies in a human IgG1 $N_{297}A$ format at different doses followed 10 minutes later by a lethal dose of free rocuronium (160 µg/kg). A vitality score was defined based on visual cues: 5, no symptom of neuromuscular blockade; 4, transient (<30s) symptoms of flattening, slowing down, difficulty to stand on legs; 3, longer symptoms (<1min) with respiratory distress; 2, inactivity, impossibility to stand on legs, severe respiratory difficulties; 1, death.

scFv production, purification and characterization

Rocuronium-specific V_H and V_L sequences were built into scFvs with a polyglycine-serine linker (GGGGS)4 between the V_H and V_L sequences. The V_H-linker-V_L sequences were synthesized at Genscript with codon optimization for expression in Drosophila S2 cells (ATCC CRL-1963), cloned into pT-350 vector using BglII and BstBI restriction sites (the vector was a gift from F. Rey, Institut Pasteur). For transfection, $5x10^6$ Drosophila S2 cells were seeded in a T25 conical flask containing 5 ml Schneider's Drosophila medium (Gibco) complemented with 10% FBS and incubated at 28°C overnight. Twenty-four hours later, 2 µg of pMT-Roc-scFv-Strep plasmid were co-transfected with 0.1 µg (ratio 20:1) of selection plasmid pCoBlast carrying a gene that confers resistance to puromycin. Effectene transfection kit was used (Qiagen) according to the vendor's protocol. Forty-eight hours after transfection, the selection process was started by addition of puromycin (Invivogen) to the cells at a final concentration of 7 µg/ml. Transfected cells were collected every 4 to 5 days by centrifugation at 90g for 5 min, and cell pellets were resuspended in fresh medium containing 7 µg/ml puromycin. Cell propagation was initiated approximately 2 weeks after transfection. Puromycin-selected cells were adapted to serum-free HyClone Insect cell culture media (GE healthcare life science) and were amplified in large volume flasks as needed.

Protein expression was induced with 0.5 mM CuSO4 when the cell density reached approximately $7.5x10^6$ cells/ml. Seven days after induction, S2 cell suspension was centrifuged for 30 min at 15,000g to remove the cells, and the supernatant was collected. Avidin was added at 15 mg/L to sequester any biotin present in the medium. The supernatant, cleared by centrifugation at 20,000g for 30 min and filtration, was loaded onto a Strep-Tactin Superflow high-capacity 5 mL column (IBA GmbH) using a peristaltic pump or ÄKTA high-pressure liquid chromatography (HPLC) system (Cytiva). The column was washed with 15 mL of 0.1 M Tris pH 8, 0.15 M NaCl, 1 mM EDTA, and the protein was eluted with 8 mL of the same buffer containing 2.5 mM desthiobiotin.

Fab preparation

Fabs were prepared following Pierce Fab Preparation Kit (Thermo Fisher Scientific) instructions. Samples were digested for 4h with papain in the presence of 4 mM cysteine. After purification on protein A columns, a gel filtration was performed with Tris 50mM pH, 7.4; 100 mM NaCl.

Crystallization and X-ray data collection

Crystallization screening trials were carried out by the vapor diffusion method using a Mosquito nanodispensing system (STPLabtech) following established protocols (*88*). Briefly, we set up crystallization sitting drops of 400 nL containing a 1:1 mixture of protein sample (Fab-m2B1 or scFv of Fabm1B6) in complex with 10 mM of rocuronium and commercially available crystallization solutions (*88*) equilibrated against 150 µL of reservoir solution in multiwell plates (Greiner Bio-One). The crystallization plates were stored at 18°C in a RockImager (Formulatrix) automated imaging system to monitor crystal growth. Manual optimization was performed in Linbro plates with the hanging-drop method by mixing 2 µl of protein samples with 2 µl of reservoir solution. The best crystals were obtained with the conditions shown in table S2. The crystals were flash cooled in liquid nitrogen for data collection using the crystallization solution as cryoprotectant. X-ray diffraction data were collected on beamlines PROXIMA-1 and PROXIMA-2A at the synchrotron SOLEIL. Diffraction images were integrated with autoPROC (*89*) and XDS (*90*), and crystallographic calculations were carried out with programs from the CCP4 program suite (*91*).

Structure determination and model refinement.

The structures of Fab-m2B1 and scFv-m1B6 in complex with rocuronium were solved by molecular replacement with Phaser (*92*) using the structures of the catalytic antibody Fab7A1 (pdb 2AJU) as search model. The final models of the complexes were obtained through interactive cycles of manual model building with Coot (*93*) and reciprocal space refinement with Refmac5 (*94*). X-ray data collection and model refinement statistics are summarized in table S2. Figures showing the crystallographic models were generated with Pymol (Schrodinger, LLC).

Anesthesia and reversal of neuromuscular blockade in cynomolgus macaques

Adult cynomolgus macaques (*Macaca fascicularis*) were randomly assigned to this study. All animals were housed within IDMIT animal facilities at CEA, Fontenay-aux-Roses in Bio Safety Level (BSL)-2 facilities (Animal facility authorization #D92-032-02, Préfecture des Hauts de Seine, France) and in compliance with the European Directive 2010/63/EU, the French regulations and the Standards for Human Care and Use of Laboratory Animals of the Office for Laboratory Animal Welfare (OLAW, insurance number #A5826-01, US). Animals tested negative for Campylobacter, Yersinia, Shigella, and Salmonella before being used in the study. Experiments using macaques were approved by the local ethical committee (CEtEA #44) and the French Research, Innovation, and Education Ministry under registration number APAFIS#36723-2022041910357437 v1.

Anesthesia and monitoring of neuromuscular blockade in cynomolgus macaques was performed as described in (*46*). All animals were anaesthetized according to institutional guidelines. For all procedures, the animals were first sedated with ketamine (Imalgene 1000, 5 mg/kg) and medetomidine (Domitor, 0.5 mg/kg). An intravenous (IV) line was placed, followed by tracheal intubation allowing mechanical ventilation (Hallowell EMC Matrix 3002Pro veterinary ventilator), and anesthesia was maintained with isofluorane (Isoflu-vet 1,000 mg/g, 0.5-1.5%). Once complete anesthesia was assessed, macaques received rocuronium bromide (Esmeron, MSD 50 mg/5mL) by IV bolus infusion. When indicated, animals also received sugammadex (Bridion, MSD, 1 mg/kg) or antibody m1B6 (2.5-5-10-15 mg/kg) for rocuronium-induced neuromuscular blockade reversal. Animals were monitored using a Nihon Kohden PVM-2703 monitor during all the anesthesia procedures. Physiological parameters (capnography, heart rate, respiratory rate, oxygen saturation, arterial blood pressure, and temperature) were followed in real-time and

recorded in a chart every 10 minutes. Neuromuscular blockade monitoring devices (TOF-Watch and ToFscan) measuring the T4/T1 ratio were installed before NMBA infusion. Mechanical ventilation was maintained for the whole procedure until complete recovery of the neuromuscular function, assessed with a TOF ratio > 90%. All experiments were performed under the supervision of a trained anesthesiologist and a veterinarian. After the procedures, anesthesia was reversed with atipamezole (Antisedan, 0.5 mg/kg), and animals were resumed to their cage under supervision until complete recovery.

Animals were clinically followed for three days post-infusion. Clinical examination, body weight, and rectal temperature were recorded at each bleeding time, including a complete blood count on each day and a blood biochemistry evaluation on days 0 and 1. Blood sampling did not exceed 7.5% of the total blood volume per week, following ethical recommendations.

Statistical analyses

Individual-level data are presented in data file S2. The R environment v4.3.1 was used for all the analyses (R foundation, https://www.r-project.org/). Data were neither averaged nor normalized prior to analyses. Response variables were log2 converted when required for better adjustment to linear models. For Fig. 2F and Fig. 3A, a mixed models using the lmer() function of the lme4 package was used in order to consider the repeated measures on each mouse. For the other figures, data were fitted to a simple linear model. Resulting effects of interest of the linear model were two-by-two compared (contrast comparisons) using the emmeans() function of the emmeans package. Statistical significance was set to a P value of 0.05 or less. In each panel, type I error was controlled by correcting the P values according to the Benjamini & Hochberg method ("BH" option in the p.adjust() function of R).

Supplemental Materials

Figs. S1 to S

Tables S1 and S2

MDAR Reproducibility Checklist

Data files S1 and S2

REFERENCES

1. S. R. Thilen, W. A. Weigel, M. M. Todd, R. P. Dutton, C. A. Lien, S. A. Grant, J. W. Szokol, L. I. Eriksson, M. Yaster, M. D. Grant, M. Agarkar, A. M. Marbella, J. F. Blanck, K. B. Domino, 2023 American Society of Anesthesiologists Practice Guidelines for Monitoring and Antagonism of Neuromuscular Blockade: A Report by the American Society of Anesthesiologists Task Force on Neuromuscular Blockade. *Anesthesiology* **138**, 13-41 (2023).
2. T. Fuchs-Buder, C. S. Romero, H. Lewald, M. Lamperti, A. Afshari, A. M. Hristovska, D. Schmartz, J. Hinkelbein, D. Longrois, M. Popp, H. D. de Boer, M. Sorbello, R. Jankovic, P. Kranke, Peri-operative management of neuromuscular blockade: A guideline from the European Society of Anaesthesiology and Intensive Care. *Eur J Anaesthesiol* **40**, 82-94 (2023).
3. P. M. Mertes, I. Aimone-Gastin, R. M. Gueant-Rodriguez, C. Mouton-Faivre, G. Audibert, J. O'Brien, D. Frendt, M. Brezeanu, H. Bouaziz, J. L. Gueant, Hypersensitivity reactions to neuromuscular blocking agents. *Curr Pharm Des* **14**, 2809-2825 (2008).
4. P. H. Sadleir, R. C. Clarke, D. L. Bunning, P. R. Platt, Anaphylaxis to neuromuscular blocking drugs: incidence and cross-reactivity in Western Australia from 2002 to 2011. *Br J Anaesth* **110**, 981-987 (2013).
5. G. Cammu, Residual Neuromuscular Blockade and Postoperative Pulmonary Complications: What Does the Recent Evidence Demonstrate? *Curr Anesthesiol Rep* **10**, 131-136 (2020).
6. C. Zaouter, S. Mion, A. Palomba, T. M. Hemmerling, A Short Update on Sugammadex with a Special Focus on Economic Assessment of its Use in North America. *J Anesth Clin Res* **8**, (2017).
7. W. Ji, X. Zhang, J. Liu, G. Sun, X. Wang, L. Bo, X. Deng, Efficacy and safety of neostigmine for neuromuscular blockade reversal in patients under general anesthesia: a systematic review and meta-analysis. *Ann Transl Med* **9**, 1691 (2021).
8. C. Rex, U. A. Bergner, F. K. Puhringer, Sugammadex: a selective relaxant-binding agent providing rapid reversal. *Curr Opin Anaesthesiol* **23**, 461-465 (2010).
9. L. Savic, S. Savic, P. M. Hopkins, Anaphylaxis to sugammadex. *Anaesth Intensive Care* **42**, 7-9 (2014).
10. B. A. Baldo, Anaphylaxis caused by sugammadex- rocuronium inclusion complex: What is the basis of the allergenic recognition? *J Clin Anesth* **54**, 48-49 (2019).
11. D. G. Ebo, B. A. Baldo, A. L. Van Gasse, C. Mertens, J. Elst, L. Sermeus, C. H. Bridts, M. M. Hagendorens, L. S. De Clerck, V. Sabato, Anaphylaxis to sugammadex-rocuronium inclusion complex: An IgE-mediated reaction due to allergenic changes at the sugammadex primary rim. *J Allergy Clin Immunol Pract* **8**, 1410-1415 e1413 (2020).
12. M. Orihara, T. Takazawa, T. Horiuchi, S. Sakamoto, K. Nagumo, Y. Tomita, A. Tomioka, N. Yoshida, A. Yokohama, S. Saito, Comparison of incidence of anaphylaxis between sugammadex and neostigmine: a retrospective multicentre observational study. *Br J Anaesth* **124**, 154-163 (2020).
13. L. Savic, S. Savic, P. M. Hopkins, Anaphylaxis to sugammadex: should we be concerned by the Japanese experience? *Br J Anaesth*, (2020).
14. P. M. Mertes, D. G. Ebo, T. Garcez, M. Rose, V. Sabato, T. Takazawa, P. J. Cooke, R. C. Clarke, P. Dewachter, L. H. Garvey, A. B. Guttormsen, D. L. Hepner, P. M. Hopkins, D. A. Khan, H. Kolawole, P. Kopac, M. Kroigaard, J. J. Laguna, S. D. Marshall, P. R. Platt, P. H. M. Sadleir, L. C. Savic, S. Savic, G. W. Volcheck, S. Voltolini, Comparative epidemiology of suspected perioperative hypersensitivity reactions. *Br J Anaesth* **123**, e16-e28 (2019).
15. P. Bruhns, S. Chollet-Martin, Mechanisms of human drug-induced anaphylaxis. *J Allergy Clin Immunol* **147**, 1133-1142 (2021).
16. F. Jonsson, L. de Chaisemartin, V. Granger, A. Gouel-Cheron, C. M. Gillis, Q. Zhu, F. Dib, P. Nicaise-Roland, C. Ganneau, M. Hurtado-Nedelec, C. Paugam-Burtz, S. Necib, H. Keita-Meyer, M. Le Dorze, B. Cholley, O. Langeron, L. Jacob, B. Plaud, M. Fischler, C. Sauvan, M. T. Guinnepain, P. Montravers, M. Aubier, S. Bay, C. Neukirch, F. Tubach, D. Longrois, S. Chollet-Martin, P. Bruhns, An IgG-induced neutrophil activation pathway contributes to human drug-induced anaphylaxis. *Sci Transl Med* **11**, (2019).
17. P. Vadas, M. Gold, B. Perelman, G. M. Liss, G. Lack, T. Blyth, F. E. Simons, K. J. Simons, D. Cass, J. Yeung, Platelet-activating factor, PAF acetylhydrolase, and severe anaphylaxis. *N Engl J Med* **358**, 28-35 (2008).
18. K. Arias, M. Baig, M. Colangelo, D. Chu, T. Walker, S. Goncharova, A. Coyle, P. Vadas, S. Waserman, M. Jordana, Concurrent blockade of platelet-activating factor and histamine prevents life-threatening peanut-induced anaphylactic reactions. *J Allergy Clin Immunol* **124**, 307-314, 314 e301-302 (2009).

19. M. M. van der Poorten, A. L. Van Gasse, M. M. Hagendorens, M. A. Faber, L. De Puysseleyr, J. Elst, C. M. Mertens, V. Sabato, D. G. Ebo, Serum specific IgE antibodies in immediate drug hypersensitivity. *Clin Chim Acta* **504**, 119-124 (2020).
20. Decuyper, II, D. G. Ebo, A. P. Uyttebroek, M. M. Hagendorens, M. A. Faber, C. H. Bridts, L. S. De Clerck, V. Sabato, Quantification of specific IgE antibodies in immediate drug hypersensitivity: More shortcomings than potentials? *Clin Chim Acta* **460**, 184-189 (2016).
21. A. P. Uyttebroek, V. Sabato, C. H. Bridts, L. S. De Clerck, D. G. Ebo, Immunoglobulin E antibodies to atracurium: a new diagnostic tool? *Clin Exp Allergy* **45**, 485-487 (2015).
22. B. A. Baldo, M. M. Fisher, Substituted ammonium ions as allergenic determinants in drug allergy. *Nature* **306**, 262-264 (1983).
23. W. J. Russell, C. Lee, D. Milne, Is allergy to rocuronium a high probability cross-reaction with suxamethonium? *Anaesth Intensive Care* **31**, 333 (2003).
24. M. A. Rose, J. Anderson, S. L. Green, J. Yun, S. L. Fernando, Morphine and pholcodine-specific IgE have limited utility in the diagnosis of anaphylaxis to benzylisoquinolines. *Acta Anaesthesiol Scand* **62**, 628-634 (2018).
25. B. A. Baldo, M. M. Fisher, N. H. Pham, On the origin and specificity of antibodies to neuromuscular blocking (muscle relaxant) drugs: an immunochemical perspective. *Clin Exp Allergy* **39**, 325-344 (2009).
26. M. Peyneau, L. de Chaisemartin, N. Gigant, S. Chollet-Martin, S. Kerdine-Romer, Quaternary ammonium compounds in hypersensitivity reactions. *Front Toxicol* **4**, 973680 (2022).
27. E. Florvaag, S. G. Johansson, The Pholcodine Case. Cough Medicines, IgE-Sensitization, and Anaphylaxis: A Devious Connection. *World Allergy Organ J* **5**, 73-78 (2012).
28. P. M. Mertes, N. Petitpain, C. Tacquard, M. Delpuech, C. Baumann, J. M. Malinovsky, D. Longrois, A. Gouel-Cheron, D. Le Quang, P. Demoly, J. L. Gueant, P. Gillet, A. S. Group, Pholcodine exposure increases the risk of perioperative anaphylaxis to neuromuscular blocking agents: the ALPHO case-control study. *Br J Anaesth*, (2023).
29. R. Jimenez-Saiz, Y. Ellenbogen, K. Bruton, P. Spill, D. D. Sommer, H. Lima, S. Waserman, S. U. Patil, W. G. Shreffler, M. Jordana, Human BCR analysis of single-sorted, putative IgE(+) memory B cells in food allergy. *J Allergy Clin Immunol* **144**, 336-339 e336 (2019).
30. J. M. Davies, T. A. Platts-Mills, R. C. Aalberse, The enigma of IgE+ B-cell memory in human subjects. *J Allergy Clin Immunol* **131**, 972-976 (2013).
31. B. Laffleur, S. Duchez, K. Tarte, N. Denis-Lagache, S. Peron, C. Carrion, Y. Denizot, M. Cogne, Self-Restrained B Cells Arise following Membrane IgE Expression. *Cell Rep*, (2015).
32. R. A. Hoh, S. A. Joshi, J. Y. Lee, B. A. Martin, S. Varma, S. Kwok, S. C. A. Nielsen, P. Nejad, E. Haraguchi, P. S. Dixit, S. V. Shutthanandan, K. M. Roskin, W. Zhang, D. Tupa, B. J. Bunning, M. Manohar, R. Tibshirani, N. Q. Fernandez-Becker, N. Kambham, R. B. West, R. G. Hamilton, M. Tsai, S. J. Galli, R. S. Chinthrajah, K. C. Nadeau, S. D. Boyd, Origins and clonal convergence of gastrointestinal IgE(+) B cells in human peanut allergy. *Sci Immunol* **5**, (2020).
33. K. Haniuda, S. Fukao, T. Kodama, H. Hasegawa, D. Kitamura, Autonomous membrane IgE signaling prevents IgE-memory formation. *Nat Immunol* **17**, 1109-1117 (2016).
34. I. Hoof, V. Schulten, J. A. Layhadi, T. Stranzl, L. H. Christensen, S. Herrera de la Mata, G. Seumois, P. Vijayanand, C. Lundegaard, K. Niss, A. Lund, J. Ahrenfeldt, J. Holm, E. Steveling, H. Sharif, S. R. Durham, B. Peters, M. H. Shamji, P. S. Andersen, Allergen-specific IgG(+) memory B cells are temporally linked to IgE memory responses. *J Allergy Clin Immunol* **146**, 180-191 (2020).
35. X. M. Luo, E. Maarschalk, R. M. O'Connell, P. Wang, L. Yang, D. Baltimore, Engineering human hematopoietic stem/progenitor cells to produce a broadly neutralizing anti-HIV antibody after in vitro maturation to human B lymphocytes. *Blood* **113**, 1422-1431 (2009).
36. A. Sokal, G. Barba-Spaeth, L. Hunault, I. Fernandez, M. Broketa, A. Meola, S. Fourati, I. Azzaoui, A. Vandenberghe, P. Lagouge-Roussey, M. Broutin, A. Roeser, M. Bouvier-Alias, E. Crickx, L. Languille, M. Fournier, M. Michel, B. Godeau, S. Gallien, G. Melica, Y. Nguyen, F. Canoui-Poitrine, F. Pirenne, J. Megret, J. M. Pawlotsky, S. Fillatreau, C. A. Reynaud, J. C. Weill, F. A. Rey, P. Bruhns, M. Mahevas, P. Chappert, SARS-CoV-2 Omicron BA.1 breakthrough infection drives late remodeling of the memory B cell repertoire in vaccinated individuals. *Immunity*, (2023).
37. D. R. Glass, A. G. Tsai, J. P. Oliveria, F. J. Hartmann, S. C. Kimmey, A. A. Calderon, L. Borges, M. C. Glass, L. E. Wagar, M. M. Davis, S. C. Bendall, An Integrated Multi-omic Single-Cell Atlas of Human B Cell Identity. *Immunity* **53**, 217-232 e215 (2020).

38. N. T. Gupta, J. A. Vander Heiden, M. Uduman, D. Gadala-Maria, G. Yaari, S. H. Kleinstein, Change-O: a toolkit for analyzing large-scale B cell immunoglobulin repertoire sequencing data. *Bioinformatics* **31**, 3356-3358 (2015).
39. J. Elst, V. Sabato, M. A. Faber, C. H. Bridts, C. Mertens, M. Van Houdt, A. L. Van Gasse, M. M. Hagendorens, V. Van Tendeloo, M. Maurer, D. Campillo-Davo, J. P. Timmermans, I. Pintelon, D. G. Ebo, MRGPRX2 and Immediate Drug Hypersensitivity: Insights From Cultured Human Mast Cells. *J Investig Allergol Clin Immunol* **31**, 489-499 (2021).
40. A. Gouel-Cheron, A. Dejoux, E. Lamanna, P. Bruhns, Animal Models of IgE Anaphylaxis. *Biology (Basel)* **12**, (2023).
41. L. Fielding, G. H. Grant, Conformational equilibria in amino steroids. 1. A proton and carbon-13 NMR spectroscopy and molecular mechanics study of 3.alpha.-hydroxy-2.beta.-(4-morpholinyl)-5.alpha.H-androstan-17-one. *J. Am. Chem. Soc.* **113**, 9785-9790 (1991).
42. B. A. Baldo, M. M. Fisher, Anaphylaxis to muscle relaxant drugs: cross-reactivity and molecular basis of binding of IgE antibodies detected by radioimmunoassay. *Mol Immunol* **20**, 1393-1400 (1983).
43. P. M. Jones, T. P. Turkstra, Mitigation of rocuronium-induced anaphylaxis by sugammadex: the great unknown. *Anaesthesia* **65**, 89-90; author reply 90 (2010).
44. A. E. Funnell, J. Griffiths, I. Hodzovic, A further case of rocuronium-induced anaphylaxis treated with sugammadex. *Br J Anaesth* **107**, 275-276 (2011).
45. B. Conte, L. Zoric, G. Bonada, B. Debaene, J. Ripart, Reversal of a rocuronium-induced grade IV anaphylaxis via early injection of a large dose of sugammadex. *Can J Anaesth* **61**, 558-562 (2014).
46. H. Letscher, J. Lemaitre, E. Burban, R. Le Grand, P. Bruhns, F. Relouzat, A. Gouel-Chéron, Optimization of neuromuscular blockade protocols in cynomolgus macaques: monitoring, doses and antagonism. *bioRxiv*, (2023).
47. J. I. Reddy, P. J. Cooke, J. M. van Schalkwyk, J. A. Hannam, P. Fitzharris, S. J. Mitchell, Anaphylaxis is more common with rocuronium and succinylcholine than with atracurium. *Anesthesiology* **122**, 39-45 (2015).
48. T. Takazawa, H. Mitsuhata, P. M. Mertes, Sugammadex and rocuronium-induced anaphylaxis. *J Anesth* **30**, 290-297 (2016).
49. C. Tacquard, O. Collange, P. Gomis, J. M. Malinovsky, N. Petitpain, P. Demoly, S. Nicoll, P. M. Mertes, Anaesthetic hypersensitivity reactions in France between 2011 and 2012: the 10th GERAP epidemiologic survey. *Acta Anaesthesiol Scand* **61**, 290-299 (2017).
50. J. M. Hunter, Rocuronium: the newest aminosteroid neuromuscular blocking drug. *Br J Anaesth* **76**, 481-483 (1996).
51. W. J. Pichler, Anaphylaxis to drugs: Overcoming mast cell unresponsiveness by fake antigens. *Allergy*, (2020).
52. R. C. Aalberse, I. Kleine Budde, M. Mulder, S. O. Stapel, W. Paulij, F. Leynadier, M. W. Hollmann, Differentiating the cellular and humoral components of neuromuscular blocking agent-induced anaphylactic reactions in patients undergoing anaesthesia. *Br J Anaesth* **106**, 665-674 (2011).
53. A. Dejoux, L. de Chaisemartin, P. Bruhns, D. Longrois, A. Gouel-Cheron, Neuromuscular blocking agent induced hypersensitivity reaction exploration: an update. *Eur J Anaesthesiol* **40**, 95-104 (2023).
54. M. M. Fisher, B. A. Baldo, Immunoassays in the diagnosis of anaphylaxis to neuromuscular blocking drugs: the value of morphine for the detection of IgE antibodies in allergic subjects. *Anaesth Intensive Care* **28**, 167-170 (2000).
55. D. Laroche, S. Chollet-Martin, P. Leturgie, L. Malzac, M. C. Vergnaud, C. Neukirch, L. Venemalm, J. L. Gueant, P. N. Roland, Evaluation of a new routine diagnostic test for immunoglobulin e sensitization to neuromuscular blocking agents. *Anesthesiology* **114**, 91-97 (2011).
56. J. Leysen, A. Uyttebroek, V. Sabato, C. H. Bridts, L. S. De Clerck, D. G. Ebo, Predictive value of allergy tests for neuromuscular blocking agents: tackling an unmet need. *Clin Exp Allergy* **44**, 1069-1075 (2014).
57. J. Anderson, S. Green, M. Capon, B. Krupowicz, J. Li, R. Fulton, S. L. Fernando, Measurement of pholcodine-specific IgE in addition to morphine-specific IgE improves investigation of neuromuscular blocking agent anaphylaxis. *Br J Anaesth* **125**, e450-e452 (2020).
58. K. L. Chow, K. Patchett, G. Reeves, T. de Malmanche, D. Gillies, M. Boyle, Morphine-specific IgE testing in the assessment of neuromuscular blocking agent allergy: a single centre experience. *Br J Anaesth*, (2023).
59. T. J. Looney, J. Y. Lee, K. M. Roskin, R. A. Hoh, J. King, J. Glanville, Y. Liu, T. D. Pham, C. L. Dekker, M. M. Davis, S. D. Boyd, Human B-cell isotype switching origins of IgE. *J Allergy Clin Immunol* **137**, 579-586 e577 (2016).

60. M. Ota, K. B. Hoehn, W. Fernandes-Braga, T. Ota, C. J. Aranda, S. Friedman, M. G. C. Miranda-Waldetario, J. Redes, M. Suprun, G. Grishina, H. A. Sampson, A. Malbari, S. H. Kleinstein, S. H. Sicherer, M. A. Curotto de Lafaille, CD23(+)IgG1(+) memory B cells are poised to switch to pathogenic IgE production in food allergy. *Sci Transl Med* **16**, eadi0673 (2024).
61. J. F. E. Koenig, N. P. H. Knudsen, A. Phelps, K. Bruton, I. Hoof, G. Lund, D. D. Libera, A. Lund, L. H. Christensen, D. R. Glass, T. D. Walker, A. Fang, S. Waserman, M. Jordana, P. S. Andersen, Type 2-polarized memory B cells hold allergen-specific IgE memory. *Sci Transl Med* **16**, eadi0944 (2024).
62. J. Elst, M. Van Houdt, M. M. van der Poorten, A. L. Van Gasse, C. Mertens, A. Toscano, M. Beyens, E. De Boeck, V. Sabato, D. G. Ebo, Comparison of the passive mast cell activation test with the basophil activation test for diagnosis of perioperative rocuronium hypersensitivity. *Br J Anaesth*, (2023).
63. S. Asrat, N. Kaur, X. Liu, L. H. Ben, D. Kajimura, A. J. Murphy, M. A. Sleeman, A. Limnander, J. M. Orengo, Chronic allergen exposure drives accumulation of long-lived IgE plasma cells in the bone marrow, giving rise to serological memory. *Sci Immunol* **5**, (2020).
64. S. Asrat, J. C. Devlin, A. Vecchione, B. Klotz, I. Setliff, D. Srivastava, A. Limnander, A. Rafique, C. Adler, S. Porter, A. J. Murphy, G. S. Atwal, M. A. Sleeman, W. K. Lim, J. M. Orengo, TRAPnSeq allows high-throughput profiling of antigen-specific antibody-secreting cells. *Cell Rep Methods* **3**, 100522 (2023).
65. N. Stawicki, P. Gessner, Residual Neuromuscular Blockade in the Critical Care Setting. *AACN Adv Crit Care* **29**, 15-24 (2018).
66. L. Saager, E. M. Maiese, L. D. Bash, T. A. Meyer, H. Minkowitz, S. Groudine, B. K. Philip, P. Tanaka, T. J. Gan, Y. Rodriguez-Blanco, R. Soto, O. Heisel, Incidence, risk factors, and consequences of residual neuromuscular block in the United States: The prospective, observational, multicenter RECITE-US study. *J Clin Anesth* **55**, 33-41 (2019).
67. P. Goncalves, A. V. Vieira, C. Silva, R. S. Gomez, Residual neuromuscular blockade and late neuromuscular blockade at the post-anesthetic recovery unit: prospective cohort study. *Braz J Anesthesiol* **71**, 38-43 (2021).
68. J. Ross, D. P. Ramsay, L. J. Sutton-Smith, R. D. Willink, J. E. Moore, Residual neuromuscular blockade in the ICU: a prospective observational study and national survey. *Anaesthesia* **77**, 991-998 (2022).
69. C. Baillard, C. Clec'h, J. Catineau, F. Salhi, G. Gehan, M. Cupa, C. M. Samama, Postoperative residual neuromuscular block: a survey of management. *Br J Anaesth* **95**, 622-626 (2005).
70. S. Esteves, F. Correia de Barros, C. S. Nunes, A. Puga, B. Gomes, F. Abelha, H. Machado, M. Ferreira, N. Fernandes, P. Vitor, S. Pereira, T. A. Lapa, V. Pinho-Oliveira, Incidence of postoperative residual neuromuscular blockade - A multicenter, observational study in Portugal (INSPIRE 2). *Porto Biomed J* **8**, e225 (2023).
71. A. D. Raval, V. R. Anupindi, C. P. Ferrufino, D. L. Arper, L. D. Bash, S. J. Brull, Epidemiology and outcomes of residual neuromuscular blockade: A systematic review of observational studies. *J Clin Anesth* **66**, 109962 (2020).
72. S. Koethe, L. Zander, S. Koster, A. Annan, A. Ebenfelt, J. Spencer, M. Bemark, Pivotal advance: CD45RB glycosylation is specifically regulated during human peripheral B cell differentiation. *J Leukoc Biol* **90**, 5-19 (2011).
73. K. Suzuki, T. Takazawa, S. Saito, History of the development of antagonists for neuromuscular blocking agents. *J Anesth* **34**, 723-728 (2020).
74. A. Gouel-Cheron, L. de Chaisemartin, F. Jonsson, P. Nicaise-Roland, V. Granger, A. Sabahov, M. T. Guinnepain, S. Chollet-Martin, P. Bruhns, C. Neukirch, D. Longrois, N. s. group, Low end-tidal CO2 as a real-time severity marker of intra-anaesthetic acute hypersensitivity reactions. *Br J Anaesth* **119**, 908-917 (2017).
75. J. Sprung, T. N. Weingarten, L. B. Schwartz, Presence or absence of elevated acute total serum tryptase by itself is not a definitive marker for an allergic reaction. *Anesthesiology* **122**, 713-714 (2015).
76. D. G. Ebo, L. Venemalm, C. H. Bridts, F. Degerbeck, H. Hagberg, L. S. De Clerck, W. J. Stevens, Immunoglobulin E antibodies to rocuronium: a new diagnostic tool. *Anesthesiology* **107**, 253-259 (2007).
77. S. Goyard, B. Balbino, R. S. Chinthrajah, S. C. Lyu, Y. L. Janin, P. Bruhns, P. Poncet, S. J. Galli, K. C. Nadeau, L. L. Reber, T. Rose, A highly sensitive bioluminescent method for measuring allergen-specific IgE in microliter samples. *Allergy* **75**, 2952-2956 (2020).
78. D. A. Mancardi, B. Iannascoli, S. Hoos, P. England, M. Daeron, P. Bruhns, FcgammaRIV is a mouse IgE receptor that resembles macrophage FcepsilonRI in humans and promotes IgE-induced lung inflammation. *J Clin Invest* **118**, 3738-3750 (2008).

79. A. Watanabe, K. Y. Su, M. Kuraoka, G. Yang, A. E. Reynolds, A. G. Schmidt, S. C. Harrison, B. F. Haynes, E. W. St Clair, G. Kelsoe, Self-tolerance curtails the B cell repertoire to microbial epitopes. *JCI Insight* **4**, (2019).
80. T. Tiller, E. Meffre, S. Yurasov, M. Tsuiji, M. C. Nussenzweig, H. Wardemann, Efficient generation of monoclonal antibodies from single human B cells by single cell RT-PCR and expression vector cloning. *J Immunol Methods* **329**, 112-124 (2008).
81. Docker. *https://www.docker.com*.
82. Apptainer. *https://apptainer.org*.
83. Nextflow. *https://www.nextflow.io*.
84. Git. *https://about.gitlab.com*.
85. M. Djaffardjy, G. Marchment, C. Sebe, R. Blanchet, K. Bellajhame, A. Gaignard, F. Lemoine, S. Cohen-Boulakia, Developing and reusing bioinformatics data analysis pipelines using scientific workflow systems. *Comput Struct Biotechnol J* **21**, 2075-2085 (2023).
86. Immcantation. *https://immcantation.readthedocs.io/en/stable/*.
87. IMGT. *https://www.imgt.org*.
88. P. Weber, C. Pissis, R. Navaza, A. E. Mechaly, F. Saul, P. M. Alzari, A. Haouz, High-Throughput Crystallization Pipeline at the Crystallography Core Facility of the Institut Pasteur. *Molecules* **24**, (2019).
89. C. Vonrhein, C. Flensburg, P. Keller, A. Sharff, O. Smart, W. Paciorek, T. Womack, G. Bricogne, Data processing and analysis with the autoPROC toolbox. *Acta Crystallogr D Biol Crystallogr* **67**, 293-302 (2011).
90. W. Kabsch, Xds. *Acta Crystallogr D Biol Crystallogr* **66**, 125-132 (2010).
91. J. Agirre, M. Atanasova, H. Bagdonas, C. B. Ballard, A. Basle, J. Beilsten-Edmands, R. J. Borges, D. G. Brown, J. J. Burgos-Marmol, J. M. Berrisford, P. S. Bond, I. Caballero, L. Catapano, G. Chojnowski, A. G. Cook, K. D. Cowtan, T. I. Croll, J. E. Debreczeni, N. E. Devenish, E. J. Dodson, T. R. Drevon, P. Emsley, G. Evans, P. R. Evans, M. Fando, J. Foadi, L. Fuentes-Montero, E. F. Garman, M. Gerstel, R. J. Gildea, K. Hatti, M. L. Hekkelman, P. Heuser, S. W. Hoh, M. A. Hough, H. T. Jenkins, E. Jimenez, R. P. Joosten, R. M. Keegan, N. Keep, E. B. Krissinel, P. Kolenko, O. Kovalevskiy, V. S. Lamzin, D. M. Lawson, A. A. Lebedev, A. G. W. Leslie, B. Lohkamp, F. Long, M. Maly, A. J. McCoy, S. J. McNicholas, A. Medina, C. Millan, J. W. Murray, G. N. Murshudov, R. A. Nicholls, M. E. M. Noble, R. Oeffner, N. S. Pannu, J. M. Parkhurst, N. Pearce, J. Pereira, A. Perrakis, H. R. Powell, R. J. Read, D. J. Rigden, W. Rochira, M. Sammito, F. Sanchez Rodriguez, G. M. Sheldrick, K. L. Shelley, F. Simkovic, A. J. Simpkin, P. Skubak, E. Sobolev, R. A. Steiner, K. Stevenson, I. Tews, J. M. H. Thomas, A. Thorn, J. T. Valls, V. Uski, I. Uson, A. Vagin, S. Velankar, M. Vollmar, H. Walden, D. Waterman, K. S. Wilson, M. D. Winn, G. Winter, M. Wojdyr, K. Yamashita, The CCP4 suite: integrative software for macromolecular crystallography. *Acta Crystallogr D Struct Biol* **79**, 449-461 (2023).
92. A. J. McCoy, R. W. Grosse-Kunstleve, P. D. Adams, M. D. Winn, L. C. Storoni, R. J. Read, Phaser crystallographic software. *J Appl Crystallogr* **40**, 658-674 (2007).
93. P. Emsley, K. Cowtan, Coot: model-building tools for molecular graphics. *Acta Crystallogr D Biol Crystallogr* **60**, 2126-2132 (2004).
94. G. N. Murshudov, P. Skubak, A. A. Lebedev, N. S. Pannu, R. A. Steiner, R. A. Nicholls, M. D. Winn, F. Long, A. A. Vagin, REFMAC5 for the refinement of macromolecular crystal structures. *Acta Crystallogr D Biol Crystallogr* **67**, 355-367 (2011).

ACKNOWLEDGMENTS

We would like to thank our colleagues from the Institut Pasteur, Paris, France for their help and advice: D. Brun and A. Meola (Structural virology unit) for ScFv generation and production; B. Raynal, S. Brulé and S. Hoos for assistance with affinity measurements (Molecular Biophysics Core Facility), F. Agou for access to the BLI instrument (Plateforme de Criblage Chémogénomique et Biologique; PF-CCB), the Cytometry and Biomarkers technological unit (UTechS CB); and M. Perez for advice and support (Direction Des Applications De la Recherche et des Relations Industrielles; DARRI). We would like to thank G. Kelsoe (Duke University) for providing us with invaluable advice and the human B cell culture system; the team of the Pharmacoepidemiology, Center of the Assistance Publique-Hôpitaux de Paris (AP-HP) and, in particular, N. Yelles, K. Chandirakumaran, and I. Younes at the Bichat Hospital for help with the NASA clinical study logistics; G. Chabot and O. Kacimi at Hôpital Bichat for the MEDIREP study; J. Lehacaut and C. Da Costa Ribeiro Coutinho from the CIC at Hôpital Bichat; and the staff of the crystallography platform at Institut Pasteur for crystallization screening. We would also like to acknowledge synchroton SOLEIL for granting access to their facility and the staff of Proxima1 and Proxima2A for helpful assistance.

FUNDING

Work in the Bruhns lab was supported by the Institut Pasteur, Institut National de la Santé et de la Recherche Médicale (Inserm), Fondation pour la Recherche Médicale, Paris, France (Programme Equipe FRM grant EQU202203014631 to PB), Accélérateur de l'innovation de l'Institut Pasteur (grant rocuCEPT), Agence Nationale de la Recherche (ANR grant ANR-21-CE15-0027), European Research Council (ERC)–Seventh Framework Program (ERC-2013-CoG 616050). Data partially resulted from the work performed in the International Research Program IRP "ALLERGYMINE" (Inserm grant call 2022-2026) to PB. AD and LH were doctoral fellows of Sorbonne Université. AD was partly supported by a fellowship from the Fondation pour la Recherche Médicale grant FDT202304016860 to AD. QZ received a PhD scholarship from the Chinese Science Council. AGC was a recipient of a poste d'accueil 2017 Institut Pasteur – Assistance Publique des Hôpitaux de Paris (APHP) and from a grant provided by INSERM, SFAR (Société Française d'Anesthésie et de Réanimation), and SRLF (Société de Réanimation de

Langue Française) through the “Bourse de Recherche du Comité d’interface INSERM-SFAR-SRLF 2012. CMG was supported partly by a stipend from the Pasteur-Paris University (PPU) International PhD program and by the Institut Carnot Pasteur Maladies Infectieuses. PB benefited from an additional support from AP-HP through a “Contrat Local d’Interface 2014” and the “Département Hospitalo-Universitaire” (DHU) FIRE. The sponsor of the NASA study was the Direction de la Recherche Clinique et de l’Innovation de l’AP-HP (France).

AUTHOR CONTRIBUTIONS

SB, SCM, AGC and PB designed experiments. AD, QZ, C Ganneau, C Pecalvel, LH, TD, BI, TR, CM, PNR, and C Pissis conducted in vitro experiments. AD, QZ, ORL, OG, JL, FR, C Gillis and YW conducted in vitro experiments. AD, FH, AS, AV, C Pecalvel, LH and TD conducted flow experiments. AD, QZ, C Ganneau, ORL, OG, JL, FH, C Gillis, TR, PE, MM, LdC, RLG, HL, FS, AH, LLR, PC, FJ, DGE, GAM, SB, SCM, AG, and PB analyzed and interpreted data. PB acquired funding. AD and PB wrote the original draft of the manuscript, and all authors reviewed and edited the manuscript.

COMPETING INTERESTS

Unrelated to the submitted work, PB received consulting fees from Regeneron Pharmaceuticals. LdC reports lecture fees from MSD France, without any relation to the content of this manuscript. LLR has received grants or consulting fees from Neovacs, CEVA, Novartis and Argenx, not related to this work. The other authors declare no competing interests.

DATA AND MATERIALS AVAILABILITY

All data associated with this study are in the paper or supplementary materials. The code of the Nextflow pipeline developed to analyze batches of nucleotide sequence fasta files is deposited under DOI: 10.5281/zenodo.13221082. Coordinates and structure factors of crystallographic data have been deposited in the Protein Data Bank under the accession codes 8S4K (Fab2B1 in complex with rocuronium) and 8S4H (scFv-1B6 in complex with rocuronium). Further information and

requests under MTA for resources, reagents, and materials that are not commercially available should be directed to and will be fulfilled by the corresponding author (bruhns@pasteur.fr).

In addition to the members of the NASA study group who are authors (Pierre Bruhns, Friederike Jönsson, Caitlin M. Gillis, Pascale Nicaise-Roland, Luc de Chaisemartin, Sylvie Chollet-Martin, Qianqian Zhu, Aurélie Gouel-Chéron, Sylvie Bay, Christelle Ganneau), the following study group members are collaborators who have contributed to study design, data analysis, and interpretation: David A. Mancardi[1], Vanessa Granger[3], Dan Longrois[16,17], Philippe Montravers[16,17], Caroline Sauvan[19], Michel Aubier[18,19], Catherine Neukirch[18,19], Fadia Dib[20], Catherine Paugam-Burtz[21], Skander Necib[21], Hawa Keita-Meyer[22], Valentina Faitot[22], Alexandre Mebazaa[23], Matthieu Le Dorze[23], Bernard Cholley[24], Jean Mantz[24] (deceased), Olivier Langeron[25], Sabrine Roche[25], Laurent Jacob[26], Benoit Plaud[26], Julie Bresson[26], Carole Chahine[26], Marc Fischler[27], Marie-Thérèse Guinnepain[28], Florence Tubach[29], Antoine Mignon[30].

Affiliations 1 to 18 can be found on the first page of the paper.

[19]APHP, Hôpital Bichat, Service de Pneumologie A, HUPNVS, Paris, France; [20]APHP, Hôpital Bichat, Department of Epidemiology and Clinical Research, INSERM, Paris, France; [21]Département d'Anesthésie-Réanimation, Hôpital Beaujon, AP-HP, Clichy, France, and Université Paris Diderot, Paris, France; [22]Service d'anesthésie, Hôpital Louis Mourier, AP-HP, Colombes, France and Université Paris Diderot, Sorbonne Paris Cité, EA Recherche Clinique coordonnée ville-hôpital, Méthodologies et Société (REMES), Paris, France; [23]Département d'Anesthésie-Réanimation, Hôpital Lariboisière, AP-HP, Paris, France; [24]Service d'Anesthésie-Réanimation, Hôpital Européen Georges Pompidou, UMR1140 INSERM, AP-HP, Paris, France and Université Paris Descartes, Sorbonne Paris Cité, Paris, France; [25]Department of Anesthesia and Critical Care, Hôpital Pitié Salpêtrière, AP-HP, Sorbonne Université, Paris, France and Infection and Epidemiology Department, Institut Pasteur Human Histopathology and Animal Models Unit, Paris, France; [26]Département d'Anesthésie-Réanimation, Hôpital Saint Louis, AP-HP, Paris, France; [27]Service d'Anesthésie, Hôpital Foch, Suresnes, France; [28]Hôpital Foch, Service de médecine interne, Suresnes, France; [29]Sorbonne Université, INSERM, Institut Pierre Louis d'Epidémiologie et de Santé Publique, PEPITES, AP-HP, Hôpitaux Universitaires Pitié Salpêtrière - Charles Foix, Département Biostatistique Santé Publique et Information Médicale,

1339 Centre de Pharmacoépidémiologie (Cephepi), CIC-1421, F75013, Paris, France; [30]Département
1340 d'anesthésie-réanimation, Hôpital Cochin, AP-HP, Paris, France.

Figure 1. Identification of rocuronium-specific IgG repertoires from NMBA-allergic patients. (**A**) Structural formula of rocuronium with its major groups circled and named. (**B**) IgE anti-rocuronium ImmunoCAP results from the serum of indicated patients (each value is a replicate, n≥2), or serum from five blood bank donors (each value represents one donor). The cut-off was set at 0.13 kUA/L and is indicated by the dotted line. (**C**) IgG anti-rocuronium ELISA results ($OD_{HSA\text{-}roc}$ minus OD_{HSA}) from the serum of indicated patients (each value is a replicate, n=3), or serum from five blood bank donors (each value represents one sample from one donor). The cut-off was set at 0.28 OD and is indicated by the dotted line. (**D**) Example of gating strategy for the single-cell sort of rocuronium-binding memory B cells ($CD3^-$ $CD14^-$ $CD19^+$ $CD38^-$ $CD27^+$ IgD^- HSA-roc^+ HSA^-) from the PBMCs of Patient #1_2014. Numbers in the panels indicate the percentage of cells gated among the represented cells in each panel. BV, brilliant violet; PE, phycoerythrin; AF, Alexa Fluor. (**E**) Donut plot of V_H and V_L gene usage among the monoclonal B cell cultures secreting anti-rocuronium IgG from the indicated patients. The total number of cells is indicated in the center of the donut. The major V-J recombination and their frequency (in parentheses) are indicated in color. Means ± standard deviations are indicated in (B) and (C). Statistical comparisons in (B) and (C) were obtained using contrast analysis after simple linear modeling and multiple-testing P-value adjustment. ****, $P \leq 0.0001$; ***, $P \leq 0.001$; **, $P \leq 0.01$; ns, not significant.

Figure 2: Characterization of recombinant roc-specific mAbs from patients. (**A**) IgG anti-rocuronium ELISA results are shown for mAbs isolated from indicated patients. A non-specific human IgG1 was used as a control. (**B**) Shown are results of an anti-IgG rocuronium competitive ELISA using fixed concentration of mAb 1F10 but increasing concentrations of indicated molecules free in solution. 5α-DHT, 5α-dihydrotestosterone; IC_{50}, half-maximal inhibitory concentration. (**C**) Bio-layer interferometry avidity measurement of the interaction between immobilized HSA-rocuronium and varying concentrations of mAb 1F10 in solution. (**D**) Surface Plasmon Resonance affinity measurement of the interaction between immobilized 1F10 and varying concentrations of free rocuronium in solution. In (C) and (D), K_D values were obtained by fitting the curves using a heterogenous ligand model. (**E**) Human mast cell activation test using mAb 1F10 in a human IgE format for sensitization, followed by challenge with HSA or HSA-roc,

with degranulation measured using fluorescent avidin binding by flow cytometry (n=3). Unsti., unstimulated. Means ± standard deviations are indicated. Statistical comparisons were obtained using contrast analysis after linear modeling and multiple-testing P-value adjustment. ***, $P \leq 0.001$. (**F**) Passive systemic anaphylaxis was measured by changes in body temperature (Δ°C) in hFcεRI-transgenic mice sensitized twice with hIgE 1F10 and challenged with HSA-roc intravenously. Mean ± standard deviation of 3 mice per group are indicated. Each of the three post injection effects were analyzed separately, comparing the contrast between 1F10 and isotype control groups after mixed linear modeling and multiple-testing P-value adjustment. P values are indicated at the end of each time period analyzed. **, $P \leq 0.01$; ns, not significant. (**G**) Experimental timeline (left panel), establishment of the lethal dose of rocuronium and time to death (middle panel; n≥2), and prophylaxis of neuromuscular blockade (right, n=2) in wild-type mice. Prophylaxis was evaluated by vitality scores of mice injected first with sugammadex (sugam.) or 400μg/mouse of indicated anti-rocuronium mAbs, followed by rocuronium injection. Vitality is scored as follows: 5 (no behavior changes), 4 (transient inactivity; ≤30 sec), 3 (respiratory distress and intermediate inactivity; >30 sec), 2 (flipping or inactivity; >1 min), 1 (death).

Figure 3. mAbs isolated from immunized mice exclusively bind rocuronium. (**A**) IgG anti-rocuronium ELISA results from sera of mice immunized with KLH or KLH-roc. Means are indicated by horizontal bars. Each dot represents a mouse. Statistical comparisons were obtained using contrast analysis after mixed linear modeling and multiple-testing P-value adjustment. ****, $P \leq 0.0001$; *, $P \leq 0.05$; ns, not significant. (**B**) IgG anti-rocuronium ELISA results from indicated mouse mAbs or a non-specific mouse IgG as isotype control. (**C**) Anti-IgG rocuronium competition ELISA results are shown, using fixed concentrations of mouse mAbs but increasing concentrations of indicated molecules free in solution. 5α-DHT, 5-alpha-Di-Hydro-Testosterone; QAM, Quaternary Ammonium Molecule.

Figure 4: X-ray crystal structures of mAbs in complex with rocuronium. (**A**) Surface representation of co-crystal structures of rocuronium-specific mouse Fab-m2B1 (top) and scFv-m1B6 (bottom) in complex with rocuronium. (**B**) Superposition of the rocuronium and key

residues (indicated by the one-letter code of the amino acid, and their position in the chain) of the binding site for the Fab-m2B1-rocuronium complex (top) and scFv-m1B6-rocuronium (bottom). The antibody heavy chain is colored in green and light chain in cyan. In both panels, the different atoms of the rocuronium molecule are colored as: C atoms in yellow, O atoms in red, and N atoms in dark blue.

Figure 5: mAb m1B6 demonstrates therapeutic capacity to reverse neuromuscular blockade. (**A**) Prophylactic effect of indicated mAbs on rocuronium-induced neuromuscular blockade with vitality scores of wild-type mice (n≥3) as in Fig. 2E. Means ± standard deviations are indicated. Each dot represents a mouse. Statistical comparisons were obtained using contrast analysis after linear modeling and multiple-testing P-value adjustment. ***, $P \leq 0.001$, **, $P \leq 0.01$. Results for m2B1 1 to 8 mg/kg are not significant. (**B**) Scheme of the experimental protocol in macaques. (**C and D**) TOF measurement are shown for one representative macaque following rocuronium injection to monitor neuromuscular reversal without capture molecule (C) or following mAb m1B6 injection (D). The rocuronium injection time point and the time point of resumption of spontaneous ventilation (SV) and of TOF ratio T4/Tref > 0.9 are indicated. (**E and F**) Dose-dependent therapeutic effect of mAb m1B6 in macaques was assessed by time to spontaneous ventilation (E) or time for the TOF ratio T4/Tref to reach 90% (F). n=3 for all groups except n=4 for sugammadex (Suga., in mg/kg). Statistical comparisons were obtained using contrast analysis after linear modeling and multiple-testing P-value adjustment. ***, $P < 0.001$; **, $P < 0.01$; *, $P < 0.05$.

TABLES

Table 1: Clinical signs and therapeutic interventions of the allergic patients included in the study. ICU, intensive care unit; IV, intravenous; N.A., not available; ACEI, Angiotensin-Converting-Enzyme Inhibitor; ARA, Angiotensin II Receptor Antagonist; BB, Beta-blocker; CI: Calcium channel inhibitor. *includes drugs, latex, food, Hymenoptera venom, pollen/moth, and animals/mold.

Variable	**Patient #1**	**Patient #2**	**Patient #3**
Gender	Female	Male	Female
Age (years)	43	47	69
Previous general anesthesia	Yes	No	N.A.
Medication (ACEI/ARA/BB/CI)	No	N.A.	N.A.
History of allergy			
Allergy*/Asthma/Atopy	No	No	No
Mastocytosis	N.A.	No	No
Type of surgery	Visceral	Neurosurgery	Orthopedic
Scheduled surgery	Yes	Yes	Yes
Surgery with a context of infection	No	No	No
NMBA used during surgery	Atracurium	Rocuronium	Rocuronium
Clinical signs			
Erythema	No	Yes	Yes
Tachycardia	Yes	No	Yes
Highest heart rate value (/min)	100	N.A.	115
Bradycardia	No	No	No
Arrhythmia	No	No	No
Arterial hypotension	Yes	Yes	Yes
Bronchospasm	No	Yes	Yes
Hypoxemia	No	No	No
Cardiac arrest	No	No	No
Ring and Messmer severity scale	2	3	4
Delay between anesthesia induction and first signs of the reaction (min)	5	5	5
Delay between first signs of the reaction and treatment initiation (min)	15	10	10
Therapeutic interventions			
Epinephrine IV alone	No	Yes	Yes
Phenylephrine IV alone	Yes	No	No
Glucocorticoids	No	Yes	No
Histamine receptor antagonists	No	Yes	No
Fluid resuscitation with crystalloids	No	Yes	Yes
Evolution			
Surgery cancelled	No	rescheduled	rescheduled
Admission to ICU	Yes	Yes	Yes
Delay between anaphylaxis and PBMC collection (months)	24	3.5	3
Allergy exploration			
QAM IgE ImmunoCAP (threshold 0.35)	0.1	2.58	0.28
Rocuronium Basophil Activation Test (BAT)	Negative	Positive	Positive
Rocuronium Skin Prick Test (SPT)	Negative	Positive	Positive
Allergen Exposure			
Pholcodine consumption in the past 12 months prior AHR	No	No	N.A.
Previous exposure to NMBA	Yes(1993, 1996, 1999)	N.A.	Yes, once
Occupational exposure to QAM (Patients reporting current or past cleaning profession or hairdressers)	No	N.A.	N.A.
Hair coloring frequency	Regular	No	N.A.

Table 2: Characteristics of anti-rocuronium antibodies with identical heavy chain rearrangements and CDR3 amino acid sequence. Antibodies produced recombinantly with demonstrated binding to rocuronium (roc) by ELISA are indicated in bold and their ELISA values indicated for a 1µg/mL antibody concentration. nd, not determined. Number of amino acid (AA) mutations compared to the imgt database are indicated.

Patient	mAb name	V_H	CDR3 V_H	AA mutation # in V_H	V_L	CDR3 V_L	AA mutation # in V_L	roc ELISA (OD)
#1_2023	I8F7	V3−7*01 J4*02	CARGYYGSGTYYASVFDYW	7	nd	nd	nd	nd
	I8D1				nd	nd	nd	nd
	5GI5				LV2-11*01 LJ3*02	CCSFAGTKTWMF	8	nd
	I2G11				KV4-1*02 KJ1*01	CQQYYNTPWTF	9	0.16
	I1G9	V4−59*01 J4*02	CARIWGSSGNYFDFW	7	IGLV2-11*01 LJ1*01	CCSYAGSFPYVF	6	nd
	I2H6				LV2-11*01 LJ1*01	CCSYAGSFPYVF	8	0.21
	I4D10							
	I7A2	V4-59*01 J4*02	CARGTGYSSDWHVEYW	5	LV3-1*01 LJ2*01	CQAWDSSTFVMF	20	nd
	I7C8				LV1-47*01 LJ1*01	CASWDDSLRGYVF	7	nd
	I1C10	V3-7*01 J6*02	CARTDYGYYYYYGVDVW	6	LV1-51*02 LJ3*02	CGTWDSSLSAEVF	6	1.13
	I1D8							
	I7B8							
	I2H10	V4-39*01 J4*02	CVAMVRGVPAYYW	6	LV2-8*01 LJ1*01	CSSYAGSNNPYVF	4	nd
	I5G8				KV3-20*01 KJ2*01	CQQYGSSPYTF	7	nd
	I7D10	V3-53*01 IGHJ3*01	CARAQTRNLYDGSGHYYKGAFDLW	11	KV1-5*03 F KJ1*01	CQQYNSYWTF	2	nd
	I7BI7							
	I7F5	V4-61*02 J6*02	CARERRYSNGWGSYYYYGLDVW	15	LV2-18*02 LJ3*02	CSSYTNTKNWVF	10	0.23
	I2G10							
#2	G4E12	V4−38*02 J5*02	AMYYCARAPCAGECRTLNIWFDPW	41	KV3-20*01 KJ2*02	CQQYGTSPSTF	5	nd
	G5H9							nd
#3	**B1G2**	V3−21*01 J5*02	CARGHSSFDDFWSGYSPNWFDPW	1	KV4-1*01 KJ2*04	CQQYYSTPCSF	1	0.96
	B5G9							

Table 3: Characteristics of human anti-rocuronium antibodies. Antibodies were produced recombinantly and demonstrated binding to rocuronium by ELISA. They are ranked by their K_D value to HSA-rocuronium. roc, rocuronium; K_D, dissociation constant determined using biolayer interferometry for HSA-rocuronium and using surface plasmon resonance for free roc; nd, not determined; IC_{50}, half-maximal inhibitory concentration.

		Heavy chain			Light chain				
Patient	**human mAb**	**V_H gene**	**D_H gene**	**J_H gene**	**V_L gene**	**J_L gene**	**K_D to HSA-roc (nM)**	**IC_{50} free roc (μM)**	**K_D to free roc (μM)**
#1_2014	**h1F10**	V3-48	D3-10	J4*02	KV2-30	KJ2*01	21	351	140
	A4E5	V4-61*07	D2-21*01	J6*02	KV3-11*01	KJ4*01	22	917	760
	h1G12	V4-61*02	D3-3*01	J3*02	LV2-8*01	LJ1*01	28	735	>1,000
	h6E11	V3-15*07	D3-22*01	J6*02	KV1-5*03	KJ2*01	30	nd	nd
	A6H7	V4-39*01	D2-15*01	J6*02	KV3-11*01	KJ4*01	35	917	>2,000
#2	**D3F8**	V4-39*08	D2-21*01	J6*03	KV3-15*01	J4*01	40	464	>2,000
#1_2014	**hA3E12**	V3-30*18	D6-13*01	J6*02	KV1-9*01	KJ2*01	49	539	nd
	h1B8	V4-39*01	D3-3*01	J3*02	KV4-1*01	KJ1*01	50	375	nd
	hA5H5	V4-61*02	D6-19*01	J3*02	GKV3-11*01	KJ1*01	63	684	nd
	h6A12	V1-2	D3-16	J4*02	KV1-5	KJ3*01	74	2,100	nd
	hA10A9	V1-18	D2-8	J1*01	LV2-14	LV2-14*03	249	2,718	nd
	hA8D8	V1-69*06	D3-22*01	J6*02	KV1-5*03	KJ2*01	257	473	nd
#2	**E9B10**	V4-34*01	D3-22*01	J3*01	KV1-39*01	KJ4*01	275	2,105	nd
#1_2014	**h2D6**	V3-30-3	D2-15	J5*02	KV2-28	KJ2*01	922	612	nd
#2	**E11B8**	V4-30-4*09	D3-10*02	J6*03	KV3-20*01	KJ1*01	nd	2,191	nd
	E11G7	V4-61*01	D6-6*01	J4*02	KV1-39*01	KJ4*01	nd	nd	nd

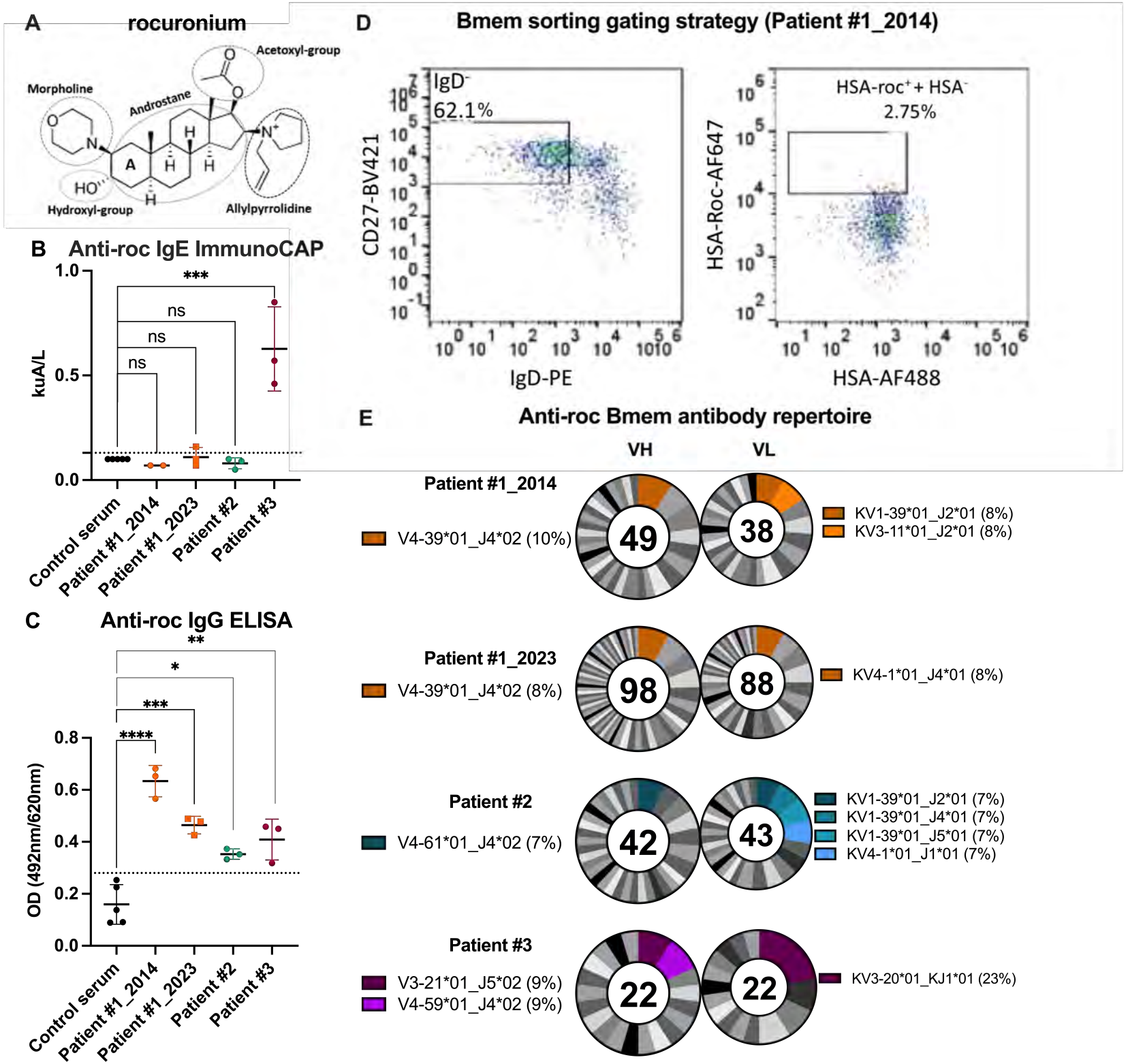
A
rocuronium
Acetoxyl-group
Morpholine
Androstane
Hydroxyl-group
Allylpyrrolidine
B
Anti-roc IgE ImmunoCAP
kuA/L
***
ns
ns
ns
Control serum
Patient #1_2014
Patient #1_2023
Patient #2
Patient #3
C
Anti-roc IgG ELISA
OD (492nm/620nm)
**
*
***
****
D
Bmem sorting gating strategy (Patient #1_2014)
IgD-
62.1%
CD27-BV421
IgD-PE
HSA-roc+ + HSA-
2.75%
HSA-Roc-AF647
HSA-AF488
E
Anti-roc Bmem antibody repertoire
VH
VL
Patient #1_2014
V4-39*01_J4*02 (10%)
49
38
KV1-39*01_J2*01 (8%)
KV3-11*01_J2*01 (8%)
Patient #1_2023
V4-39*01_J4*02 (8%)
98
88
KV4-1*01_J4*01 (8%)
Patient #2
V4-61*01_J4*02 (7%)
42
43
KV1-39*01_J2*01 (7%)
KV1-39*01_J4*01 (7%)
KV1-39*01_J5*01 (7%)
KV4-1*01_J1*01 (7%)
Patient #3
V3-21*01_J5*02 (9%)
V4-59*01_J4*02 (9%)
22
22
KV3-20*01_KJ1*01 (23%)

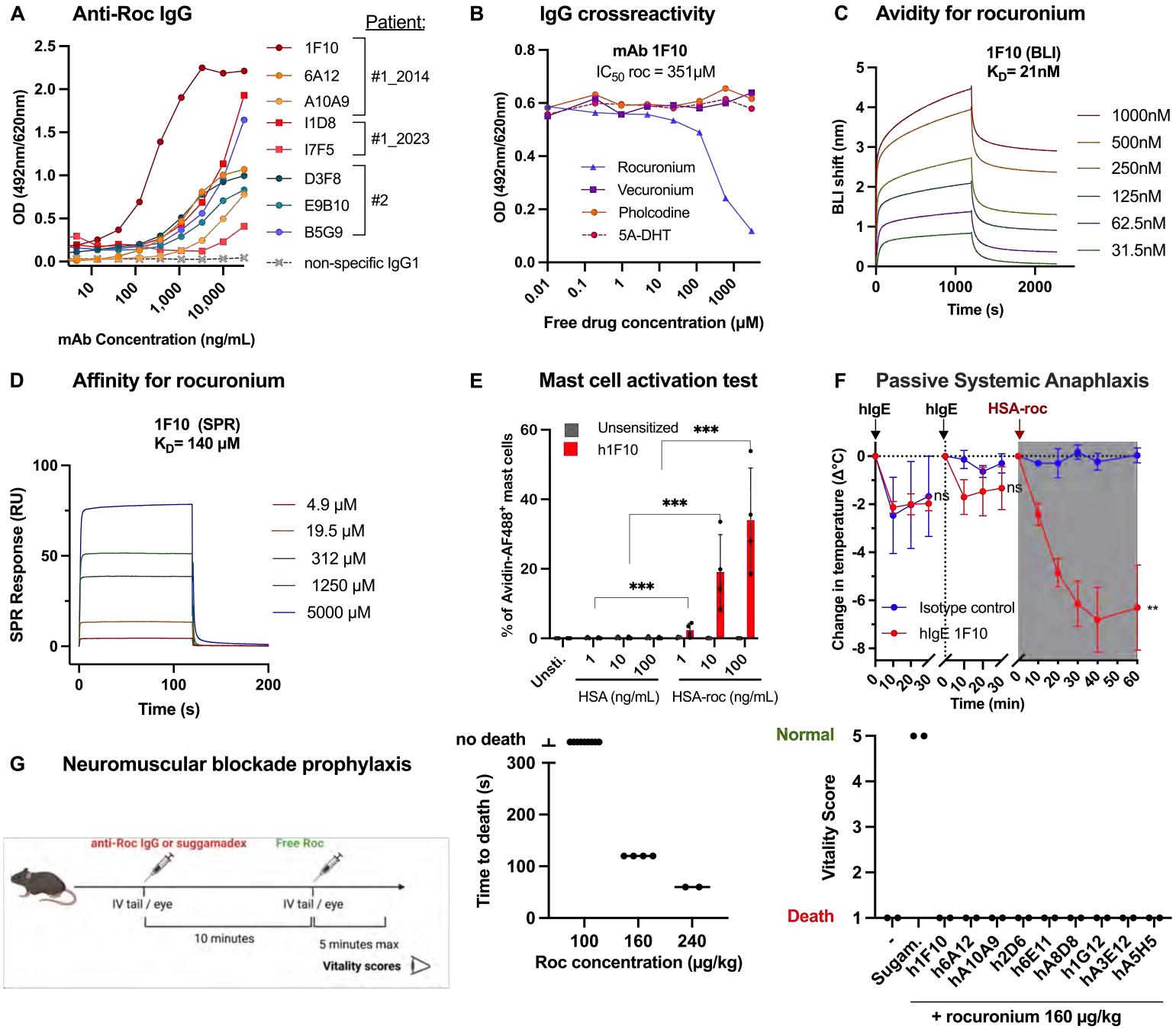
A
Anti-Roc IgG
Patient:
1F10
6A12
A10A9
I1D8
I7F5
D3F8
E9B10
B5G9
non-specific IgG1
#1_2014
#1_2023
#2
OD (492nm/620nm)
mAb Concentration (ng/mL)
B
IgG crossreactivity
mAb 1F10
IC50 roc = 351µM
Rocuronium
Vecuronium
Pholcodine
5A-DHT
Free drug concentration (µM)
C
Avidity for rocuronium
1F10 (BLI)
KD= 21nM
1000nM
500nM
250nM
125nM
62.5nM
31.5nM
BLI shift (nm)
Time (s)
D
Affinity for rocuronium
1F10 (SPR)
KD= 140 µM
4.9 µM
19.5 µM
312 µM
1250 µM
5000 µM
SPR Response (RU)
Time (s)
E
Mast cell activation test
Unsensitized
h1F10
% of Avidin-AF488+ mast cells
Unsti.
HSA (ng/mL)
HSA-roc (ng/mL)
F
Passive Systemic Anaphlaxis
hIgE
hIgE
HSA-roc
Isotype control
hIgE 1F10
Change in temperature (Δ°C)
Time (min)
G
Neuromuscular blockade prophylaxis
anti-Roc IgG or suggamadex
Free Roc
IV tail / eye
IV tail / eye
10 minutes
5 minutes max
Vitality scores
no death
Time to death (s)
Roc concentration (µg/kg)
Normal
Death
Vitality Score
Sugam.
h1F10
h6A12
hA10A9
h2D6
h6E11
hA8D8
h1G12
hA3E12
hA5H5
+ rocuronium 160 µg/kg

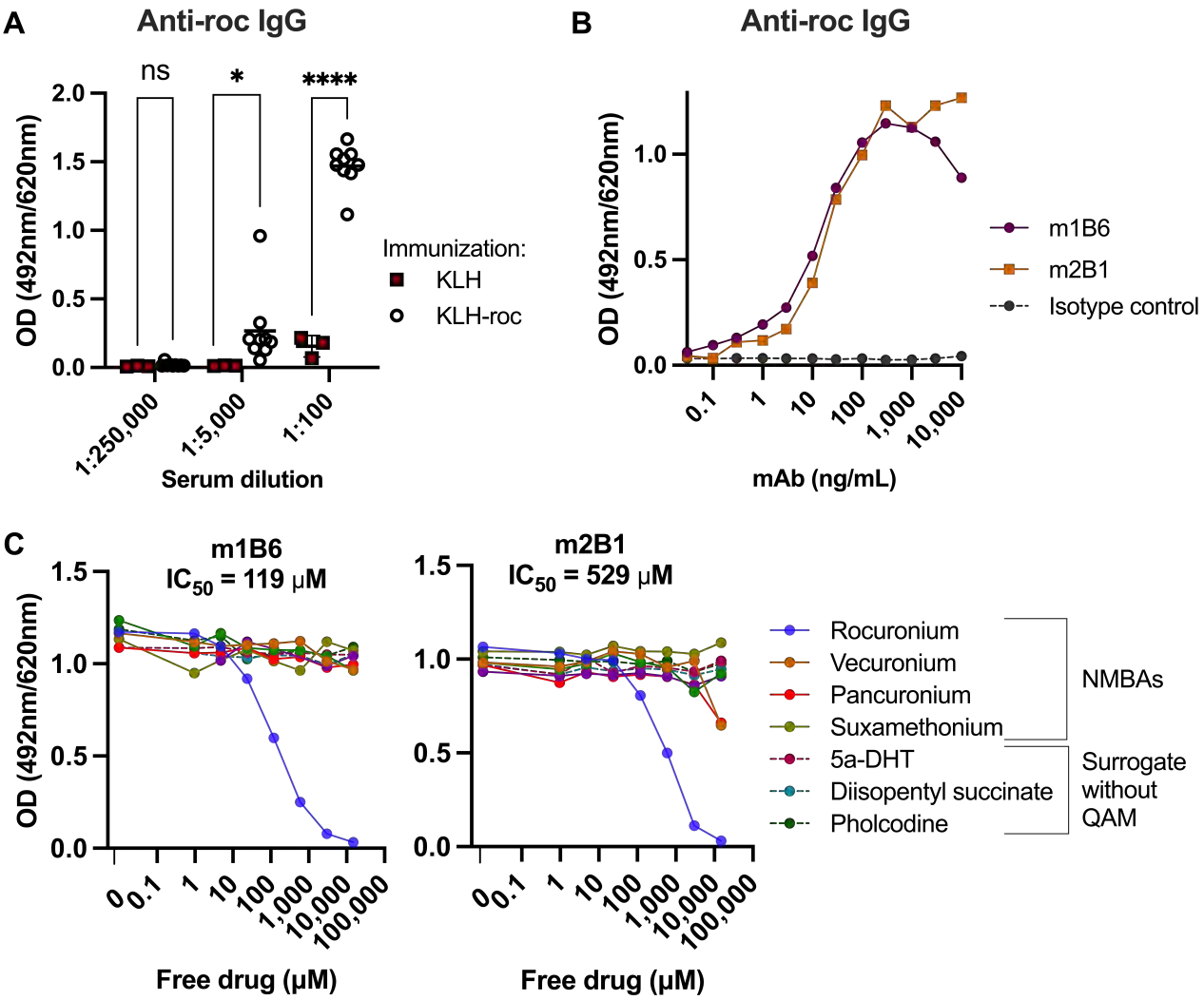
A
Anti-roc IgG
ns
*
****
OD (492nm/620nm)
2.0
1.5
1.0
0.5
0.0
1:250,000
1:5,000
1:100
Serum dilution
Immunization:
KLH
KLH-roc
B
Anti-roc IgG
OD (492nm/620nm)
1.0
0.5
0.0
0.1
1
10
100
1,000
10,000
mAb (ng/mL)
m1B6
m2B1
Isotype control
C
m1B6
IC50 = 119 µM
m2B1
IC50 = 529 µM
OD (492nm/620nm)
1.5
1.0
0.5
0.0
0
0.1
1
10
100
1,000
10,000
100,000
Free drug (µM)
Rocuronium
Vecuronium
Pancuronium
Suxamethonium
5a-DHT
Diisopentyl succinate
Pholcodine
NMBAs
Surrogate without QAM

A

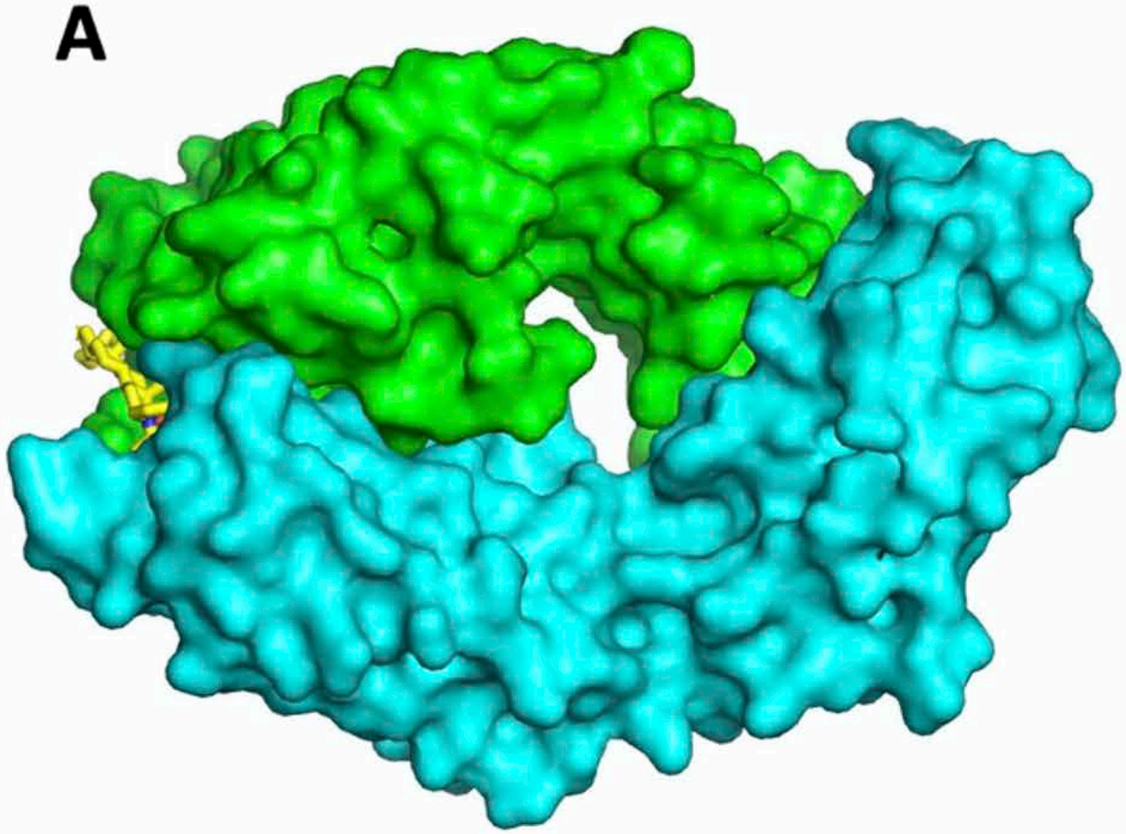

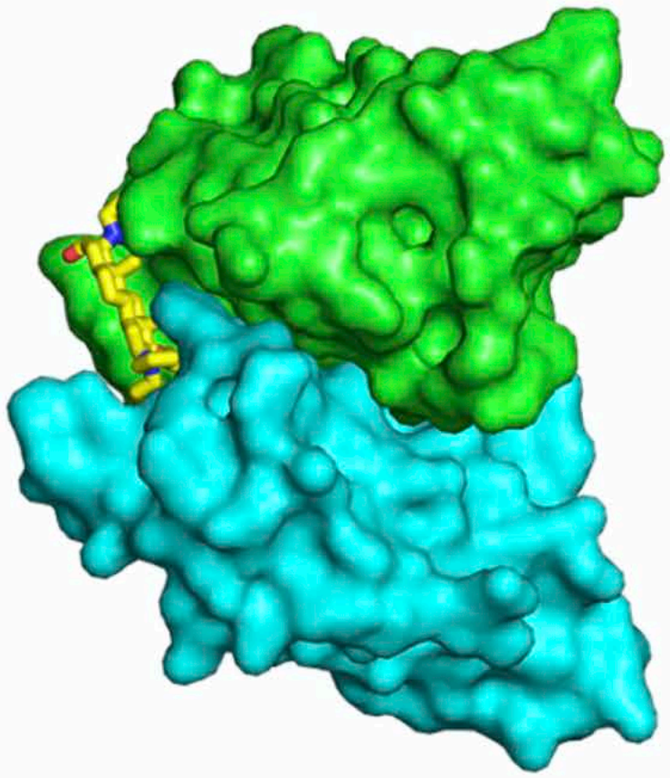

B

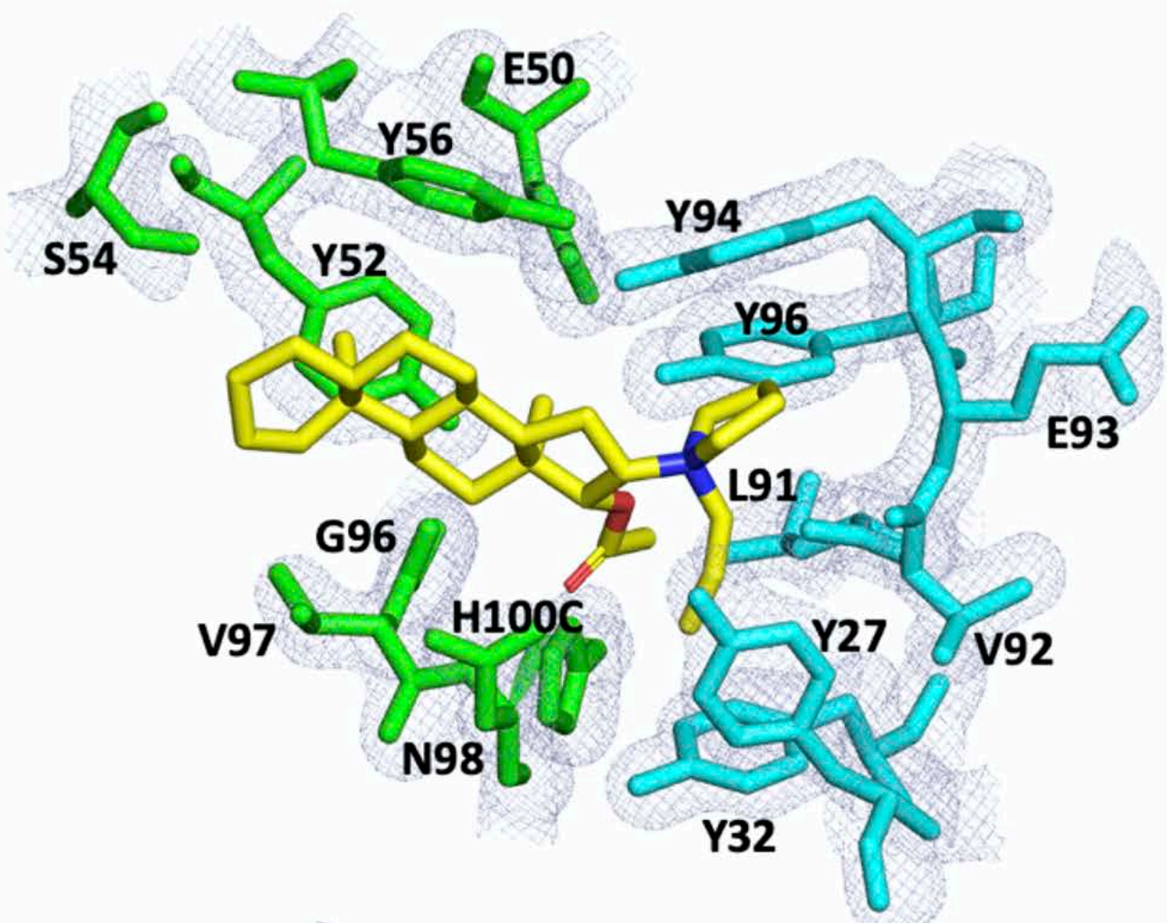
E50
Y56
S54
Y52
Y94
Y96
E93
L91
G96
V97
H100C
Y27
V92
N98
Y32

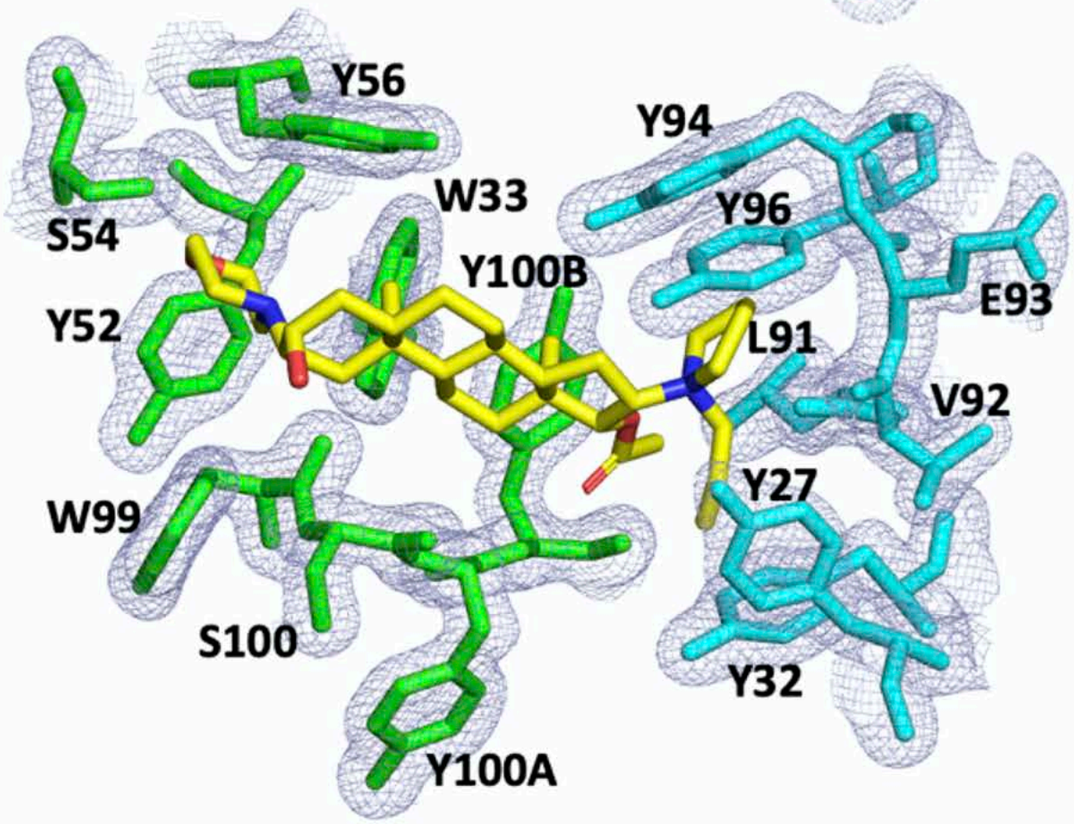
Y56
Y94
W33
S54
Y96
Y100B
E93
Y52
L91
V92
Y27
W99
S100
Y32
Y100A

Neuromuscular blockade prophylaxis

Neuromuscular blockade reversal

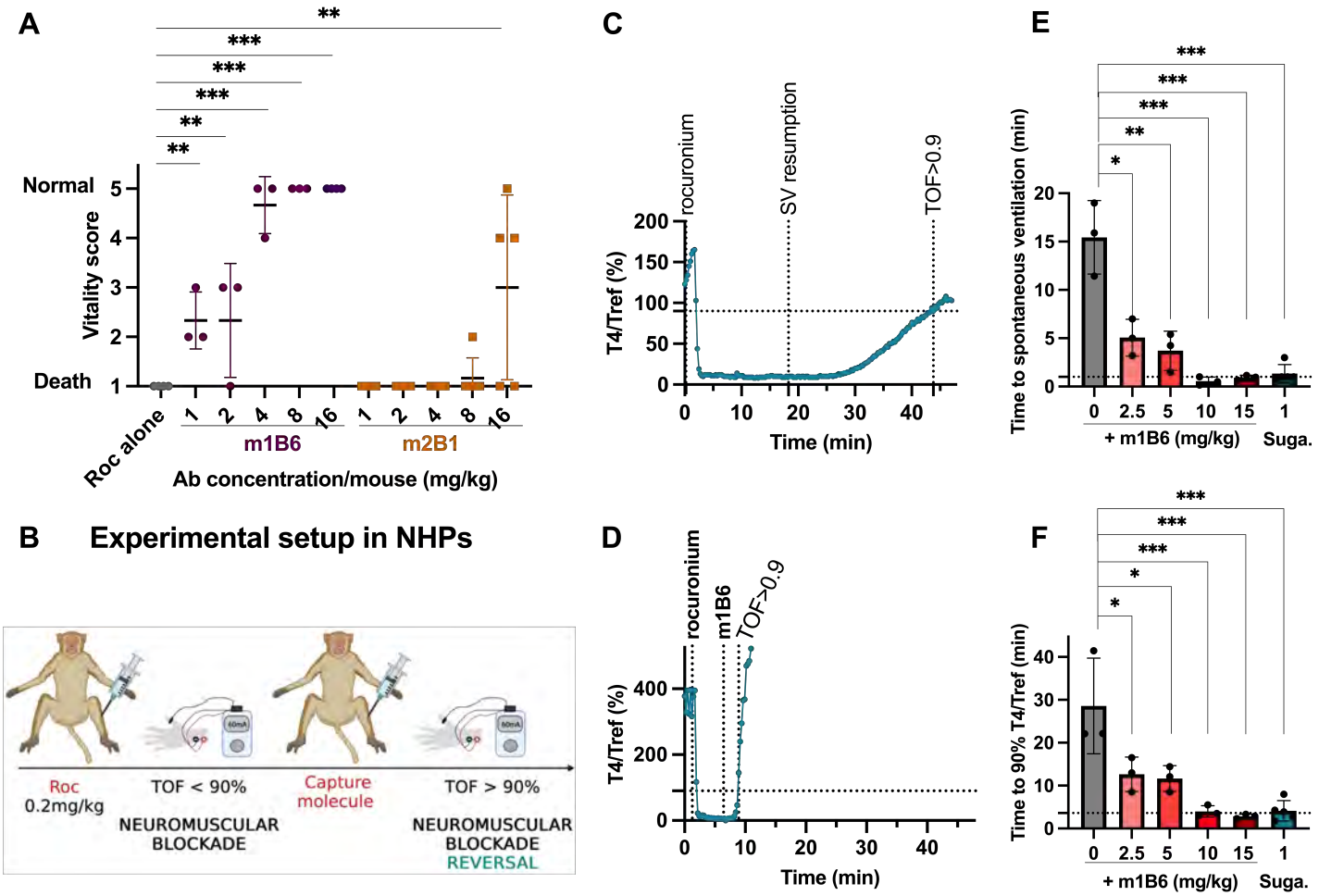

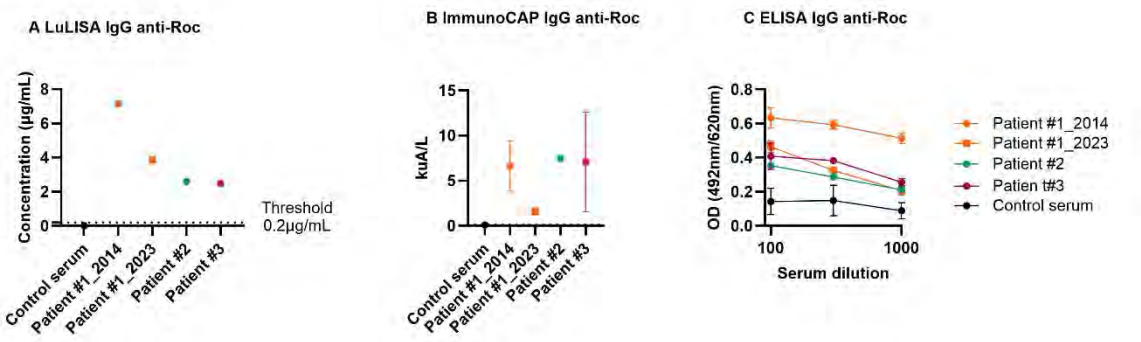

Fig. S1. **Screening for anti-rocuronium (roc) IgG in patients' serum samples.** (**A to C**) IgG anti-rocuronium detection by Luciferase-linked immunosorbent **assay (**LuLISA) with a cut-off at 0.2 µg/mL (n=1 replicate) (**A**), ImmunoCAP with a cut-off at 0.13 kUA/L (n≥1 replicates) (**B**), and ELISA performed in triplicate (**C**), in the serum of indicated patients or serum from five blood bank donors. Data are presented as Mean± Standard Error of Mean (SEM).

A

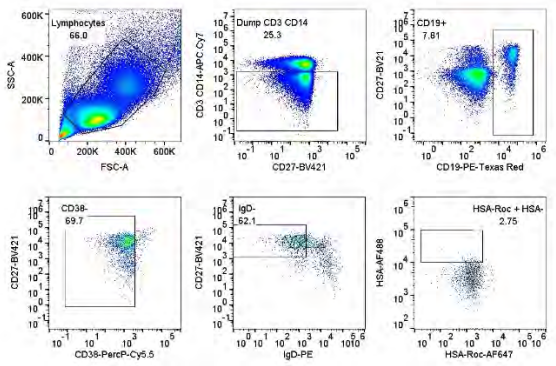

B

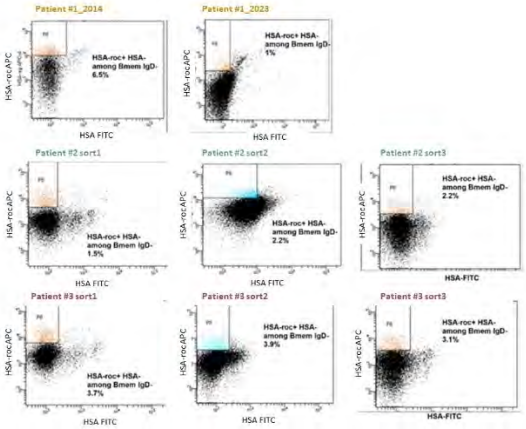

C

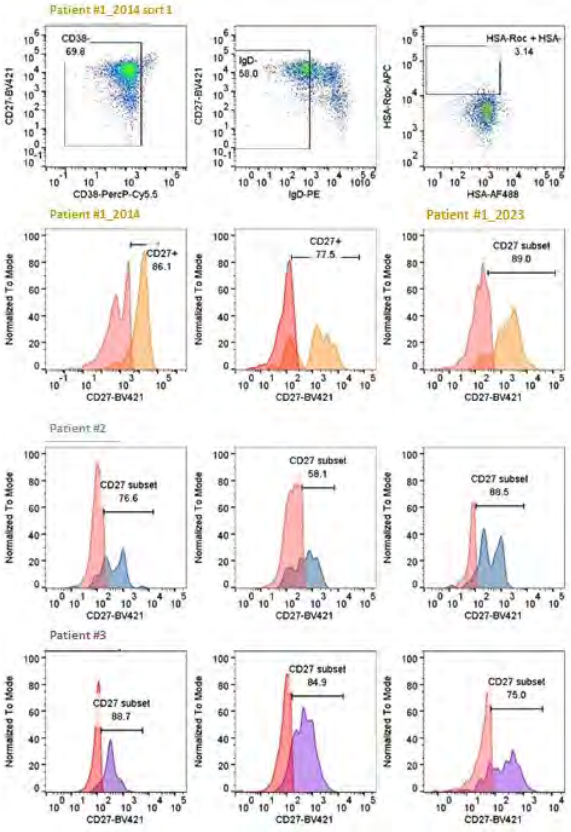

Fig. S2. Gating strategy for the sorting of rocuronium-binding human memory B cells from human peripheral blood mononuclear cells (PBMCs). (**A**) Full gating strategy for the single-cell sort of rocuronium-binding memory B cells ($CD3^-$ $CD14^-$ $CD19^+$ $CD38^-$ $CD27^+$ IgD^- Human serum albumin (HSA)-roc^+ HSA^-) from the PBMCs of Patient #1_2014, as in Fig. 1D. (**B**) Dot plots showing the final sorting gate for all the sorts with percentages of cells gated among the represented cells in each panel. (**C**) Back gating of the $CD27^+$ population among $CD3^-$, $CD14^-$, $CD38^-$, $CD19^+$, HSA-Roc^+, HSA^-, IgD^- cell populations. Histogram of the $CD27^+$ population for Patient #1 (orange), Patient #2 (blue) and Patient #3 (purple) are superimposed on the histogram of the $CD3^-$, $CD14^-$, $CD38^-$, and $CD27^-$ population. Percentage of $CD27^+$ among antigen-specific cells are calculated compared to the $CD27^-$ population.

A

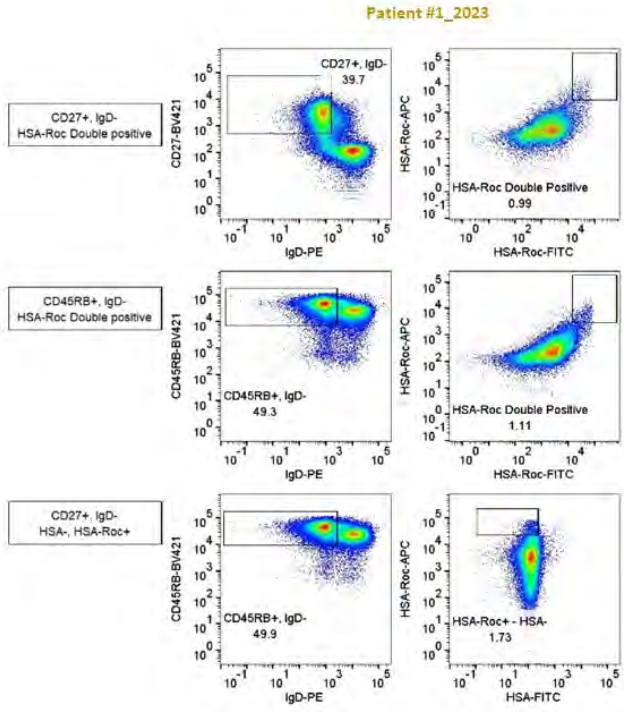

B

		Sorting data			Monoclonal cultures				
		IgD⁻ among Bmem (%)	**Antigen screen**	**Sorted cells among IgD⁻ Bmem (%)**	**(i) cultured cells #**	**Positive HSA-roc ELISA # (% of i)**	**Not inhibited by free rocuronium # (% of i)**	**(ii) Total rocuronium-binding cultures # (% of i)**	**Strong binders # (% of ii)**
CD27⁺ memory B cells	**Patient #1_2023**	39.7%	HSA-rocuronium-APC *versus* HSA-rocuronium-AF488	0.99%	**768**	78 (10.2%)	9 (1.2%)	**69 (9%)**	57 (81%)
CD45RB⁺ memory B cells		49.3%		1.11%	**672**	34 (5.0%)	2 (0.3%)	**32 (4.7%)**	18 (56%)
CD45RB⁺ memory B cells		*49.9%*	HSA-rocuronium-APC versus HSA-AF488	*1.72%*	**672**	*38 (5.7%)*	*5 (0.7%)*	***33 (4.9%)***	*16 (48%)*

Fig. S3. Analysis and quantification of single-cell sorts of rocuronium-binding memory B cells (Bmem). (**A**) Analysis of single-cell sorts of rocuronium-binding $CD27^+$ memory B cells and $CD45RB^+$ memory B cells. $CD3^-$ $CD14^-$ $CD19^+$ $CD38^-$ PBMCs from Patient #1_2023 were gated for (top, left) $CD27^+$ IgD^- cells, or (middle, left and bottom, left) $CD45RB^+$ IgD^- cells, and immediately on their right for (top and middle) HSA-roc-allophycocyanin (APC)$^+$/HSA-roc-Alexa Fluor (AF)488^+ ("HSA-roc double positive") or HSA-roc-APC^+/HSA-$AF488^-$ ("HSA-roc^+ HSA^-"). Numbers in the panels indicate the percentage of cells gated among the represented cells in each panel. The gates in the right column were used for single cell sorting. (**B**) Summary of sorting data and monoclonal cultures. The middle and bottom row correspond to data of sorts performed with antigen (HSA-rocuronium) labeled with two different fluorophores and gated on double-positive cell populations, or with antigen labeled with a single fluorophore and gated on the corresponding positive cell population, respectively. Rocuronium specificity was assessed using competition ELISA for which free rocuronium inhibited a minimum of 50% of the optical density (OD) value in the absence of free rocuronium. Strong binding to HSA-roc (extreme right column) was determined by the ratio of the OD of the HSA-rocuronium ELISA on the OD of the IgG ELISA, with a ratio>1 being considered a strong binder.

A

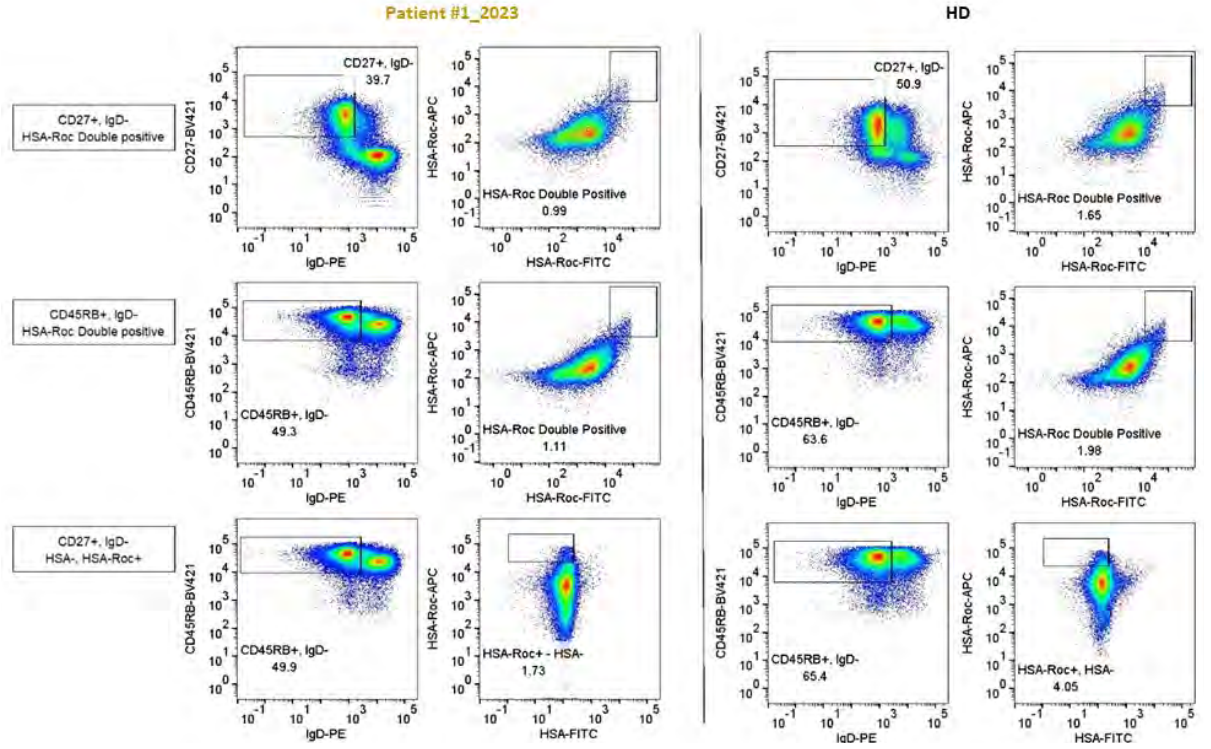

B

	Sorting data			Monoclonal cultures				
Patient	**Sort**	**CD27+ IgD- or CD45RB+ IgD- among Bmem cells %**	**Sorted cells %**	**(A) cultured cells #**	**Positive HSA-roc ELISA #**	**Not inhibited by free rocuronium #**	**(B) Total rocuronium-binding cultures # (% of A)**	**Strong binders # (% of B)**
#1_2023	CD27+ double positive	39.7	0.99	768	78	9	69 (9.0%)	56 (**81**%)
HD		50.9	1.65	768	36	0	36 (4.7%)	22 (**61**%)
#1_2023	CD45RB+ double positive	49.3	1.11	672	34	6	28 (4.2%)	19 (**67**%)
HD		63.6	1.98	288	15	2	13 (4.5%)	5 (**38**%)
#1_2023	CD45RB+ HSA-roc+ HSA-	49.9	1.73	672	38	13	25 (3.7%)	21 (**84**%)
HD		65.4	4.05	288	14	0	14 (4.8%)	4 (**29**%)

Fig. S4. Analysis of single-cell sorts of rocuronium-binding CD27$^+$ memory B cells and CD45RB$^+$ memory B cells from Patient #1_2023 and a healthy donor (HD). (**A**) CD3$^-$ CD14$^-$ CD19$^+$ CD38$^-$ PBMCs from indicated individuals were gated for (top) CD27$^+$ IgD$^-$ cells, or (middle and bottom) CD45RB$^+$ IgD$^-$ cells, and immediately on their right for (top & middle) HSA-roc-APC$^+$/HSA-roc-AF488$^+$ ("HSA-roc double positive") or HSA-roc-APC$^+$/HSA-AF488$^-$ ("HSA-roc$^+$ HSA$^-$"). Numbers in the panels indicate the percentage of cells gated among the represented cells in each panel. The gates in the right column were used for single cell sorting. (**B**) Summary of sorting data and monoclonal cultures. Rocuronium specificity was assessed using competition ELISA for which free rocuronium inhibited a minimum of 50% of the OD value in the absence of free rocuronium. Strong binding to HSA-roc (extreme right column) was determined by the ratio of the OD of the HSA-rocuronium ELISA on the OD of the IgG ELISA, with a ratio>1 being considered a strong binder.

A

	VH mutations			VL mutations		
Patient	**mean**	median	standard deviation	**mean**	median	standard deviation
#1_2014	**16.9**	14	12.9	**9.2**	10	4.9
#1_2023	**11.5**	11	6.5	**5.0**	4	3.6
#2	**15.0**	15	8.4	**7.8**	8	4.8
#3	**6.0**	2	8.7	**2.9**	1	3.7
All	**13.0**	12	9.6	**6.3**	5.5	4.7

B

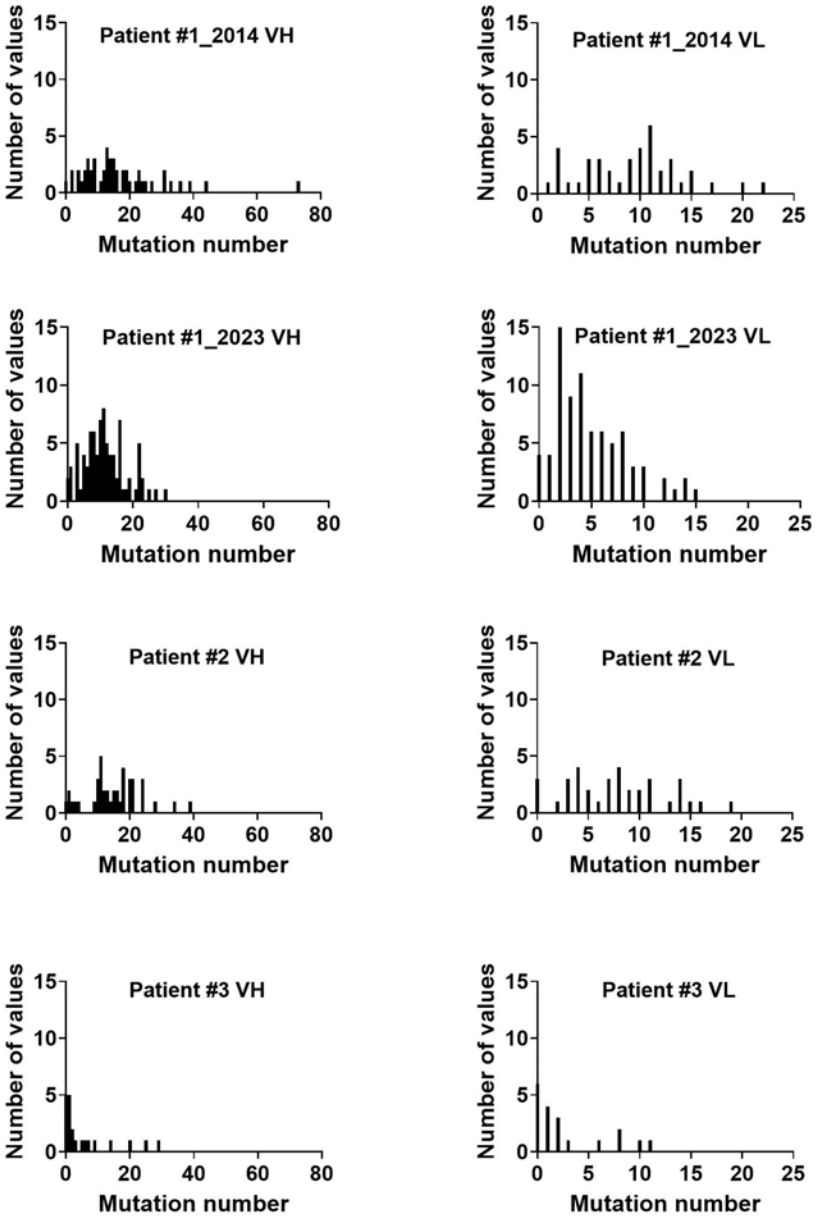

Fig. S5. **Anti-rocuronium human VH and VL nucleotide mutation frequency**. (**A**) VH and VL mutation frequencies compared to germline for each patient. (**B**) Distribution of mutation frequency among (left) VH sequences and (right) VL sequences compared to germline in indicated patient samples.

A

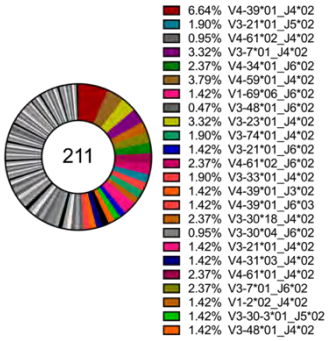
211
6.64% V4-39*01_J4*02
1.90% V3-21*01_J5*02
0.95% V4-61*02_J4*02
3.32% V3-7*01_J4*02
2.37% V4-34*01_J6*02
3.79% V4-59*01_J4*02
1.42% V1-69*06_J6*02
0.47% V3-48*01_J6*02
3.32% V3-23*01_J4*02
1.90% V3-74*01_J4*02
1.42% V3-21*01_J6*02
2.37% V4-61*02_J6*02
1.90% V3-33*01_J4*02
1.42% V4-39*01_J3*02
1.42% V4-39*01_J6*03
2.37% V3-30*18_J4*02
0.95% V3-30*04_J6*02
1.42% V3-21*01_J4*02
1.42% V4-31*03_J4*02
2.37% V4-61*01_J4*02
2.37% V3-7*01_J6*02
1.42% V1-2*02_J4*02
1.42% V3-30-3*01_J5*02
1.42% V3-48*01_J4*02

B

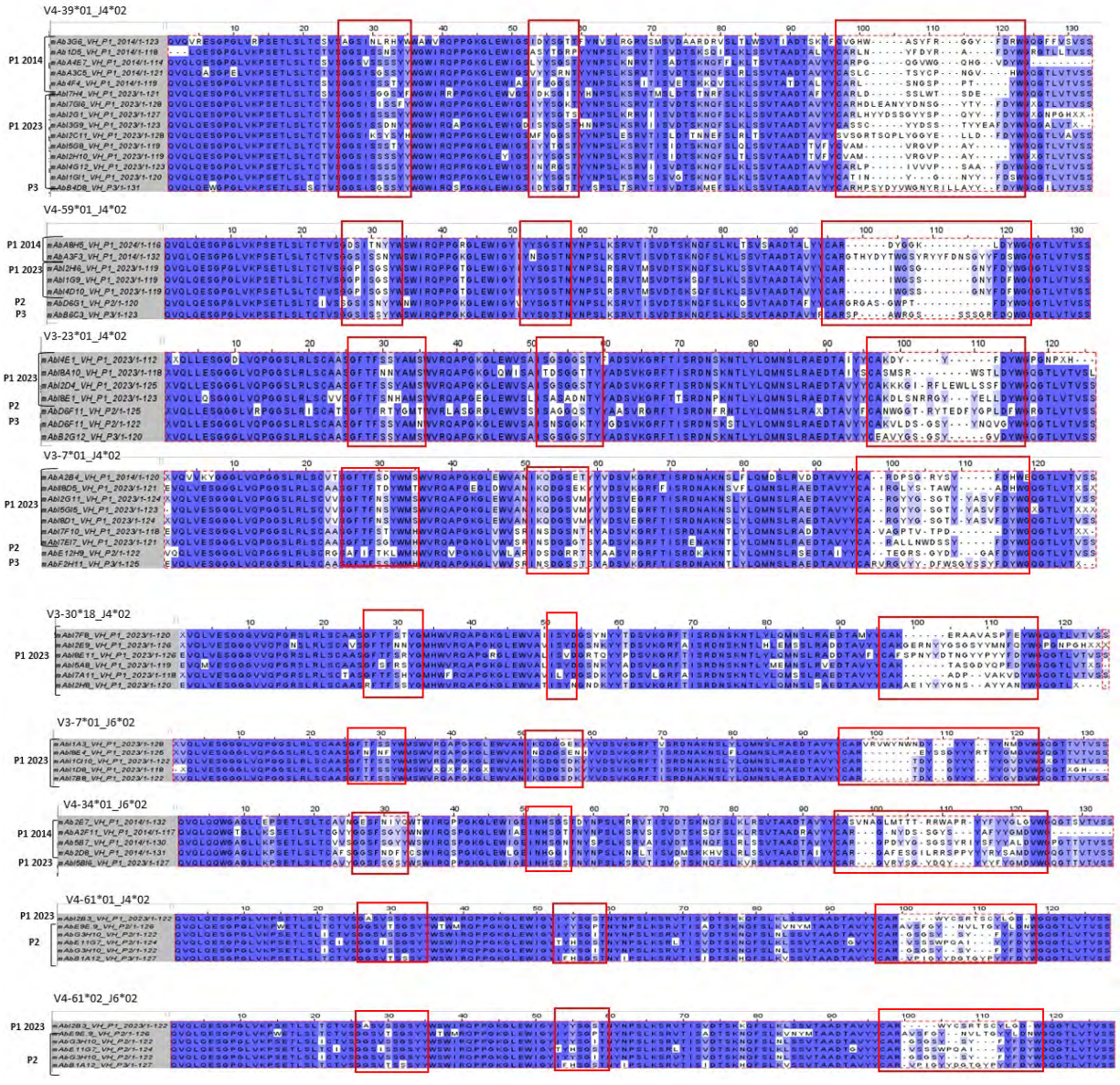
V4-39*01_J4*02
V4-59*01_J4*02
V3-23*01_J4*02
V3-7*01_J4*02
V3-30*18_J4*02
V3-7*01_J6*02
V4-34*01_J6*02
V4-61*01_J4*02
V4-61*02_J6*02
P1 2014
P1 2023
P2
P3

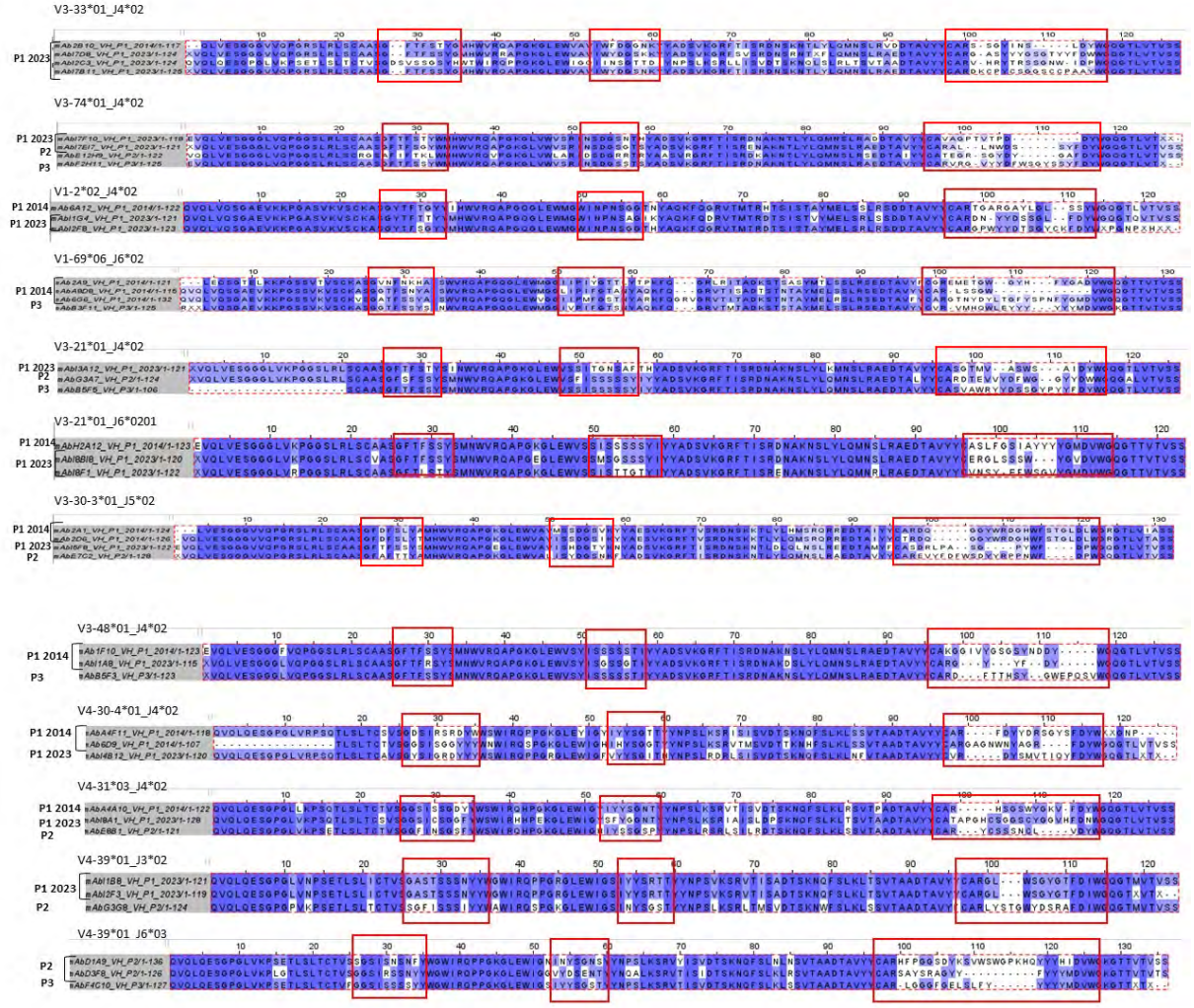

Fig. S6. Antibody repertoire analysis of the different patients. (**A**) Donut plot of V-J gene usage among all the VH (n=211, indicated in the center of the donut) sequenced from monoclonal B cell cultures of the 3 patients (P1 2014, Patient #1_2014; P1 2023, Patient #1_2023; P2, Patient #2; P3, Patient #3). The major V-J recombinations and their percentage are indicated in color. (**B**) Sequence alignment of the amino acid VH sequences from the 22 V-J families composed of at least 3 members using MUltiple Sequence Comparison by Log- Expectation (Muscle) and colored by percentage identity. Complementary determining regions (CDRs) are framed in red. Names of the V-J families are indicated over the alignments.

A

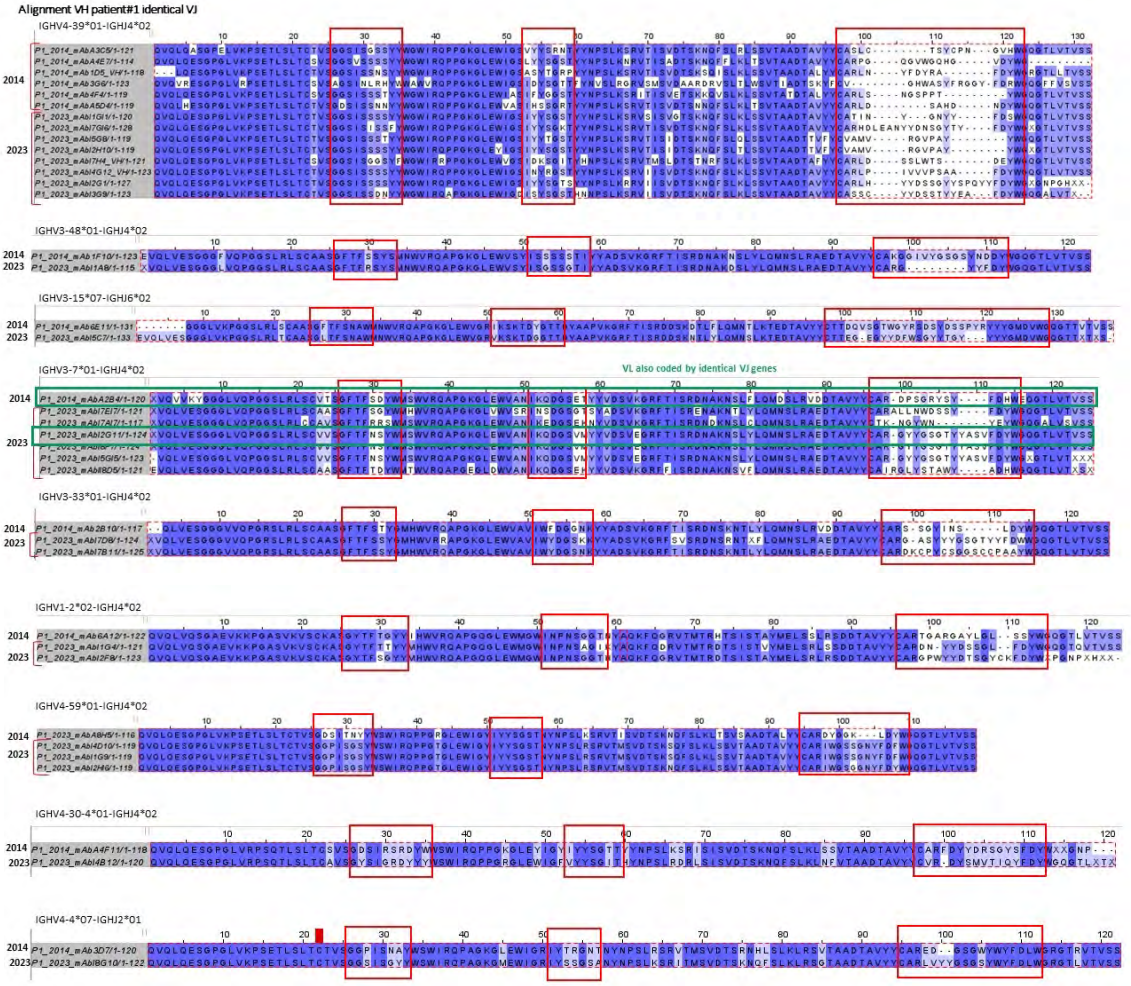

B

	VH CDR3	% ID VH	VL CDR3	% ID VL
mAb A2B4 Patient #1_2014	CARDPSGRYSYFDHW	81	CQQYYSIPPGTF	86
mAb I2G11 Patient #1_2023	CARGYYGSGTYYASVFDYW		CQQYYNTPWTF	

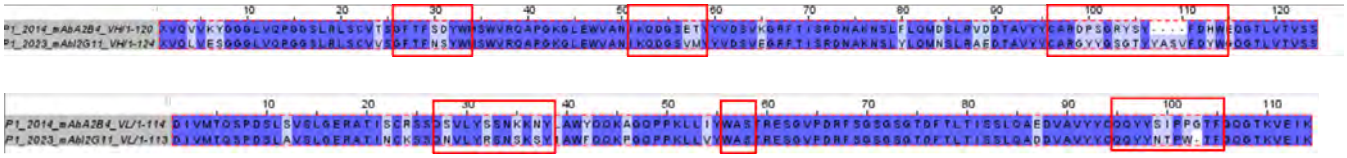

Fig. S7. Anti-rocuronium antibody repertoire comparison between Patient #1_2014 and Patient #1_2023. (**A**) Sequence alignment of the amino acid VH sequences coded by identical V-J genes using MUltiple Sequence Comparison by Log- Expectation (Muscle) and colored by percentage identity. CDRs are framed in red. Among those, two VH sequences (A2B4 and I2G11) also share the same light chain rearrangement and are highlighted in green. (**B**) Comparison of monoclonal antibodies (mAbs) A2B4 and I2G11 with percentage similarities of pairwise alignment of the complete VH amino acid sequence. (P1_2014, Patient #1_2014; P1_2023, Patient #1_2023).

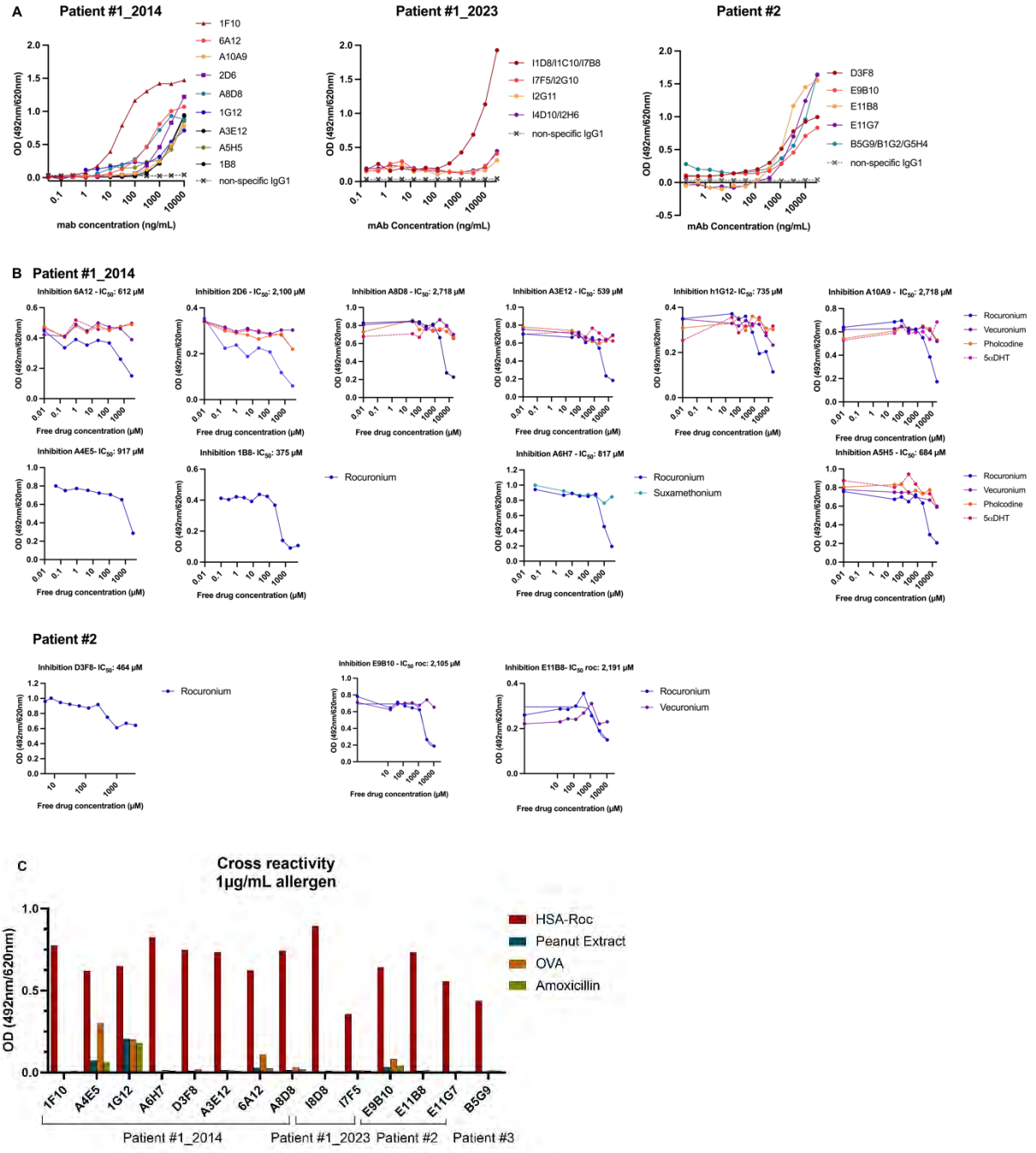

Fig. S8. Characterization of human anti-rocuronium mAbs. (**A**) Binding of human mAbs to HSA-rocuronium by ELISA. (**B**) "Competitive ELISA" of anti-IgG rocuronium ELISA from Patient #1_2014 and Patient #2 at fixed mAb concentration (1.5 μg/mL) but increasing concentrations of indicated molecules free in solution. 5αDHT: 5-alpha-Di-Hydro-Testosterone; IC50, Half-maximal inhibitory concentration. (**C**) Cross-reactivity test by ELISA of representative mAbs. Various allergens [peanut extract, amoxicillin, and ovalbumin (OVA)] were coated at 1 μg/mL with mAb concentrations (2μg/mL to 0.03 μg/mL). For a fixed mAb concentration giving a signal of approximately OD 0.7, the signal given for the representative allergen is represented.

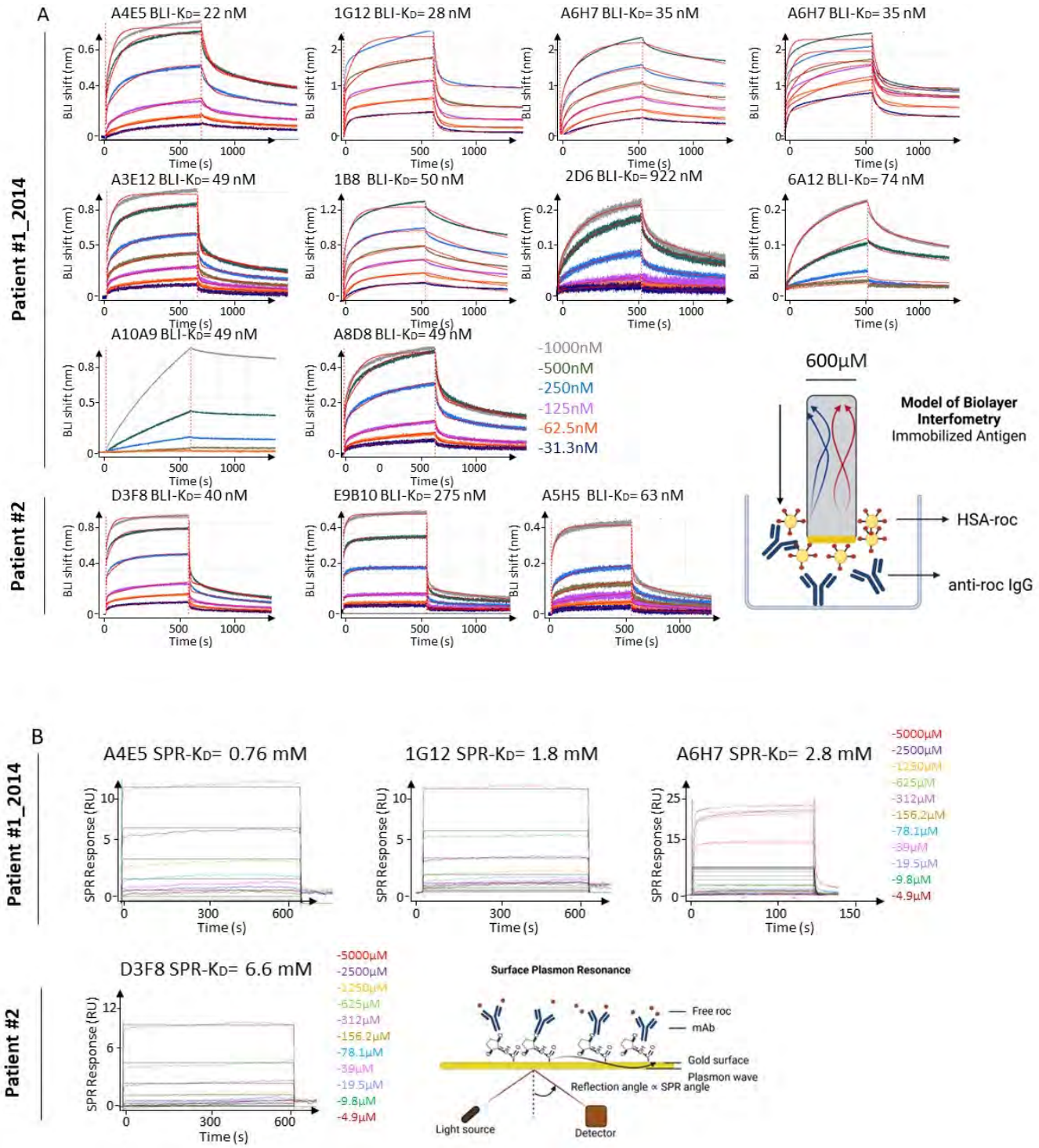

Fig. S9. Avidity and affinity of human anti-rocuronium mAbs for haptenized or free rocuronium. (**A**) Bio-layer interferometry (BLI) avidity measurement of the interaction between immobilized HSA-roc and varying concentrations of human mAbs in solution. A scheme of the setup is provided. (**B**) Surface Plasmon Resonance affinity measurement of the interaction between immobilized human mAbs captured by an anti-Fc and varying concentrations of free rocuronium in solution. A scheme of the setup is provided. For (A and B), the dissociation constant (K_D) was obtained by fitting the curves using a heterogenous ligand model.

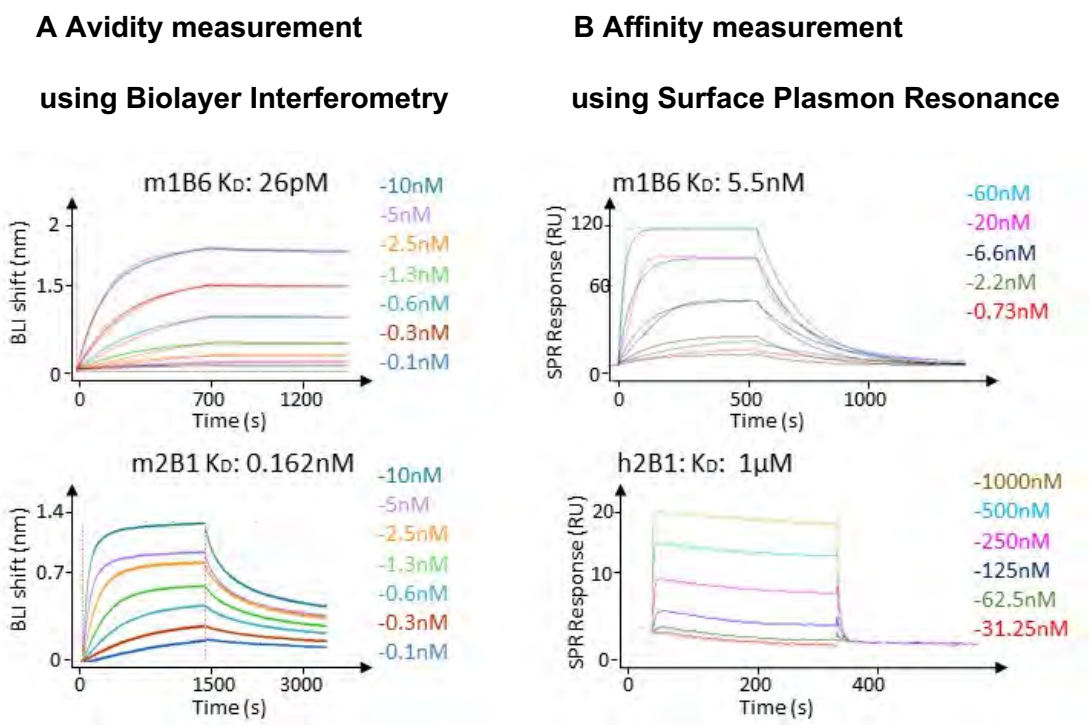

Fig. S10. Avidity and Affinity of mouse anti-rocuronium mAbs for haptenized or free rocuronium. (**A**) Bio-layer interferometry avidity measurement of the interaction between immobilized HSA-roc and varying concentrations of mouse mAbs in solution. (**B**) Surface plasmon resonance (SPR) affinity measurement of the interaction between immobilized mouse mAbs captured by an anti-Fc and varying concentrations of free rocuronium in solution. RU, response units. In (A and B), fitting was performed using kinetic analysis and 1:1 binding. The dissociation constant (K_D) values are indicated.

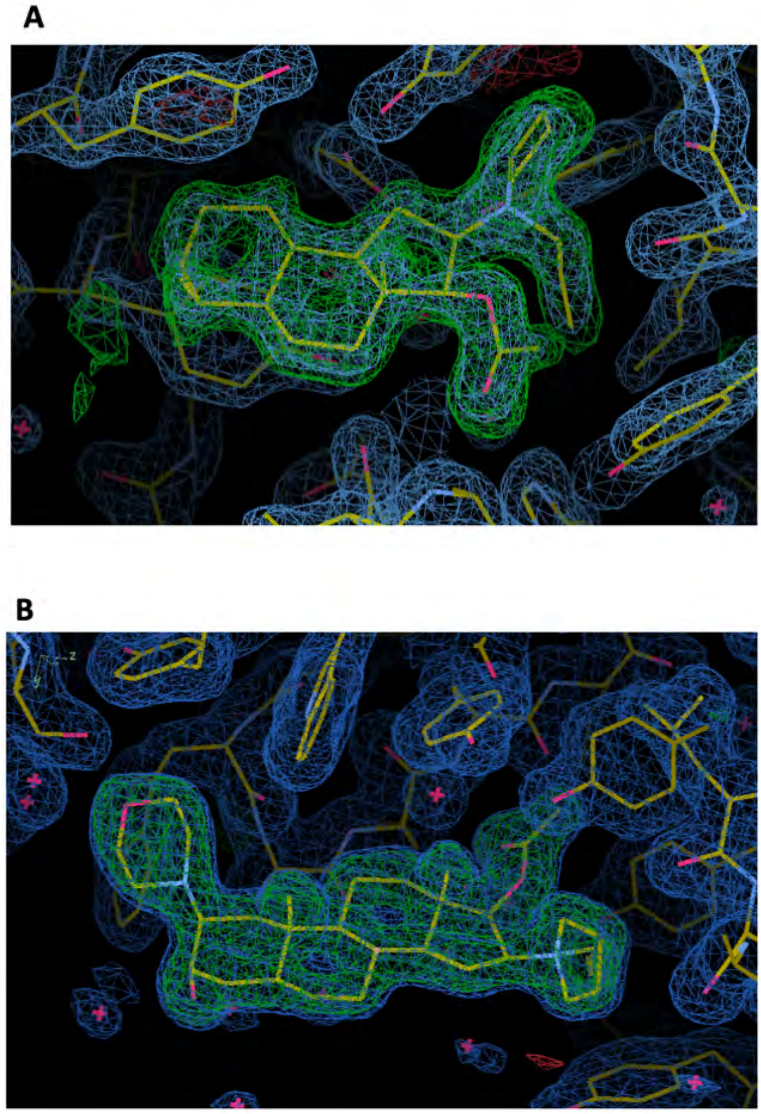

Fig. S11. Density map of rocuronium within the binding cleft of mAb m2B1 and mAb m1B6. (**A and B**) 2Fo-Fc electron density omitmap contoured at 3.5σ of Fab-m2B1-rocuronium (A) and scFv-m1B6-rocuronium (B), showing the rocuronium molecule in the binding site of both antibodies.

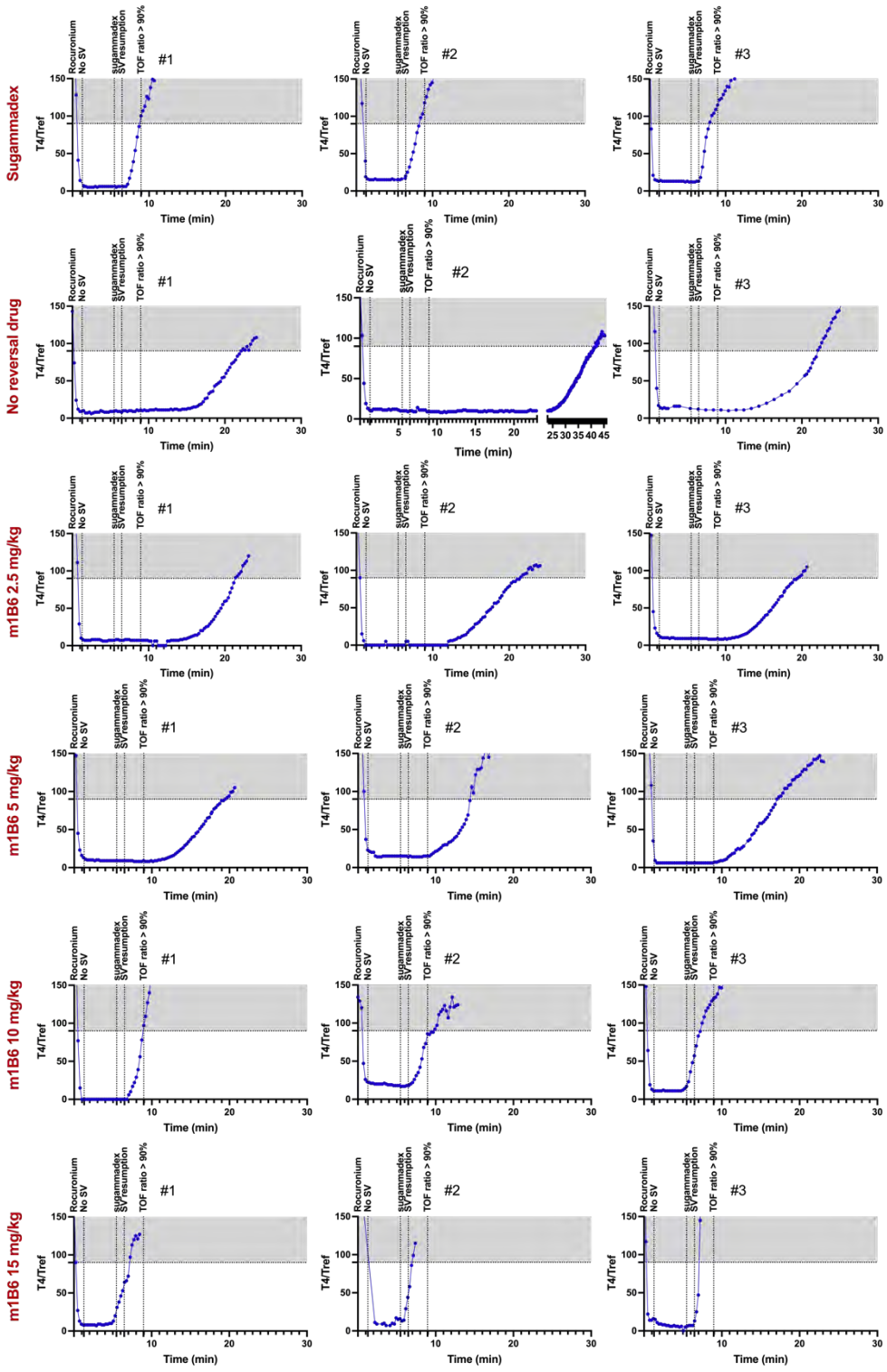

Fig. S12. Train of four (TOF) measurement in the non-human primate cohort. TOF measurement in macaques following rocuronium injection (200 µg/kg) to monitor neuromuscular reversal following injection of indicated compounds. The time points of rocuronium injection, compound injection, resumption of spontaneous ventilation (SV) and TOF ratio T4/Tref > 0.9 are indicated in shaded gray. Once deep neuromuscular blockade was established (absence of T1 response), indicated concentrations of (first row) sugammadex, (second row) vehicle, (third row) m1B6 at 2.5 mg/mL, (fourth row) m1B6 at 5 mg/mL, (fifth row) m1B6 at 10 mg/mL, or (sixth row) m1B6 at 15 mg/mL were injected. The ID of each macaque is indicated. The red box indicates an involuntary interruption of monitoring for the 15 mg/mL condition of non-human primate #2.

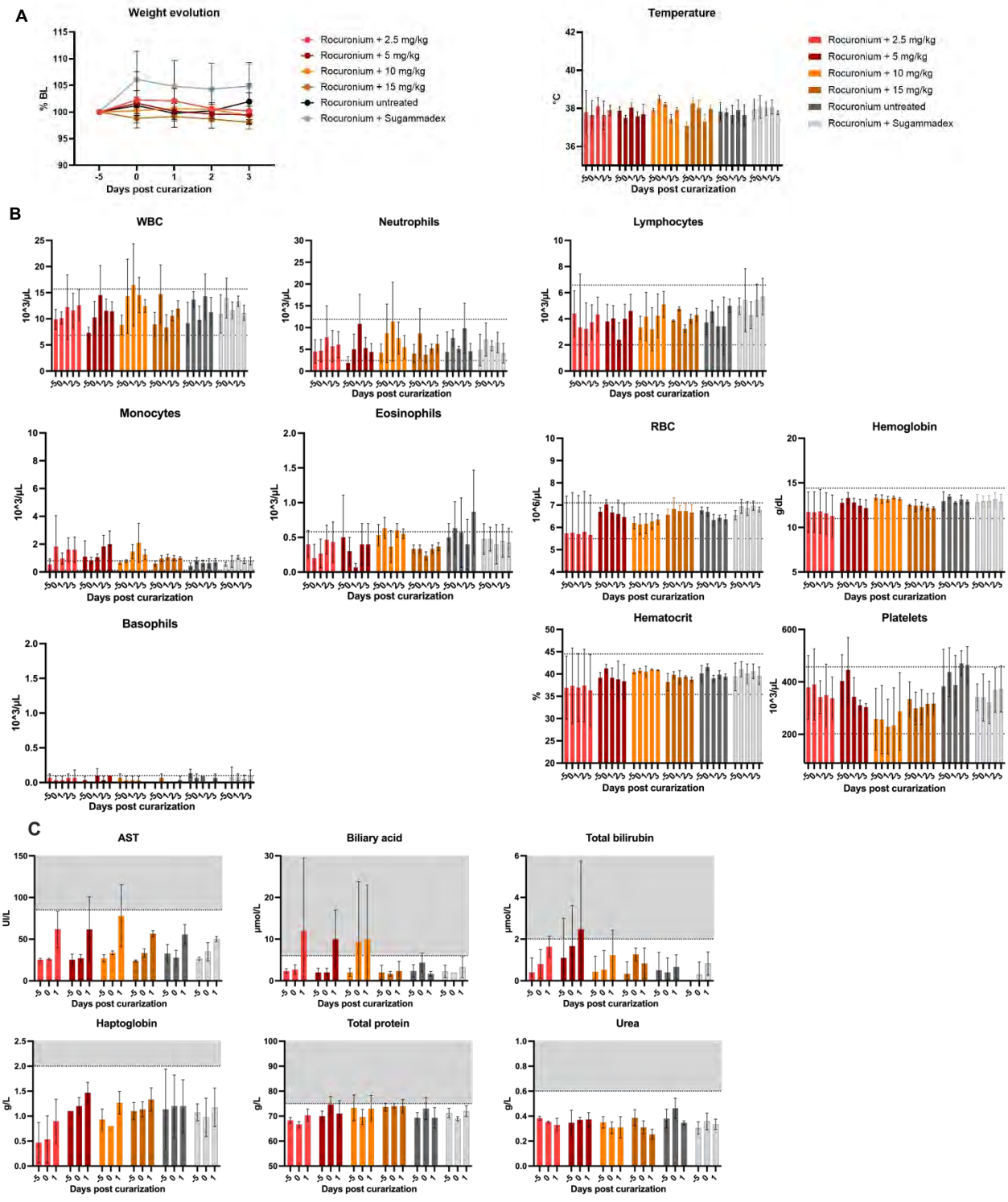

Fig. S13. Follow-up of physiological parameters in macaques. (**A**) Mean and standard deviation of the macaques' body weight and body temperature modification considering day 0 as the day of curare-enhanced anesthesia (n=5 per group). BL, baseline. (**B**) Mean and standard deviation of indicated cell populations and hematocrit in circulating blood reported considering day 0 as the day of curare enhanced anesthesia for each macaque (n=5 per group). Upper and lower normal values are indicated in dotted lines. (**C**) Mean and standard deviation of the macaques' blood biochemistry results for indicated parameters of the macaques (n=3 per group). Normal values reside in the white background, and abnormal values in the gray background. For (A to C), blood draws on day 0 were performed before curare injection. No statistical significance was found for any measurement or cell population count using non parametric Mann-Whitney and Kruskal-Wallis tests.

Table S1. Summary of sorting data and monoclonal culture data of rocuronium-binding human CD27$^+$ memory B cells. (Left) For each sort of each patient, the percentage of memory B cells sorted (IgD$^-$) is indicated. IgD$^-$ memory B cells stained with HSA-roc but not with HSA (HSA-roc$^+$ HSA$^-$) are considered to bind rocuronium. (Right) The number of rocuronium-specific monoclonal B cell cultures (identified by positive anti-rocuronium ELISA and at least 50% signal inhibition using competitive ELISA with free rocuronium) are shown, as well as the number of paired VH/VL sequences retrieved.

		Sorting data		Monoclonal cultures				
Patient	**Sort**	**IgD- among CD27+ Bmem and among total cells %**	**HSA-roc+ HSA- among IgD- Bmem %**	**(i) cultured cells #**	**(ii) Positive HSA-roc ELISA # (% among i)**	**(iii) Not inhibited by free rocuronium # (% among ii)**	**Total rocuronium-specific cultures # (% among i)**	**Total of sequenced and paired VH + VL (#)**
#1_2014	1	62.1 – 2.7	2.7	576	49 (8.5%)	10 (20%)	**57 (3.9%)**	25
	2	46.7 – 1	6.5	864	19 (2.1%)	1 (5%)		
#1_2023	1	31.3 – 1	1	768	142 (18%)	14 (10%)	**128 (16.7%)**	76
#2	1	42.7 – 1	1.5	576	23 (4%)	1 (4%)	**45 (2.6%)**	32
	2	25.8 – 1	2.2	576	20 (3.5%)	5 (25%)		
	3	34.9 – 1.2	2.2	576	3 (0.5%)	0 (0%)		
#3	1	29 – 0.7	3.7	576	5 (0.8%)	0 (0%)	**23 (1.3%)**	19
	2	20.5 – 0.9	3.9	576	16 (2.8%)	2 (13%)		
	3	45.3 – 1.1	3.1	576	4 (0.7%)	0 (0%)		

Table S2 Crystallization conditions, data collection, and refinement statistics of the m1B6-rocuronium and m2B1-rocuronium co-crystal structures. Crystallization conditions, data collection and refinement statistics. Values in parentheses are for the highest resolution shell. MPD, 2-methyl-2,4-pentanediol. HEPES, 4-(2-hydroxyethyl)-1-piperazineethanesulfonic acid. PEG400, polyethylene glycol 400. MES, 2-(N-morpholino)ethanesulfonic acid.

Crystal	Fab m2B1+rocuronium	ScFv m1B6+rocuronium
Reservoir solution	70% (v/v) MPD 0.1M HEPES pH7.5	30%(v/v) PEG400 0.1M MES pH6.5 0.1 M Na Acetate
Protein concentration, mg/m	7.1	15
Data collection		
Synchrotron beamline	PROXIMA 1	PROXIMA 2
Space group	C2	C2221
Unit cell dimensions		
a,b,c (Å)	161.57, 40.52, 69.78	135.47, 165.34, 127.52
a,b,g (°)	90, 100.40, 90	90, 90, 90
Resolution, Å	47.8-1.65 (1.68-1.65)	128-1.70 (1.73-1.70)
Rmerge	0.092 (1.372)	0.079 (1.707)
Rpim	0.038 (0.561)	0.027 (0.594)
Unique reflections	53958 (2663)	93815 (4304)
<I/sigma(I)>	10.7 (1.4)	16.4 (1.4)
Mn(I) half-set correlation	0.998 (0.603)	0.999 (0.567)
Completeness, %	100.0 (100.0)	100.0 (100.0)
Multiplicity	6.9 (6.9)	9.6 (9.2)
Refinement		
Resolution, Å	37.5-1.65 (1.67-1.65)	50.0-1.70 (1.72-1.70)
No. of reflections	52843 (1948)	153886 (5647)
Rvalue, working set	0.173 (0.200)	0.167 (0.299)
Rfree	0.301 (0.344)	0.189 (0.288)
Non-hydrogen protein	3644	6409
atoms	340	818
No. of Waters		
RMS deviations from ideal	0.012	0.015
bond length, Å	1.86	1.99
bond angles, °		
Ramachandran plot, %	98.07	96.15
preferred regions	1.45	3.11
allowed regions	0.48	0.74
outliers		

Data file S1. ELISA results of all monoclonal cell cultures. Supernatant of monoclonal cultures with an ELISA signal of HSA-rocuronium minus the ELISA signal of HSA ($OD_{HSA\text{-}roc} - OD_{HSA}$ = HSA-roc ELISA) superior to 3 times the background (OD>0.2) are shown. Competition was performed with 3,000 μM of free rocuronium, with a cut-off of percentage of inhibition ≥ 50%. Non-specific cultures with a percentage of inhibition <50% are indicated in gray. Cultures from which mAbs were recombinantly produced are indicated in blue.

Data file S2. Individual-level data for experiments where n<20.